INFORMATION TO USERS

This manuscript has been reproduced from the microfilm master. UMI films the text directly from the original or copy submitted. Thus, some thesis and dissertation copies are in typewriter face, while others may be from any type of computer printer.

The quality of this reproduction is dependent upon the quality of the copy submitted. Broken or indistinct print, colored or poor quality illustrations and photographs, print bleedthrough, substandard margins, and improper alignment can adversely affect reproduction.

In the unlikely event that the author did not send UMI a complete manuscript and there are missing pages, these will be noted. Also, if unauthorized copyright material had to be removed, a note will indicate the deletion.

Oversize materials (e.g., maps, drawings, charts) are reproduced by sectioning the original, beginning at the upper left-hand corner and continuing from left to right in equal sections with small overlaps. Each original is also photographed in one exposure and is included in reduced form at the back of the book.

Photographs included in the original manuscript have been reproduced xerographically in this copy. Higher quality 6" x 9" black and white photographic prints are available for any photographs or illustrations appearing in this copy for an additional charge. Contact UMI directly to order.

UMI

A Bell & Howell Information Company
300 North Zeeb Road, Ann Arbor MI 48106-1346 USA
313/761-4700 800/521-0600

SPECTROSCOPIC AND DYNAMIC PROPERTIES OF MOLECULES ADSORBED ON SURFACES

by

SERDAR OZCELIK

A dissertation submitted to the Graduate Faculty in Chemistry in partial fulfillment of the requirements of the degree of Doctor of Philosophy, The City University of New York.

1996

This manuscript has been read and accepted for the Graduate Faculty in Chemistry in satisfaction of the dissertation requirement for the degree of Doctor of Philosophy.

April 24, 1996
Date

Daniel L. Akins
Chair of Examining Committee

4/25/96
Date

Executive Officer

Supervisory Committee

THE CITY UNIVERSITY OF NEW YORK

ABSTRACT

SPECTROSCOPIC AND DYNAMIC PROPERTIES OF MOLECULES ADSORBED ON SURFACES

by

Serdar Özçelik

Adviser: Professor Daniel L. Akins

The photophysical properties of monomeric cyanines are studied because of the utility of such measured parameters as reference to spectroscopy and dynamics of the J-aggregates.

The structure and excited-state dynamics of J-aggregates of 1,1'-diethyl-2,2'-cyanine, also known as pseudoisocyanine (PIC), adsorbed onto a vesicle surface is studied. The results of spectrophotometric titrations for the interconversion of monomeric and aggregated 2,2'-cyanine and photophysical parameters of two putative adsorbed aggregates species (mono-cis- and all-trans conformers of the J-aggregates, relating to their makeup from mono-cis and all-trans stereoisomers, respectively). Superradiance and energy transfer are dominant features controlling photophysical processes. It is suggested that structure plays the crucial role in excited state dynamics.

A time-resolved, picosecond fluorescence spectroscopic study of benzimidazolocarbocyanine (BIC) adsorbed on a silica surface is presented. At the beginning, excitons are created in subpicoseconds. When two excitons close to each other, exciton-exciton interactions take place. As a result of the interaction, new states, specifically, the biexciton states in addition to the one-exciton state are created: a blue-shifted state relative to the one-exciton state, and a red-shifted state relative to the one-exciton. A kinetic model is proposed for the one-exciton and biexciton states.

The excited-state properties of 9-phenyl dibenzothiacarbocyanine (DBTC) aggregates is studied. The J-aggregate formed in homogeneous solution shows resonance fluorescence that indicates free exciton luminescence. The J-aggregates adsorbed onto silica surface show a Stokes shift. This Stokes-shift indicates the aggregate structure in the excited-state should be changed comparing to the ground-state structure. The J-aggregate formed in homogeneous solution studied has enhanced fluorescence, while another one adsorbed onto a silica surface shows nonradiative relaxations dominant in the excited-state.

ACKNOWLEDGEMENTS

I would like to thank my adviser, Dr. Daniel L. Akins, for his support, patience and encouragement throughout my studies. His unique mentorship helped me out to achieve my Ph. D. degree. His excellent research laboratory made my studies possible.

I am very grateful to the supervisory committee members who are Drs. Ronald Birke, Max Diem and Roger Dorsinville, for their stimulating suggestions and helpful comments on my studies. Additionally, I would like to thank Dr. John R. Lombardi for his special efforts during my acceptance to CUNY; and for serving in the committe until his sabbatical leave.

I acknowledge the financial support, from 1990 to 1993, of the Scientific and Technical Research Council of Turkey (Tübitak) granting a NATO science scholarship. I also acknowledge the faculty of engineering physics department of Ankara University, Turkey where I studied.

My thanks go to Dr. Dogan Bor for his continuous encouragement, who was my adviser when I was a graduate student in Turkey.

I would like to thank my wife, Isin, for her moral support, continuous encouragement and patience throughout my work. Morever, my first child to be-born, his/her due date is about the same with my defense date, is pushing me to finish up my work.

To the memory of my mother, **Ümmiye**, and mother-in-law, **Solmaz**;

and

to my wife, **Isin**.

TABLE OF CONTENTS

LIST OF TABLES

LIST OF FIGURES

CHAPTER 1

INTRODUCTION

1.1 Introduction

Interactions among organic dye molecules and resulting optical properties are important topics for study in physics and chemistry. Dye-dye interactions lead to spectral shifts and distinct changes in absorption bandshape that are indicative of incipent clustering as well as the actual formation of dye aggregates which may vary in composition from small number of molecules (i.e, oligomers) to that of a macroscopic, aligned crystal.

A particular type of dye aggregate; known as the J-aggregate or Scheibe aggregate is indicated by the appearence of a very narrow absorption band that forms when concentration is increased. This band is shifted to longer wavelengths than that of monomer's, and, often evidence a narrow resonance (1-4). Such aggregates, discovered by Edwin E. Jelley and Günter Scheibe in the late 1930s, are formed in homogeneous aqueous solution and glasses, such as ethylene-glycol/water mixture at low temperatue, as well as at solid-liquid interfaces, such as silver halide crystals, mica, vesicles and bilayers, and may be organized in insoluble monolayers at the air-water interface.

Aggregates play crucial roles in nature and have important technological applications. Aggregates are found in biological systems where they function to convert optical radiation into chemical energy and promote charge transfer reactions (5). Dye aggregates adsorbed onto silver halide semiconductor substrates have found extensive use as spectral sensitizers to inject electrons into semiconductors (6); the resultant mobile electrons can lead to important processes and reactions in solar cells, photographic film, photocatalytic and electrophotographic systems. Recently, aggregates have increased attention due nonlinear optical properties (7-11) and superradiant behavior (12-16).

In order to optimize the use of aggregates in these applications, it is necessary to charaterize and understand their optical and electronic properties.

The subject of this thesis is to characterize spectroscopic and dynamical properties of J-aggregates. In this study some cyanine dyes were used and various techniques such as absorption, excitation, emission, synchronized emission, Raman scattering, pisosecond fluorescence lifetime and picosecond time resolved fluorescence measurements were applied.

The following summary of the contents of the chapters will facilitate reading of this thesis.

Chapter 1 is summary of the the molecular exciton model for aggregates, and reviews structural, spectral and dynamical properties of aggregates.

Starting with chapter 2, the experimental studies are presented for monomeric cyanines: photophysical properties of monomers are in particularly presented because of the utility of such measured parameters as reference to spectroscopy and dynamics of aggregates.

In chapter 3 a study is provided of the structure and excited-state dynamics of J-aggregates of 2,2'-cyanine, also known as pseudoisocyanine (PIC) which is formed upon adsorption of the molecule onto a vesicle surface. Spectrophotometric titration and phase-modulation fluorescence lifetime measurements provides important information regarding the effective size of the aggregate and its superradiance.

In chapter 4 reports time-resolved, picosecond fluorescence dynamics and concentration dependent spectral properties of benzimidazolocarbocyanine (BIC) is reported; interpreted as revealing exciton-exciton interactions resulting in formation of blue-shifted and red-shifted biexciton states.

Chapter 5 presents an investigation of the excited-state properties of 9-alkly substituted thiacarbocyanine aggregates. While one of the aggregate has enhanced fluorescence, assignable possibly superradiance,

another one fluoresces only weakly, indicative of the dominance of nonradiative pathways to deplete excited state concentration.

1.1 The Molecular Exciton Model for Aggregates

Recently, basic research has focused on the excited states and nonlinear optical properties of aggregates, specifically, the creation and annihilation of excitons and biexcitons, superradiance, as well as third order optical nonlinearity. Excited electronic states of aggregates can be described using the molecular exciton model (17-19). The present section serve as an elementary primer on the molecular exciton formulation, which for the present study ignores vibronic interactions and vibronic structure in spectra.

The molecular exciton model is a construction that provides an approach for treating the coupling of excited states of molecular systems composed of interacting monomers, and the concept of the strong, intermediate or weak coupling approximations to differantiate between the coupling strength that is appropriate in different systems. The magnitude of the coupling strength can be can be inferedfrom a comparison of the exciton bandwidth (or the related spectral shift) to the the monomer's absorption bandwidth.

The mathematical formalism is the linear combination of wavefunctions for the individual molecules, one of which is excited, that comprise the aggregate system. The electronic states of the aggregate are then expressed in terms of the electronic states of the monomers and interactive energy terms between the monomers. Thus, the spectral properties of a molecular aggregate are related to the spectral properties of the component molecules by theoretical expressions involving observable experimental parameters; specifically, intermolecular distance, mutual intermolecular orientation and geometry, and intensity (oscillator strength) of light absorption by the monomeric species. Therefore, absorption intensity changes, spectral shifts and splittings may be calculable, depending upon the geometry of the aggregate. Also luminescence properties may be affected profoundly compared with those for the monomer's.

The starting point in the molecular exciton model treatment will be the singlet electronic energy states and their corresponding electronic state wavefunctions for a molecular monomers incorprated in a weakly bound aggregate. It is assumed that the electronic singlet energies $E_0, E_1, E_2, E_3, \ldots$ and wave functions $\psi_0, \psi_1, \psi_2, \psi_3, \ldots$ are known and satisfy the individual molecule Schrödinger equation

$$H_i \psi_i = E_i \psi_i . \qquad (1.1)$$

A two-level system, a ground and an excited singlet state with wave functions ψ_i and $\psi_i^\dagger$, respectively, for molecule i will be considered. All molecules of an aggregate will be considered to be identical. The zeroth-order wave functions for molecular aggregates will be constructed in order to derive first order energies for the electronic states of the aggregate.

Structure, spectral properties and energy levels for simple aggregate systems, e. g., dimers, tetramers, etc., are discussed here.

A. Molecular Dimers

The ground-state wavefunction for a molecular dimer consisting of two identical molecules is

$$\psi_{gs} = \psi_a \psi_b \tag{1.2}$$

is totally symmetric with respect to all symmetry operations. The first excited state of the dimer can be described equally well by two possible wave functions

$$\Phi_1 = \psi_a \psi_b^\dagger \text{ and } \Phi_2 = \psi_a^\dagger \psi_b \,. \tag{1.3}$$

These wavefunctions correspond to degenerate states and are not describe stationary states of the system. The correct zeroth order wavefunctions are

$$\Psi_I = \frac{1}{\sqrt{2}}(\Phi_1 + \Phi_2) = \frac{1}{\sqrt{2}}(\psi_a \psi_b^\dagger + \psi_a^\dagger \psi_b)$$

$$\Psi_{II} = \frac{1}{\sqrt{2}}(\Phi_1 - \Phi_2) = \frac{1}{\sqrt{2}}(\psi_a \psi_b^\dagger - \psi_a^\dagger \psi_b) \,. \tag{1.4}$$

In both of the stationary exciton wavefunctions, ψ_I and ψ_{II}, the excitation is on both molecules, *a* and *b*, i.e., the excitation is delocalized or collective. The node corresponds to the negative sign in the exciton wave function is an excitation node, not an electron orbital node. At an excitation node, the phase relation between transition moments on the respective molecular centers change sign.

B. A Cyclic Tetramer

In this case it will be assumed that four identical molecules are arranged in a plane with transition moments tangential to a circle in the plane. Let $\psi_a, \psi_b, \psi_c, \psi_d$ represent the wavefunctions of ground-states for molecules *a*, *b*, *c* and *d* and let $\psi_a^\dagger, \psi_b^\dagger, \psi_c^\dagger, \psi_d^\dagger$ represent the corresponding wavefunctions of excited states of the respective molecules.

The ground state of the tetramer will be the unique wave function

$$\psi_{gs} = \psi_a \psi_b \psi_c \psi_d \,. \tag{1.5}$$

The excited state wavefunctions of the tetramer can be described by four possible zeroth order wave functions, which are nonstationary

$$\begin{aligned}
\phi_1 &= \psi_a^\dagger \psi_b \psi_c \psi_d \\
\phi_2 &= \psi_a \psi_b^\dagger \psi_c \psi_d \\
\phi_3 &= \psi_a \psi_b \psi_c^\dagger \psi_d \\
\phi_4 &= \psi_a \psi_b \psi_c \psi_d^\dagger .
\end{aligned} \tag{1.6}$$

The correct symmetry adapted stationary state zeroth order wavefunctions are

$$\begin{aligned}
\psi_I &= \tfrac{1}{\sqrt{4}}(\psi_a^\dagger \psi_b \psi_c \psi_d + \psi_a \psi_b^\dagger \psi_c \psi_d + \psi_a \psi_b \psi_c^\dagger \psi_d + \psi_a \psi_b \psi_c \psi_d^\dagger) \\
\psi_{II} &= \tfrac{1}{\sqrt{4}}(\psi_a^\dagger \psi_b \psi_c \psi_d + i\psi_a \psi_b^\dagger \psi_c \psi_d - \psi_a \psi_b \psi_c^\dagger \psi_d - i\psi_a \psi_b \psi_c \psi_d^\dagger) \\
\psi_{III} &= \tfrac{1}{\sqrt{4}}(\psi_a^\dagger \psi_b \psi_c \psi_d - i\psi_a \psi_b^\dagger \psi_c \psi_d + \psi_a \psi_b \psi_c^\dagger \psi_d - i\psi_a \psi_b \psi_c \psi_d^\dagger) \\
\psi_{IV} &= \tfrac{1}{\sqrt{4}}(\psi_a^\dagger \psi_b \psi_c \psi_d - \psi_a \psi_b^\dagger \psi_c \psi_d - \psi_a \psi_b \psi_c^\dagger \psi_d + \psi_a \psi_b \psi_c \psi_d^\dagger).
\end{aligned} \tag{1.7}$$

The features for these exciton states for the cyclic tetramer are: (a) excitation is collective or completely delocalized, (b) the negative sign correspond to nodes in the exciton wavefunction, i.e., excitation nodes, corresponding a change in phase relations between the direction of

successive transition moments, and (c) the wavefunctions form orthogonal set.

C. Infinite Linear Polymer

Let us consider a simple linear chain or array of molecules forming a thread like polymer as a model for development of the exciton treatment for multimolecular aggregates.

Assuming N identical molecules, in a linear array, where N is very large or nearly infinite. The ground state wavefunction will be the unique, totally symmetric wavefunction

$$\Psi_{gs} = \psi_1\psi_2\psi_3\psi_4\ldots\psi_a\ldots\psi_N = \prod_{n=1}^{N}\psi_n \ . \qquad (1.8)$$

The lowest energy singlet excited state of the aggregate can be represented by the wavefunction

$$\Phi_a = \psi_a^{\dagger}\prod_{\substack{n=1\\ n\neq a}}^{N}\psi_n = \psi_1\psi_2\psi_3\psi_4\ldots\psi_a^{\dagger}\ldots\psi_N \qquad a=1,2,3,\ldots N \qquad (1.9)$$

where $\psi_i^{\dagger}$ indicates that the molecule i is in its lowest singlet excited state, and the remaining molecules are in their ground states. There are N such product functions Φ_i, i.e., these functions are N-fold degenerate, and they

correspond to nonstationary states of the excited states of the excited aggregate.

Symmetry adapted linear wavefunctions of the N wave functions Φ_i can be taken in order to get stationary exciton states of the aggregate. In general, the *k*th exciton stationary state wavefunction can be described by

$$\Psi_a = \frac{1}{\sqrt{N}} \sum_{a=1}^{N} C_{ak} \Phi_a \qquad (1.10)$$

where $|C_{ak}|^2$ determines the probability that the *a*th molecule is excited. Assuming ideal periodic distribution of molecules with one per unit cell, and N very large so that each molecule will have modulus unity for excitation, the various coefficients C_{ak} will differ only in their phase factors, and the wavefunctions may be written

$$\Psi_a = \frac{1}{\sqrt{N}} \sum_{a=1}^{N} e^{2\pi i k a / N} \Phi_a \qquad k=0,\pm1,\pm2,\ldots,N/2 \qquad (1.11)$$

As in the simpler cases, the N exciton stationary state wave functions show (a) collective excitation of molecular units of the aggregate, (b) excitation nodes, from a nodeless wave function to one with as many nodes as there are molecular units, and (c) orthogonality of the stationary wavefunctions.

The Hamiltonian for Aggregates. The Hamiltonian for aggregates is the sum of the Hamiltonians of individual molecules H_n in the aggregate and the potential energy terms V_{nm}, which specify the intermolecular interactions between molecules *n* and *m*

$$H = \sum_n H_n + \sum_{n,m>n} V_{mn} \tag{1.12}$$

Electron-phonon coupling is neglected throughout this chapter. However, the use of an exact coulombic potential would involve $1/r_{mn}$ as an operator, r_{mn} is the intermolecular distance between molecule m and molecule n. Therefore, a point-multiple expansion is used:

$$V_{coul} = V_{mono-mono} + V_{mono-di} + V_{di-di} + V_{quad-quad} + V_{di-quad} + V_{octo-octo} + \ldots \tag{1.13}$$

For neutral charge distrubution the monopole interactions are zero. For allowed electric-dipole transitions, the dipole-dipole term becomes the leading one and higher multipoles are neglected. Thus, corresponding to allowed electric dipole transitions

$$V_{coul} \cong V_{dipole-dipole} = -\frac{e^2}{r_{kl}^3} \sum_{i,j} (2z_k^i z_l^j - x_k^i x_l^j - y_k^i y_l^j) \tag{1.14}$$

where in the classical dipole-dipole potential r_{kl} is the distance between the point dipoles in molecules k and l, and x_k^i is the x coordinate of the ith

electron on molecule k, x_l^j the x coordinate of the jth electron on molecule l and so forth, the coordinate system being chosen with the z axis parallel to the line of molecular centers, and the summation is over all electrons in each molecule.

Thus, an approximation have been introduced which allows the physical interpretation that the excited state resonance splitting comes about from the electrostatic interaction of transition electric dipoles on neighboring molecules. Morever, in most cases electron displacement along only one coordinate is effected by the light wave causing the excitation at particular frequency.

1.2 Spectral and Structural Properties of Dimers

1.2.1 Cofacial parallel dimer

Spectral and structural properties of dimers can be evaluated using the Hamiltonians and wavefunctions discussed above for certain structural models. The energy of interaction will be given by the expectation value of the interaction potential with respect to the degenerate excited states of the dimer:

$$\varepsilon = \iint \psi_a \psi_b^{\dagger} V_{ab} \psi_a^{\dagger} \psi_b d\tau_a d\tau_b \ . \qquad (1.15)$$

Inserting the form of V_{ab} appropriate to an x-polarized electric-dipole transition in molecules a and b,

$$\varepsilon = \iint \psi_a \psi_b^{\dagger} \left(\sum_{i,j} x_k^i x_l^j\right) \psi_a^{\dagger} \psi_b d\tau_a d\tau_b$$

$$\varepsilon = \frac{1}{r_{kl}^3}\left[\int \psi_a \left(\sum_i ex_a^i\right) \psi_a^{\dagger} d\tau_a\right]\cdot\left[\int \psi_b^{\dagger}\left(\sum_j ex_b^j\right)\psi_b d\tau_b\right]. \qquad (1.16)$$

Each of the integral correspond to precisely the transition moment integral for the excitation of the individual (monomer) molecules a and b,

$$M_a = \int \psi_a \left(\sum ex_a^i\right)\psi_a^{\dagger} d\tau_a \,. \qquad (1.17)$$

At this point an arbitrary feature regarding the phase factor of the transition moment should be considered. A phase relationship exists such the exciton stationary state wavefunction Ψ_I chosen to lie lowest. Thus, in order to make the exciton wave stationary wavefunction Ψ_I correspond to a lowering of energy ε, the phase factor should be chosen

$$M_a = -M_b. \qquad (1.18)$$

The expression for the interaction energy for the parallel dimer becomes

$$\varepsilon = -\frac{M_a^2}{r_{ab}^3}. \qquad (1.20)$$

The exciton bandwidth will be 2ε. Thus the inteaction energy for the simple dimer is proportional to the probability or intensity of the electric dipole allowed transition in the monomer, divided by the intermolecular distance cubed. Thus, the stronger the absorption, the greater exciton band splitting.

A sample calculation of exciton splitting can be made by using the definition of oscillator strength

$$f = 4.704x10^{29}\,\bar{\nu}M^2 \qquad (1.21)$$

where $\bar{\nu}$ is the frequency in cm^{-1} and M is the transition moment in e.s.u., the expression,combining equ. (1.20) and (1,21), becomes

$$\varepsilon = -\frac{f}{4.704x10^{29}\,\bar{\nu}r_{ab}^3} \qquad (1.22)$$

where r_{ab} defines the nearest dipole-dipole distance. The order of the magnitude can be assessed from a choice of data. Using f=1 for a strongly allowed band, $\bar{\nu}$=20,000 cm^{-1} for absorption at 500 nm,the transition moment is calculated as $M \cong 10^{-17}$ e.s.u. or 10 deybe. Using some values of

r_{ab}, the corresponding values of ε may be estimated: -870 cm^{-1} for 1 nm, and -6960 cm^{-1} for 0.5 nm.

Let us examine **the spectral selection rules** by evaluating the matrix elements of the electric dipole operator between the ground state and the stationary exciton states of the dimer. Thus , the transition moment vector of the dimer is given by

$$M^{I} = \iint \Psi_{gs}(M_a + M_b)\Psi_{I} d\tau_a d\tau_b$$
$$M^{II} = \iint \Psi_{gs}(M_a + M_b)\Psi_{II} d\tau_a d\tau_b \qquad (1.23)$$

where M_a and M_b are the electric dipole operators corresponding to the molecular electronic coordinates of molecules a and b. Evaluating these, the two transition moments are

$$M^{I,II} = \frac{1}{\sqrt{2}} \iint \psi_a \psi_b (M_a + M_b)\left(\psi_a \psi_b^{\dagger} \pm \psi_a^{\dagger} \psi_b\right) d\tau_a d\tau_b \,. \qquad (1.24)$$

Because of orthogonality and normalization properties of the intramolecular state wavefunctions, equ. (1.24) leads to

$$M^I = \frac{1}{\sqrt{2}}\int \psi_a M_a \psi_a^\dagger d\tau_a + \frac{1}{\sqrt{2}}\int \psi_b M_b \psi_b^\dagger d\tau_b = \frac{1}{\sqrt{2}}(M_a + M_b)$$
$$M^{II} = \frac{1}{\sqrt{2}}\int \psi_a M_a \psi_a^\dagger d\tau_a - \frac{1}{\sqrt{2}}\int \psi_b M_b \psi_b^\dagger d\tau_b = \frac{1}{\sqrt{2}}(M_a - M_b) \quad .(1.25)$$

By using the phase relationship, equ. 1.18, the transition moments corresponding to the stationary exciton states are

$$M^I = \frac{1}{\sqrt{2}}(M_a + M_b) = 0$$

$$M^{II} = \frac{1}{\sqrt{2}}(M_a - M_b) = \frac{2M_a}{\sqrt{2}} . \quad (1.26)$$

Thus, the transition moments for the dimer are given as superpositions of the transition moments for the individual molecules. The oscillator strengths for electric dipole transitions between the dimer ground state and the stationary exciton states are

$$f \propto (M^I)^2 = 0$$

$$f \propto (M^{II})^2 = 2M_a^2 \quad \text{or} \quad f_{II,dimer} = 2f_{monomer}. \quad (1.27)$$

The out of phase dipole arrangement corresponds electrostaticaly to a lowering energy (ε negative), so E^I lies lower than the lowest excited state of monomer; and in the phase arrangement interaction is repulsive (ε positive), leading to higher exciton state E^{II} than the monomer excited

state. Thus, transitions from the ground state to exciton state E^I are forbidden, while transitions from the ground state to exciton state E^{II} are allowed. The parallel dimer levels and selection rules are shown below.

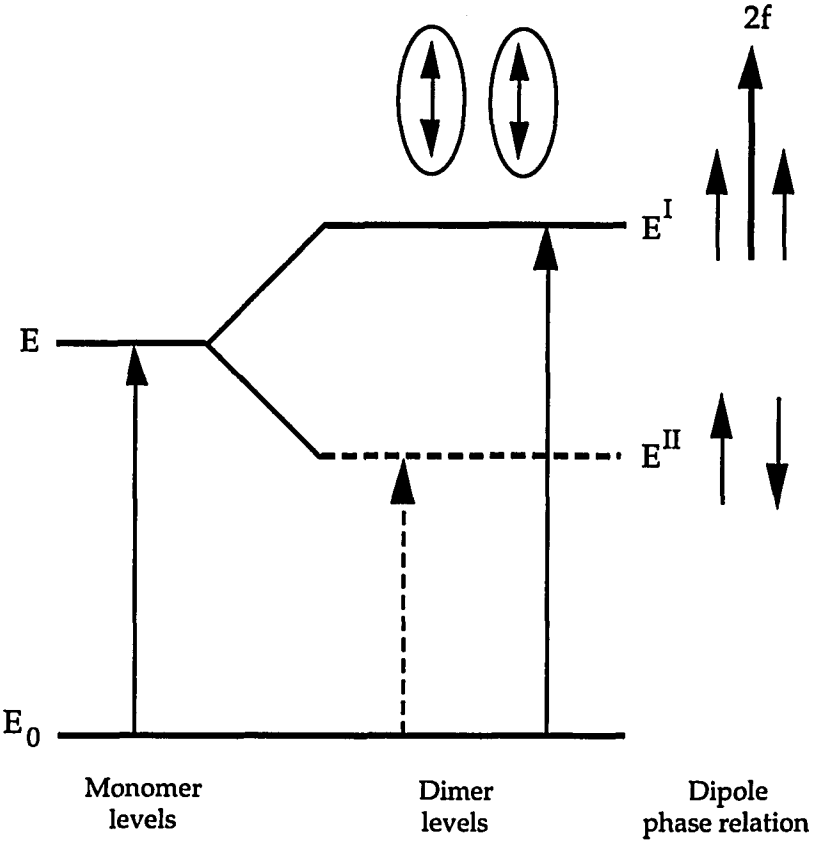

Figure 1.1: Structure and energy levels of a cofacial parallel dimer.

The characteristics of cofacial parallel dimer are (a) the absorption spectrum blue-shifts, and (b) the fluorescence is quenched. Figure 1.1 serve to illustrate spectral properties of the cofacial parallel dimer. In the monomer, absorption to the lowest singlet excited state is strongly

allowed, and fluorescence emission is observed. In the dimer, the allowed exciton states is higher than the singlet excited state of the monomer. Collisions rapidly deactivate the excited dimer to its lower stationary exciton state, a metastable singlet state with an improbable fluorescence capacity.

Other type of dimer structures are possible, and exciton model permits discussion of such dimers as well. Such dimer structures are head-to-tail dimer, oblique dimer, and co-planar inclined dimer. These are discussed below.

1.2.2 Head-to-tail dimer

Molecules in the head-to-tail orientation lead to the exciton energy level diagram shown in Figure 1.2. From the diagram it is seen readily that the in-phase arrangement of transition dipoles leads to an electrostatic attraction, producing the excited state E^{I}, whereas the out of phase arrangement of transition dipoles causes repulsion, producing the excited state E^{II}. Thus, it will be apparent that head-to-tail orientation will cause the observation of a strong spectral red shift.

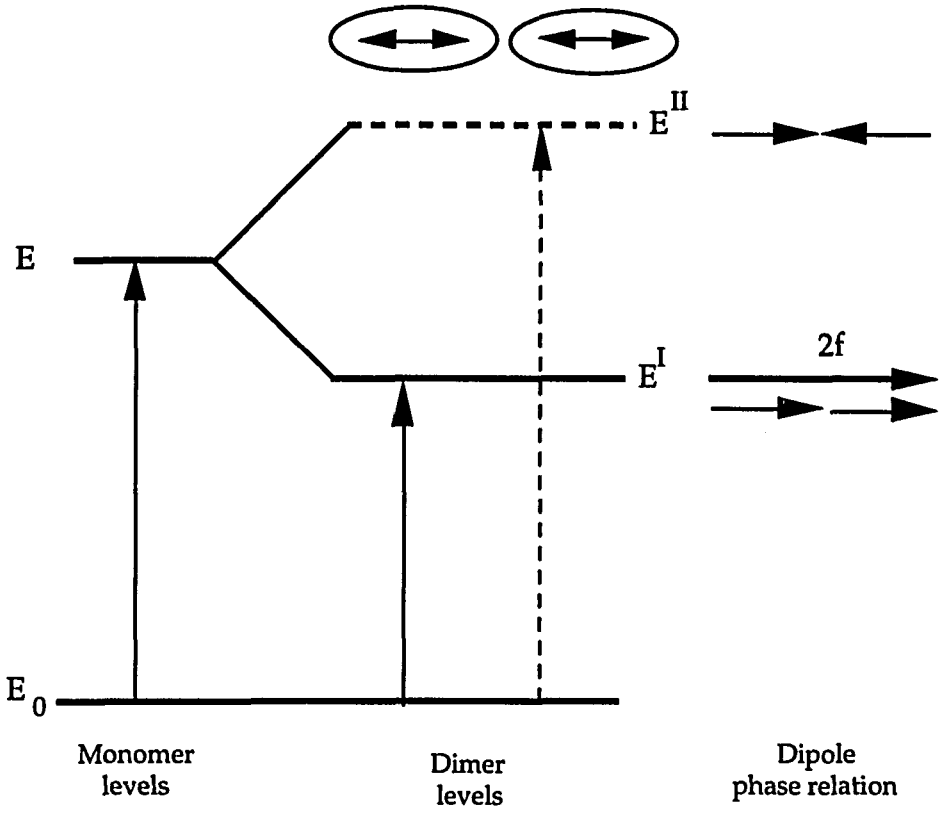

Figure 1.2 Structure and energy levels of a head-to-tail dimer.

1.2.3 Oblique dimer

In this case, orientation of the molecules lead to the exciton energy diagram shown in Figure 1.3. The in-phase arrangement of transition dipoles for the monomer is attractive and leads to a lowering of energy, and the out-of-phase arrangement of transition dipoles is repulsive and causes a raising of the excited state of the dimer. The transition moments for electric dipole transitions of the dimer are both nonvanishing. The oscillator strengths f_I and f_{II} are polarized mutually perpendicularly.

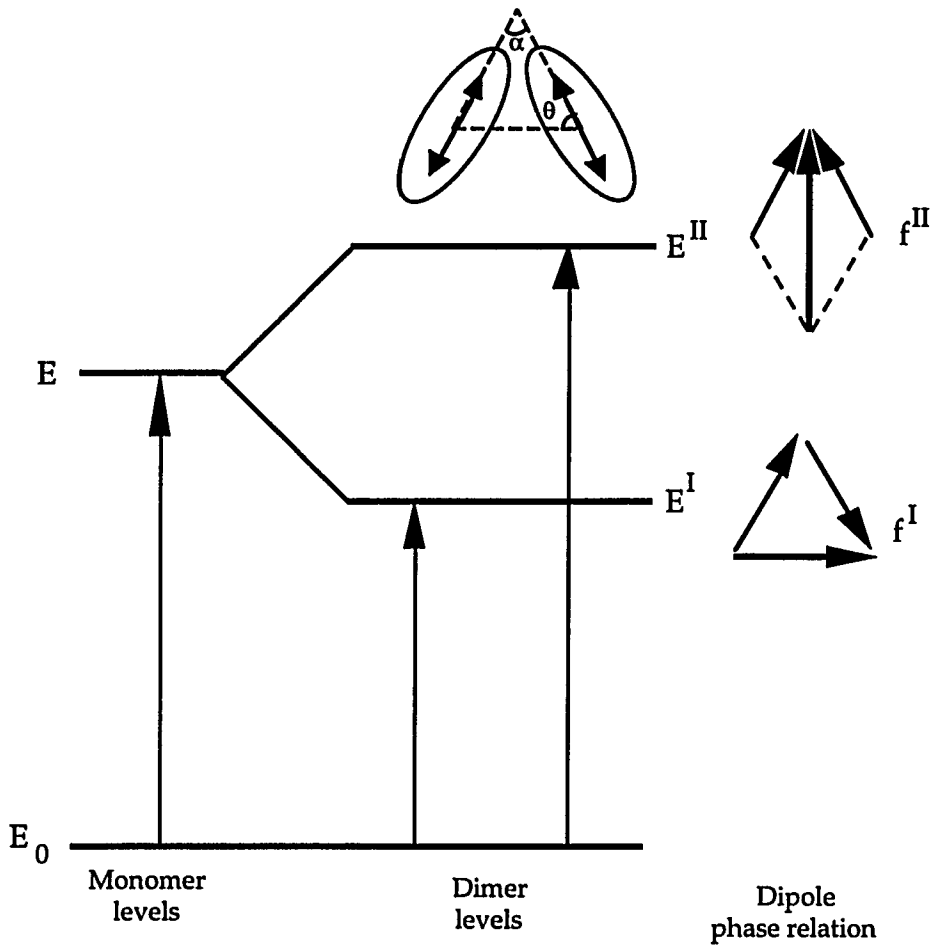

Figure 1.3 Structure and energy levels of an oblique dimer.

The exciton splitting energy, corresponding to the separation is given by

$$\Delta\varepsilon = E^{II} - E^{I} = \frac{2|M|^2}{r_{ab}^3}\left(\cos\alpha + 3\cos^2\theta\right) \qquad (1.28)$$

where M is the transition moment for the singlet-singlet transition in the monomer, r_{ab} is the centre to centre distance between molecules a and b, α

is the angle between polarization axes for the molecules and θ is the angle made by the polarization axes of the unit molecule with the line of molecular centres. The transition moments to the exciton states E^I and E^{II} are given by

$$M^I = \sqrt{2M\cos\theta}$$

$$M^{II} = \sqrt{2M\sin\theta}\ . \qquad (1.29)$$

It is seen that the exciton splitting energy is directly related to the square of the transition moment of the monomer. Thus, the greater the intensity of light absorption the greater the exciton band splitting. The square of the transition moment M is a measure of the oscillator strength f for the transition.

1.2.4 Coplanar inclined dimer

In this case, orientation of the molecules lead to the exciton energy diagram shown in Figure 1.4. This case covers continuosly the variation of angle θ between poarization axes and the line of molecule centres. Thus, 0 degrees corresponds to the parallel dimer case and 90 degrees corresponds to the head-to-tail dimer.

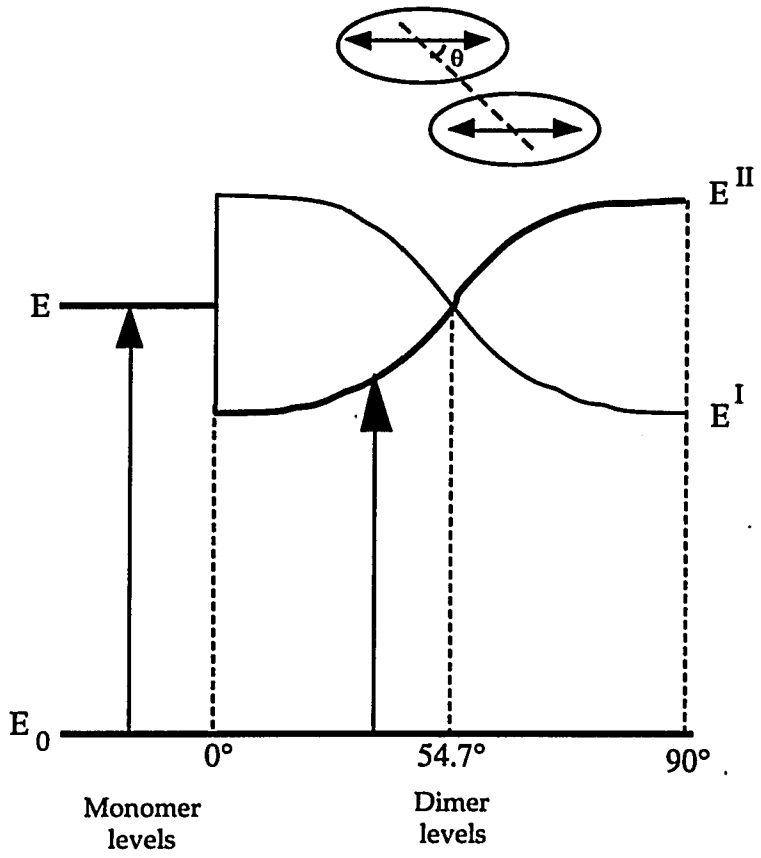

Figure 1.4 Structure and energy levels of a coplanar-inclined dimer.

The exciton band splitting in this case is given by the formula

$$\Delta\varepsilon = \frac{2|M|^2}{r_{ab}^3}\left(1-3\cos^2\theta\right) \qquad (1.30)$$

with the symbols as previously defined. It is evident that for the value of $\theta = \cos^{-1}\left(\frac{1}{\sqrt{3}}\right) = 54.7^{\circ}$, the exciton splitting is zero, i.e., the dipole dipole interaction is zero for this orientation of transition moments, irrespective of intermolecular distance r_{ab}.

The transition moments for this case are given by $M^{I} = 0$ and $M^{II} = 2M$, M^{I} and M^{II} correspond to the out-of-phase and in-phase arrangement of transition dipoles.

1.4. Spectral and Structural Properties of Linear Chain Aggregates

The exciton model will be applied to long chain linear aggregates. The exciton band width and spectral properties will be discussed. Two simple cases, offering the best illustrations of the nature of exciton bands in large molecular aggregates are: (A) long chain aggregates in which the molecular components are translationally equivalent (Figure 1.5.A), i.e. one molecule per unit. By variation the angle α, between the long molecular axis and the aggregate axis, one can go from a parallel chain aggregate to a head-to-tail chain aggregate, as α goes from $\pi/2$ to 0. In these aggregates the molecular subunits are assumed to have their optical electrons localized on each component molecule.

The other case (B) may be called the alternate transitional aggregate in which every other molecular component is translationally equivalent (Figure 1.6.A), i.e. two molecules per unit.

In this model the surroundings of neighboring molecules are equivalent, so that the excited states of the aggregate are described by wave functions of the form of equ. 1.11.

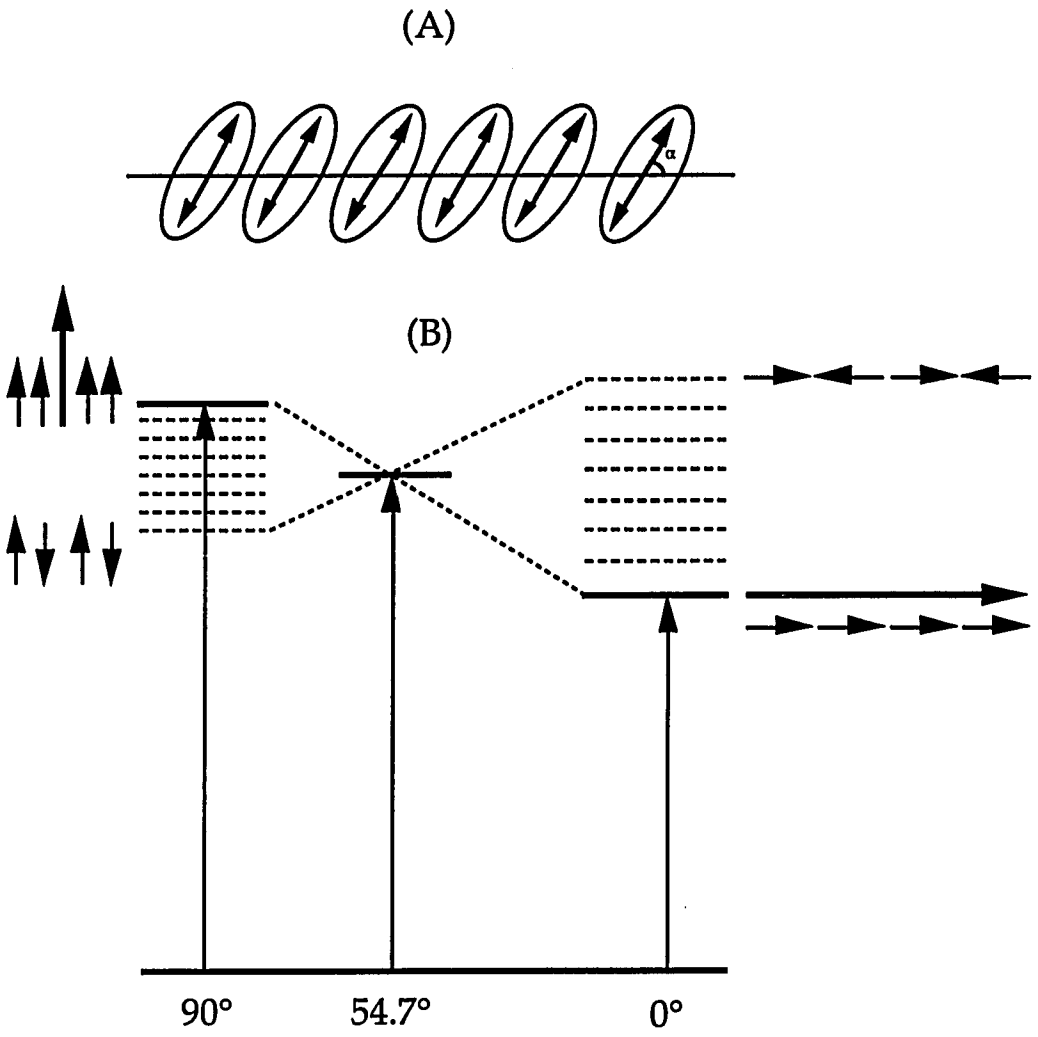

Figure 1.5: Structure (A), and energy levels (B) of long chain aggregates in which the molecular components are translationally equivalent.

$$\Psi_a = \frac{1}{\sqrt{N}} \sum_{a=1}^{N} e^{2\pi i k a / N} \Phi_a \qquad k=0,\pm1,\pm2,.....,N/2$$

The zeroth order exciton state energies for the linear chain aggregate are given by

$$E_k = E_a^0 + 2\left(\frac{N-1}{N}\right) cos\left(\frac{2\pi k}{N}\right) \varepsilon_{a,a+1} \qquad k=0,\pm1,\pm2,.....,N/2 \qquad (1.31)$$

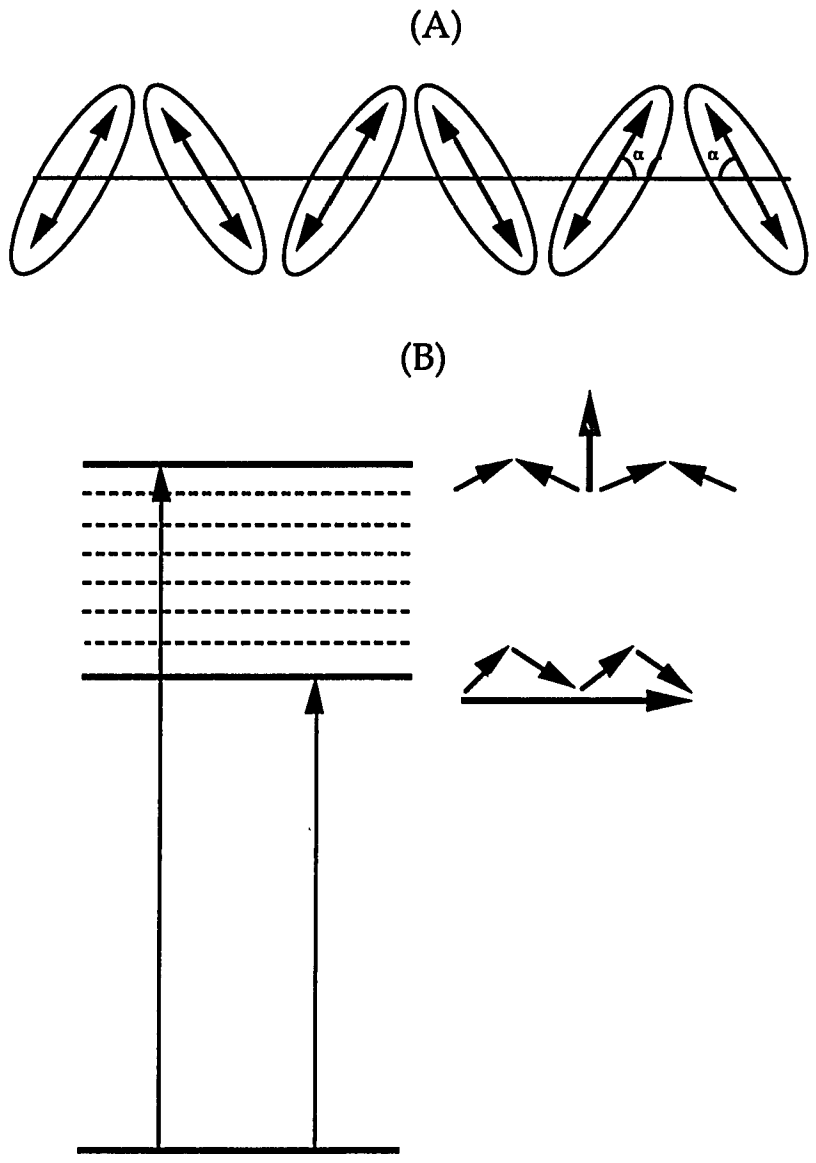

Figure 1.6: Structure (A), and energy levels (B) of alternate transitional aggregate in which every other molecular component is translationally equivalent.

where E_a^0 denotes the energy of the first excited singlet state of the isolated component molecule a of the aggregate. In equ. 1.31 $\varepsilon_{a,a+1}$ represents the matrix element for interaction between two simple product functions corresponding to excitation on two adjacent molecules. Thus

$$\varepsilon_{a,a+1} = \int \Phi_a H' \Phi_{a+1} d\tau \ . \qquad (1.32)$$

The perturbation operator H' may be taken as the appropriate form of the dipole-dipole operator in the point to point dipole approximation. Two cases will be considered here for illustration purposes: **(a)** translational chain aggregate shown in Figure 1.5.B, and **(b)** alternate translational chain aggregate shown in Figure 1.6.B. The transition moments of the individual molecules lie in the molecular plane and parallel to the aggregate axis. The matrix element for interaction is

$$\varepsilon_A = -\frac{M^2}{r^3}(1-3\cos^2\alpha) \qquad \text{for case A} \qquad (1.33)$$

and

$$\varepsilon_B = -\frac{M^2}{r^3}(1+3\cos^2\alpha) \ . \qquad \text{for case B} \qquad (1.34)$$

Therefore, the energies of the exciton states within the exciton band are given by

$$E_{k(A)} = E_k^0 - 2\left(\frac{N-1}{N}\right)\left[\cos\left(\frac{2\pi k}{N}\right)\right]\left(\frac{M^2}{r^3}\right)(1-3\cos^2\alpha) \qquad (1.34)$$

$$k=0,\pm1,\pm2,.....,N/2$$

$$E_{k(A)} = E_k^0 - 2\left(\frac{N-1}{N}\right)\left[\cos\left(\frac{2\pi k}{N}\right)\right]\left(\frac{M^2}{r^3}\right)(1+3\cos^2\alpha) \qquad (1.35)$$

The interaction energy hence **the exciton band width** is proportional to the transition moment M squared for the appropriate electronic band in the component molecule of the aggregate. Case A exhibits a feature that

for the angle $cos^{-1}\left(\frac{1}{\sqrt{3}}\right)=55^{o}$ the interaction energy and exciton band width is zero. The exciton band widths for both two cases are summarized below.

Structure	Exciton band width, 2ε
Translational chain	$4\left(\frac{N-1}{N}\right)\left(\frac{M^2}{r^3}\right)(1-3cos^2\alpha)$
Alternate translational chain	$4\left(\frac{N-1}{N}\right)\left(\frac{M^2}{r^3}\right)(1+3cos^2\alpha)$

In order to derive **selection rules** for absorption spectra for the linear chain aggregates, the matrix elements of the electric dipole operator for the aggregate wave functions should be evaluated

$$M_k=\int \Psi_{gs}^{*}\left(\sum M_a\right)\Psi_k d\tau\ . \tag{1.36}$$

Using linear aggregate wavefunctions presented in subsection 1.1.4

$$M_k=\frac{1}{\sqrt{N}}\sum_{a=1}^{N} e^{2\pi ika/N}M_a \tag{1.37}$$

and the square of the transition moment is

$$M_k^2=\frac{1}{N}\left[\sum_{a=1}^{N}\sum_{b=1}^{N}cos\{2\pi k(a-b)\}\right]M_aM_b\ , \tag{1.38}$$

where M_a and M_b represent transition moments for the ath and bth molecule.

Again the phase factors are such that two adjacent molecules are translationally-equivalent and their transition moments have opposite signs, like the parallel dimer case. For the linear chain aggregates, see Figure 1.6.B

$$M_a.M_{a+1} = -M^2,$$
$$M_a.M_{a+2} = M^2,$$
$$M_a.M_{a+3} = -M^2,$$

and so on. Hence the general form is obtained

$$M_k^2 = \frac{M^2}{N}\sum_{a=1}^{N}\sum_{b=1}^{N}(-1)^{a-b}\cos\{2\pi k(a-b)\}\,. \qquad (1.39)$$

The exciton selection rules and bandwidths for the linear chain aggregates are summarized as below.

Structure	Transition moment from ground state to **bottom** of exciton band	Transition moment from ground state to **top** of exciton band
Translational chain $\pi/2 \geq \alpha \geq \cos^{-1}\left(\frac{1}{\sqrt{3}}\right)$	0	$N^{1/2}M$
$0 \leq \alpha \leq \cos^{-1}\left(\frac{1}{\sqrt{3}}\right)$	$N^{1/2}M$	0
Alternate translational chain	$N^{1/2}M\cos\alpha$	$N^{1/2}M\sin\alpha$

All formulas apply to $2 \leq N > 10$. For linear aggregates of small and finite chain length, $N = 3...10$ the formulas are not applicable because of the end effects, a secular determinant would have to be solved to obtain the nonintegral coefficient of the wavefunctions.

1.5 Other Structural Models for Aggregates

Structural models for aggregates are proposed to explain experimental observations. A structural model for the pseudoisocyanine (PIC) aggregates has been suggested by Scheibe (20,21): the staggered and tilted chromophores form linear chain polymers; ladder or staircase arrangements. The axis of the chain is perpendicular to the transition moment of the monomer unit. PIC is not planar: the two quinoline rings are twisted around the methine due to overlap of the hydrogens in the 3 and 3′ positions (22). According to Kuhn and coworkers (23,24) the aggregates should form two-dimensional systems: brickstone model. The brickstone model has been confirmed by different experimental techniques (25-29). The suggested structures by Kuhn are depicted in Figure 1.7

In a very recent study using near-field scanning optical microscopy, a herringbone-like structural model (see Figure 1.7) has been proposed for thin films of PIC J-aggregates (30). This model was proposed originally by

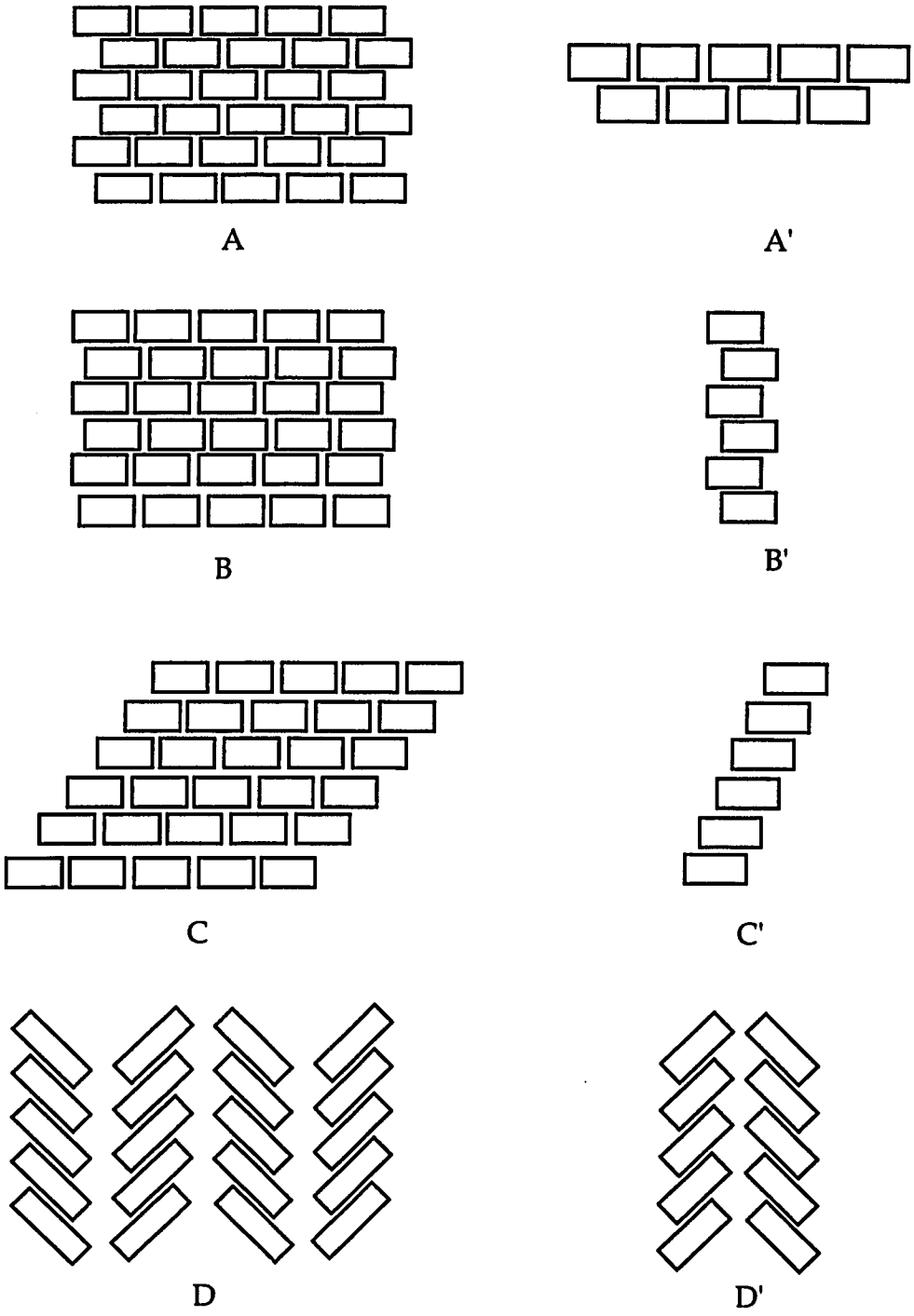

Figure 1.7. Proposed 2D (A,B,C,D) and 1D (A',B',C',D') aggregate structures. Brickwork (A,A'), ladder (B,B'), staircase (C,C') and herringbone (D,D').

Nolte (31) . Nolte has used this model to explain observed circular dichroism of the aggregates in solution. A helical structure has also been suggested as an alternative model (31). A herringbone-like structural model has also been proposed for monolayer of thiacarbocyanine aggregates (32).

Very recently, Tiddy *et al.* has proposed a new structural model for aggregates in solution, called "hollow pipe" structures (33).

1.6 Aggregate Emission Dynamics

The optical dynamics of aggregates have drawn much attention due to possible technological applications. Several experimental techniques such as femto- and picosecond pump-probe absorption, picosecond fluorescence lifetime, femto- and picosecond photon echo, etc., were applied to understand the dynamics and nonlinear optical properties of aggregates.

Fluorescence from aggregeted molecules is widely understood as resulting from radiative decay of coherently coupled molecules; morever, the physical number of molecules in an aggregate can be substantially different than the number of molecules which coherently emit. This latter concept leads to defining of an effective number of coupled molecules, termed the coherence size, represented as N_{eff}. As a result of the cooperation, the radiative rate of the aggregate is expected to be N_{eff} times faster than that for the isolated molecule.

Early measurements of the fluorescence lifetime of J-aggregates formed in solution or on glass gave very short lifetimes (34-38), on the order of picoseconds, since the high excitation intensities used resulted in exciton annihilation.

Sundström et al. (39) performed experiments on J-aggregates of 2,2'-cyanine in homogeneous aqueous solution at room temperature and determined that both the lifetime and the fluorescence yield were strongly dependent on excitation pulse intensity; a single exponential lifetime of about 400 ps was measured at low excitation intensity. Other time-dependent studies that avoided the excitation pulse intensity problem were conducted (12,13,40-42) utilizing J-aggregates of 2,2'-cyanine formed in an ethylene glycol/water glass at low temperature, and ascertained that the low-temperature fluorescence lifetimes were 70 ps for the aggregate which absorb at ca. 576 nm and 45 ps for the aggregate which absorb at ca. 573 nm . In these latter studies, the measured lifetime was found to be independent of temperature up to 50 K, and temperature dependent (increasing with temperature) above 50 K; they further concluded that molecular superradiance (due to disordered molecular aggregates) is the dominant deactivation process.

Other recent investigations provide information on fluorescence dynamics for 2,2'-cyanine. For example, Muenter et al. (43) reported the dependence of fluorescence lifetime and relative quantum yield on temperature and aggregate size for the J-aggregates of 2,2'-cyanine on a AgBr surface, and showed that the dominant process controlling the dynamics was energy transfer to a defect state—a dimer structure was suggested. This nonradiative process was postulated to lead at room

temperature to a strong diminution in fluorescence yield with increasing concentration.

Dorn and Müller (44) measured a lifetime of 8.2 ps for a Langmuir-Blodgett monolayer of 2,2'-cyanine J-aggregate at room temperature, and a value of 5.5 ps at 143 K; they interpreted the decrease in lifetime as evidence for superradiance enhancement.

Additionally, Fidder et al. (13) have shown for a Langmuir-Blodgett monolayer of 2,2'-cyanine J-aggregate at 1.5 K that the fluorescence lifetime of the initial decay process was 10 ps— a slower, secondary decay was not evaluated. These latter authors attributed the nonexponentiality of the decay to a combination of exciton transport and radiative decay. The structure of J-aggregates in a Langmuir-Blodgett monolayer was deduced to be quasi two-dimensional and more delocalized than one dimensional aggregates formed in frozen glass.

The excited-state dynamics of polymer bound J-aggregates of 2,2'-cyanine have been studied and concluded that superradiance and exciton migration are the mechanisms (45).

The fluorescence lifetime of benzimidazolocarbocyanine (BIC) J-aggregate in solution was measured by O'Brien et.al. (46) with a time correlated single photon counting technique (TCSPC) and was found to be 0.960 ns, without details such as concentration, excitation and emission wavelengths, temperature, etc.

Recently, Lindbrum et al. (47) have carried out temperature dependent fluoresence lifetime measurements of sodium salt of BIC J-

aggregates between 4 and 300K. Their conclusion was that the microscopic environment of the J-aggregate determines the lifetime.

Yoshihara and coworkers have conducted some experiments (48-50) regarding excited state dynamics of sodium salt BIC J-aggregates. They measured the picosecond pump-probe absorption spectra of J-aggregates at high pump intensities, 10^{15} - 10^{16} photons/cm^2. A fast response < 10 ps, and a slow response, 400 ps assigned to the lifetime of a single exciton on an aggregate were observed. At high excitation intensities, the excited-state dynamics was exciton-exciton annihilation processes. They studied the temperature dependence of superradiant emission of sodium salt BIC J-aggregates in ethylene glycol/water glass. They measured that the lifetime decreased with increase of the temperature in the range of 20-60K, from 100 ps at 8K to 70 ps at 65K. Additionally, emission intensity monotonically decreased with increased temperature in the range 4-100K. Possible mechanisms were discussed: internal conversion, nonradiative decay to another excited-state, or intra-aggregate electron transfer. Emission characteristics of sodium salt BIC J-aggregates in solution at room temperature were a blue shift and narrowing of emission spectrum were observed along with double exponential decay at high excitation intensities. These observations were explained as one exciton emission and emission from the two exciton to one exciton state. Reported one exciton lifetime was 110 ps and the two exciton lifetime was 30 ps (50).

Femtosecond spectroscopic studies were carried out for 2,2'-cyanine J-aggregates in solution to evaluate many exciton interactions (51,52). The results were explained in terms of exciton-exciton

interactions: formation of biexciton and many-exciton states. The decay time of the many-exciton state was reported as 200 fs.

REFERENCES

1. Jelley, E. Nature, 1936, 138, 1009.
2. Jelley, E. Nature, 1937, 139, 631.
3. Scheibe, G. Angew. Chem. 1936, 49, 563.
4. Scheibe, G. Angew. Chem. 1937, 50, 51.
5. Feher, G.; Okumura, M. Y. In "The Photosynthetic Bacteria"; Clayton, K.; Sistrom, W.F., Ed.; Plenum: New York, 1978.
6. Gilman, P. B. Photo. Sci. Eng. 1974, 18, 418.
7. Hanamura, E. Phys. Rev. B. 1988, 37, 1273.
8. Sasaki, F.; Kobayashi, S. Appl. Phys. Lett. 1993, 63, 2887.
9. Wang, Y. Chem. Phys. Lett. 1986, 126, 209.
10. Wang, Y. J. Opt. Soc. Am. B. 1991, 8, 981.
11. Kobayashi, S. Mol. Crys. Liq. Crys. 1992, 217, 77.
12. Fidder, H.; Knoster, J.; Wiersma, D. A. Chem. Phys. Lett. 1990, 171, 529.
13. Fidder, H.; Terpstra, J.; Wiersma, D. A. J. Chem. Phys. 1991, 94, 6895.
14. Grad, J.; Hernandez, G; Mukamel, S. Phys. Rev. A. 1988, 37, 3835.
15. Spano, F. C.; Mukamel, S. J. Chem. Phys. 1989, 91, 683.

16. Spano, F. C.; Kuklinski, J. R.; Mukamel, S. J. Chem. Phys. 1991, 94, 7534.

17. McRae, E.; Kasha, M. J. Chem. Phys. 1958, 28, 721.

18. Kasha, M. In Physical Processes in Radiation Biology. Academic Press, New York, 1964.

19. Kasha, M.; Rawls, H. R.; El_Bayoumi, M. A. Pure and Applied Chem., 1965, 11, 371.

20. Scheibe, G. In Optische Anregung Organischer Systeme. Ed. Foerst, W. Verlag Chemie, Weinheim, 1966.

21. Scheibe, G. Angew. Chem. 1939, 53, 631.

22. Dammeier, V. B.; Hoppe, W. Acta. Crystallogr. 1971, B27, 2364.

23. Czikklely, V.; Forsterling, H. D.; Kuhn, H. Chem. Phys. Lett. 1970, 6, 11.

24. Czikklely, V.; Forsterling, H. D.; Kuhn, H. Chem. Phys. Lett. 1970, 6, 207.

25. Stoeckli-Evans, H. Helv. Chim. Acta. 1974, 57, 1.

26. Duschl, C.; Frey, W.; Knoll, W. Thin Solid Films 1988, 160, 251.

27. Kuroda, S.; Ikegami, K.; Saito, K.; Saito, M; Sugi, M. J. Phys. Soc. Jpn. 1987, 56, 3319.

28. Mizrahi, V.; Stegeman, G. I.; Knoll, W. Phys. Rev. A 1989, 39, 3555.

29. Wolthaus, L.; Schaper, A.; Mobius, D. Chem. Phys. Lett. 1994, 225, 322.

30. Higgins, D. A.; Reid, P. J.; Barbara, P. F. J. Phys. Chem. 1996, 100, 1174.

31. Nolte, H. Chem. Phys. Lett. 1975, 31, 134.

32. Kirstein, S.; Mohwald, H. J. Chem. Phys. 1995, 103, 826.

33. Harrison, W. J., Mateer, D. L; Tiddy, G. J. T. J. Phys. Chem. 1996, 100, 2310.

34. Yu, Z. X.; Lu, P. Y.; Alfano, R. R. Chem. Phys. Lett. 1983, 79, 289.

35. Kopainsky, B.; Kaiser, W. Chem. Phys. Lett. 1982, 88, 357.

36. Rentsch, S. K.; Danielius, R. V.; Gadonas, R. A.; Piskarkas, A. Chem. Phys. Lett. 1981, 84, 446.

37. Brumbaugh, D. V.; Muenter, A. A.; Knox, W.; Mourau, G.; Wittmershaus, B.; J. Lumin. 1984, 31&32, 783.

38. Fink, F.; Klose, E.; Teuchner, K.; Dahne, S. Chem. Phys. Lett. 1977, 45, 548.

39. Sundström, V.; Gillbro, T.; Gadonas, R. A.; Piskarkas, A. J. Chem. Phys. 1988, 89, 2754.

40. De Boer, S.; Wiersma, D. A. Chem. Phys. 1989, 131, 135.

41. De Boer, S.; Wiersma, D. A. Chem. Phys. Lett. 1990, 165, 45.

42. De Boer, S.; Vink, K. J., Wiersma, D. A. Chem. Phys. Lett. 1987, 137, 99.

43. Muenter, A. A.; Brumbaugh, D. V.; Apolito, J.; Horn, L. A.; Spano, F. C.; Mukamel, S. J. Phys. Chem. 1992, 96, 2783.

44. Dorn, H-. P.; Muller, A. Appl. Phys. B. 1987, 43, 167.

45. Horng, M-L.; Quitevis, E. J. Phys. Chem. 1993, 97, 12408.

46. O'Brien, D. F. ; Kelly, T. M.; Costa, L. F. Photo. Sci. Eng. 1974, 18, 76.

47. Lindbrum, M; Glismann, A.; Moll, J.; Daehne, S. Chem. Phys. 1993, 178, 423.

48. Johnson, A. E.; Kumazaki, S.; Yoshihara, K. Chem. Phys. Lett. 1993, 211, 511.

49. Kamalov, V. F.; Struganova, I. A.; Tani, T., Y.; Yoshihara, K. Chem. Phys. Lett. 1994, 220, 257.

50. Kamalov, V. F.; Struganova, I. A.; Koyama, Y.; Yoshihara, K. Chem. Phys. Lett. 1994, 226, 132.

51. Gagel, R.; Gadonas, R.; Laubereau, A. Chem Phys. Lett. 1994, 217, 228.

52. Minoshima, K.; Taiji, M.; Misawa, K.; Kobayashi, T. Chem. Phys. Lett. 1994, 218, 67.

CHAPTER 2

EXCITED-STATE DYNAMICS AND PHOTOPHYSICS OF MONOMERIC CYANINES

In this chapter I will discuss excited-state dynamics and photophysical properties of monomeric cyanine dyes: 1,1'-diethyl-2,2'-cyanine iodide or pseudoiso-cyanine (PIC); 1,1',3,3'-tetrachloro-5,5',6,6'-tetraethyl-benzimidazolocarbocyanine iodide (BIC); 3,3'-diethyl-9-phenyl-5,5'-dichloro-thiacarbocyanine chloride (DCTC); and 3,3'-dimethyl-9-phenyl-5,5'-dibenzo-thiacarbocyanine chloride (DBTC) in homogeneous solutions. The chemical structures of BIC, DCTC and DBTC and PIC are shown in Figure 2.1.

2.1 Photophysical Parameters

Absorption is a process in which the molecule is excited from a lower to a higher electronic state by the absorption of a photon (1). The excited electronic state has a rearranged electron distribution, and can described as a promotion of one of the ground state electrons to a higher energy-orbital. This completes the absorption process which usually occurs extremely rapidly, within femtosecond (10^{-15} second). The intensity of interaction known as the oscillator strength, *f*, related to the intensity of the absorption is defined as

$$f = \frac{2303mc^2}{\pi Ne^2 n} \int_{\substack{electronic \\ absorption \\ band}} \varepsilon(\bar{\nu})d\bar{\nu} \qquad (2.1)$$

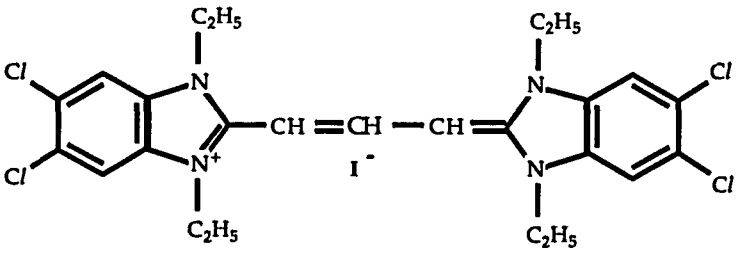

1,1',3,3'-tetrachloro-5,5',6,6'-tetraethyl-benzimidacarbocyanine iodide (BIC)

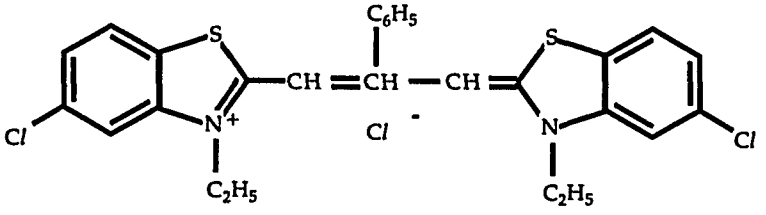

3,3'-diethyl-9-phenyl-5,5'-dichloro-thiacarbocyanine chloride (DCTC)

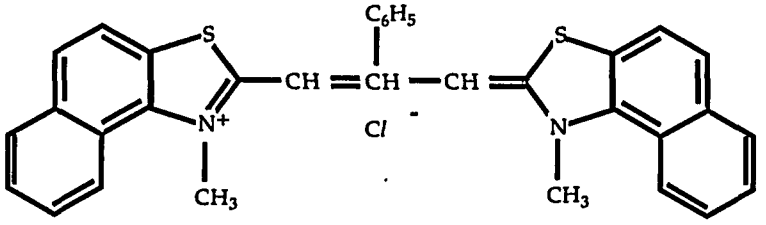

3,3'-dimethyl-9-phenyl-5,5'-dibenzo-thiacarbocyanine chloride (DBTC)

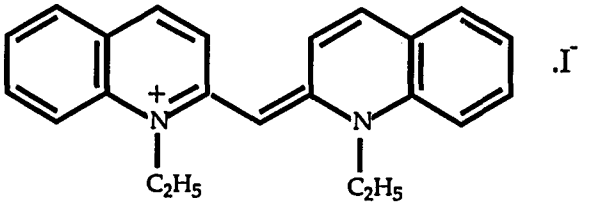

1,1'-diethyl-2,2'-Cyanine iodide

Figure 2.1. The chemical structures of cyanines.

where $\bar{\nu}$ is in cm^{-1}, n is refractive index, c is speed of light in cm s^{-1}, m and e mass and charge of electron in gram and esu, $\varepsilon(\bar{\nu})$ is extinction coefficient in M^{-1} cm^{-1}, and N is Avogadro's number.

The absorbance of a solution is defined as

$$A = \log \frac{I_0}{I_t} = \varepsilon(\bar{\nu})[M]l \qquad (2.2)$$

where I_0 and I_t are incident and transmitted intensity of light, respectively, [M] is molar concentration (moles liter^{-1}) of absorbing species, l is the optical path length (cm). The molecular absorption cross section σ (cm^2) and the absorption coefficient μ (cm^{-1}) are defined as

$$\sigma = \frac{2303\varepsilon(\bar{\nu})}{N} = 3.81x10^{-19}\varepsilon(\bar{\nu}) \qquad (2.3)$$

$$\mu = \sigma n' \qquad (2.4)$$

where $n' = 10^{-3}N[M]$ is number of molecules of the absorbing species per cm^3.

Absorption spectra are generally plotted in terms of $\varepsilon(\bar{\nu})$ or A versus wavenumber $\bar{\nu}$, or wavelength λ(nm).

Radiative deexcitation are transitions in which the molecule is deexcited from a higher to a lower electronic state by the emission of a photon. A radiative transition between states of the same multiplicity is described as **fluorescence**. A radiative transition between states of the different multiplicity is described as **phosphorescence**.

The basic fluorescence parameters of fluorescence lifetime (τ_f) and fluorescence quantum yield (ϕ_f) are related to the radiative rate constant (k_r) (if only fluorescence is radiation) and nonradiative rate constant (k_{nr}) by the photophysical equations:

$$k_r = \frac{\phi_f}{\tau_f} \tag{2.5}$$

$$k_{nr} = \frac{1-\phi_f}{\tau_f}. \tag{2.6}$$

The fluorescence quantum yield (ϕ_f) is also defined as the ratio of fluorescence lifetime (τ_f) to the radiative lifetime τ_0.

$$\phi_f = \frac{\tau_f}{\tau_o} \tag{2.7}$$

The fluorescence quantum yield is measured by comparison with a reference and calculated

$$\phi_f^{sample} = \phi_f^{reference} \cdot \left(\frac{\int_{sample} F(\overline{\nu})d\overline{\nu}}{\int_{reference} F(\overline{\nu})d\overline{\nu}} \right) \cdot \left(\frac{1-10^{-\varepsilon c l_{reference}}}{1-10^{-\varepsilon c l_{sample}}} \right) \cdot \left(\frac{n^2_{sample}}{n^2_{reference}} \right), \tag{2.8}$$

where $\int_{sample} F(\overline{\nu})d\overline{\nu}$ represents the number of emitted photon, $1-10^{-\varepsilon c l_{sample}}$ is number of absorbed photon at the excitation wavelength. n_{sample} and $n_{reference}$ are the refraction index of solvent that contains sample and that of reference, respectively. In this study, I used Rhodamine 6G in EtOH to compare the spectrally corrected, integrated emission intensity of the sample to that of a fluorescence standard, by using equ. 2.8.

It is necessary to mention the **Einstein coefficients** that define absorption and emission processes in terms of probability (1). The Einstein B coefficient determines the probability of absorption, and molecular absorption cross section σ and thus the extinction coefficient $\varepsilon(\overline{\nu})$.

$$B_{lu} = \frac{2303c}{Nhn} \int \frac{\varepsilon(\bar{\nu})d\bar{\nu}}{\bar{\nu}} \qquad (2.9)$$

The integral is over the electronic absorption spectrum.

The Einstein A coefficient determines the probability of spontaneous emission, i.e. luminescence, and its relation to the fluorescence spectrum and lifetime.

$$A_{u0\to l} = k_0 = \frac{1}{\tau_0} = \frac{8\pi.2303n^2}{c^2N} \frac{\int F(\bar{\nu})d\bar{\nu}}{\int \frac{F(\bar{\nu})d\bar{\nu}}{\bar{\nu}^3}} \int \varepsilon(\bar{\nu})d\bar{\nu} \qquad (2.10)$$

where $F(\nu)$ is fluorescence intensity, k_0 is the radiative rate constant, and τ_0 is the radiative lifetime. The integral is over the fluorescence spectrum.

If there is mirror symmetry between the fluorescence and absorption spectra, then equ. 2.10 becomes

$$\frac{1}{\tau_0} = 2.88x10^{-9} n^2 \int \frac{(2\bar{\nu}_0 - \bar{\nu})^3}{\bar{\nu}} \varepsilon(\bar{\nu})d\bar{\nu} \qquad (2.11)$$

where $\bar{\nu}_0$ is the wavenumber of the mirror symmetry point. This equation is known as **the Strickler-Berg** expression (2). For resonance fluorescence transitions where the absorption and fluorescence occur at the same wavenumber $\bar{\nu}_{ul}$, equ. 2.11 simplifies to

$$\frac{1}{\tau_0} = 2.88x10^{-9} \bar{\nu}_{ul}^2 n^2 \int \varepsilon(\bar{\nu})d\bar{\nu} \, . \qquad (2.12)$$

2.2 Photophysical Properties of 1,1'-Diethyl-2,2'-Cyanine Iodide

Figure 2.2 shows absorption spectrum of 1,1'-diethyl-2,2'-cyanine in water. The absorption spectrum consists of a vibronic progression with the band at ca. 524 nm (19083 cm^{-1}) corresponding to the 0←0 band (bandwidth 1100 cm^{-1}), the band at ca. 490 nm (20408 cm^{-1}) corresponding to the 1←0 band (bandwidth 1550 cm^{-1}), and the shoulder at ca. 454 nm (22026 cm^{-1}) corresponding to the 2←0 band (estimated bandwidth of 1800 cm^{-1}). The peak-to-peak distance of the bands is 1325 cm^{-1}, indicating a familiar vibration of skelatal mode which is observed in the Raman spectrum (3). The extinction coefficient is measured to be 7.1×10^4 M^{-1} cm^{-1}. The oscillator strength is calculated to be 0.35.

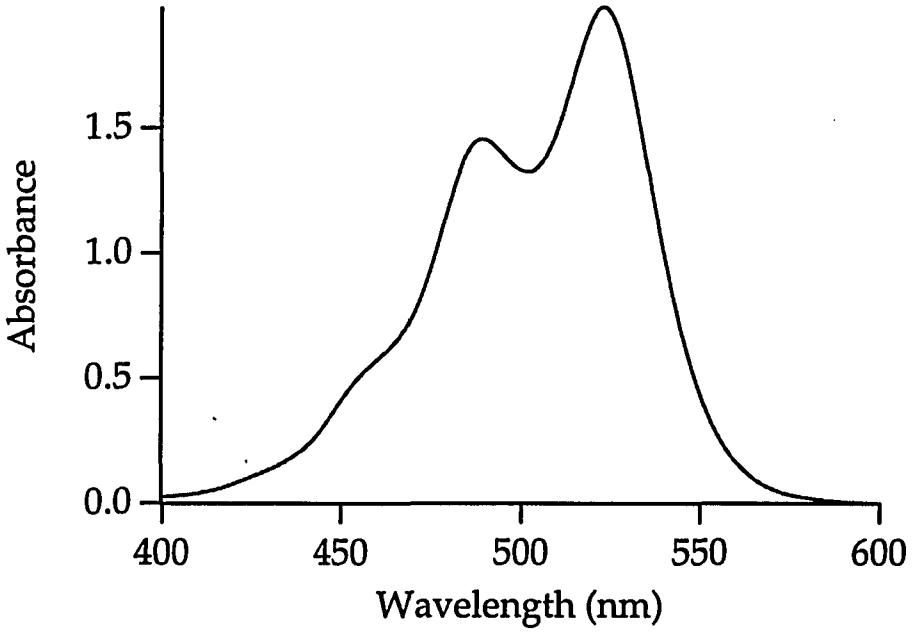

Figure 2.2 The absorption spectrum of 1×10^{-5} M 2,2'-cyanine iodide in water and/or methanol.

2,2'-cyanine iodide in water and alcoholic solvents is practically non-fluorescent at room temperature. However, the fluorescence spectrum of 2,2'-cyanine chloride in glycerol in the temperature range 84-

298 K was measured, and fluorescence maximum was found at ca. 570 nm (17543 cm^{-1}) (4). It was also reported that the fluorescence spectrum did not exhibit vibronic structure compared to the absorption spectrum. A phosphorescence spectrum was also obtained at 77K and a phosphorescence maximum was found at ca. 650 nm (15385 cm^{-1}).

Fluorescence lifetime of 2,2'-cyanine chloride in glycerol in the temperature range 84-298 K was measured by the same authors (4). It was found that fluorescence lifetime was temperature dependent and varied between 1734 to 94 ps for 84 to 298 K. The radiative lifetime was calculated at 3.7 ns by using the Strickler-Berg formula (1). The fluorescence quantum yield was calculated to be 2.6% at 298 K and 47.5% at 84 K. These parameters are important to have better understanding for the aggregate's photophysics. The Arrhenius plot of fluorescence intensities yielded a double activation curves, interpreted as indicating two different internal conversions via vibrational modes: possibly a C-H streching and torsional vibration of the quinoline ring system (4).

2.3 Photophysical Properties of 1,1',3,3'-tetrachloro-5,5',6,6'-tetraethyl-benzimidacarbocyanine iodide (BIC)

Part A of Figure 2.3 shows the absorption spectrum of BIC in methanol which consists of a band at ca. 514 nm (19455 cm^{-1}) with a shoulder at ca. 480 nm (20833 cm^{-1}); assigned, respectively, to the 0 - 0

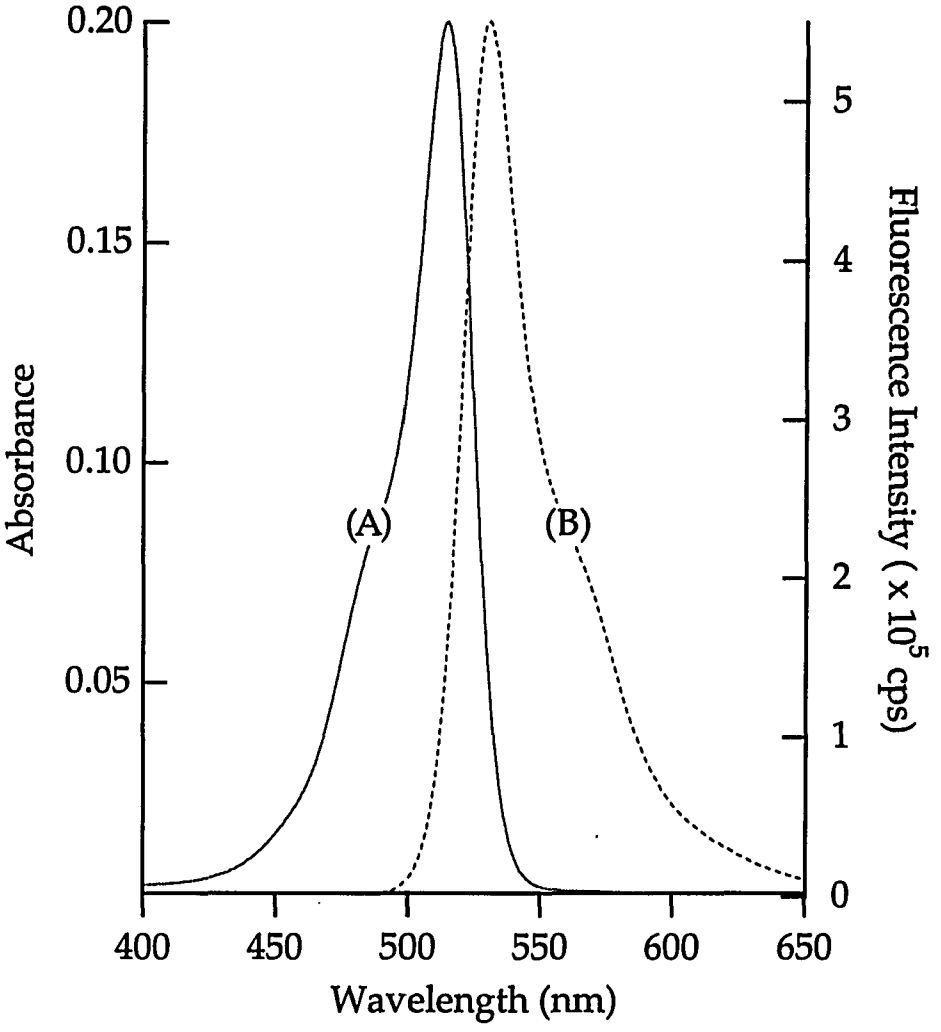

Figure 2.3. The absorption (A) and fluorescence (B) spectra of 1 x 10^{-6} M BIC in methanol. Excitation wavelength for fluorescence is 480 nm.

(bandwidth ca. 1000 cm^{-1}) and 1 - 0 (bandwidth ca. 1600 cm^{-1}) vibronic transitions. The peak-to-peak distance is 1378 cm^{-1}, indicating a skelatal mode vibration, and actually observed in the infrared (5). The extinction coefficient of BIC is calculated to be 1.85 x 10^5 M^{-1} cm^{-1}, which agrees with that reported in the literature (6). The large value of the extinction

coefficient indicates an extensive conjugation of π-electrons along the polymethine bridge, suggesting planarity; however, x-ray crystal structure analysis of BIC solvated with methanol indicates that the structure is only approximately planar despite extensive conjugation of π-electrons, and the polymethine bridge is twisted about 4° to minimize strain (7).

Part B of Figure. 2.3 provides the fluorescence spectrum of BIC in methanol, from 480 nm to ca. 650 nm, excited with 480 nm radiation. The fluorescence maximum is at ca. 530 nm (18868 cm^{-1}), and a shoulder at ca. 560 nm (17857 cm^{-1}) is also present. The peak-to-peak distance is 1010 cm^{-1}. We found that the fluorescence maximum did not shift as a function of excitation wavelength, and conclude that fluorescence originates from the lower levels of the LUMO excited state.

Part A of Figure 2.4 shows the fluorescence excitation spectrum of BIC from 400 nm to 540 nm, detected at 550 nm, the low-energy side of the fluorescence spectrum (see part B of Fig. 2.2). The spectrum consists of a band at ca. 515 nm and a shoulder at ca. 485 nm. We again assign these bands as the 0 - 0 and 1 - 0 vibronic transitions, respectively.

Part B of Figure 2.4 shows the synchronized luminescence spectrum of BIC in the range of 450 to 600 nm with 10 nm offset between excitation and emission monochromators. One peak at ca. 520 nm is found. This single peak is interpreted as indicating that only one emissive state is formed through absorption. This emissive state, as suggested by the overlap of the synchronized luminescence peak and the fluorescence excitation spectrum is the first excited singlet state.

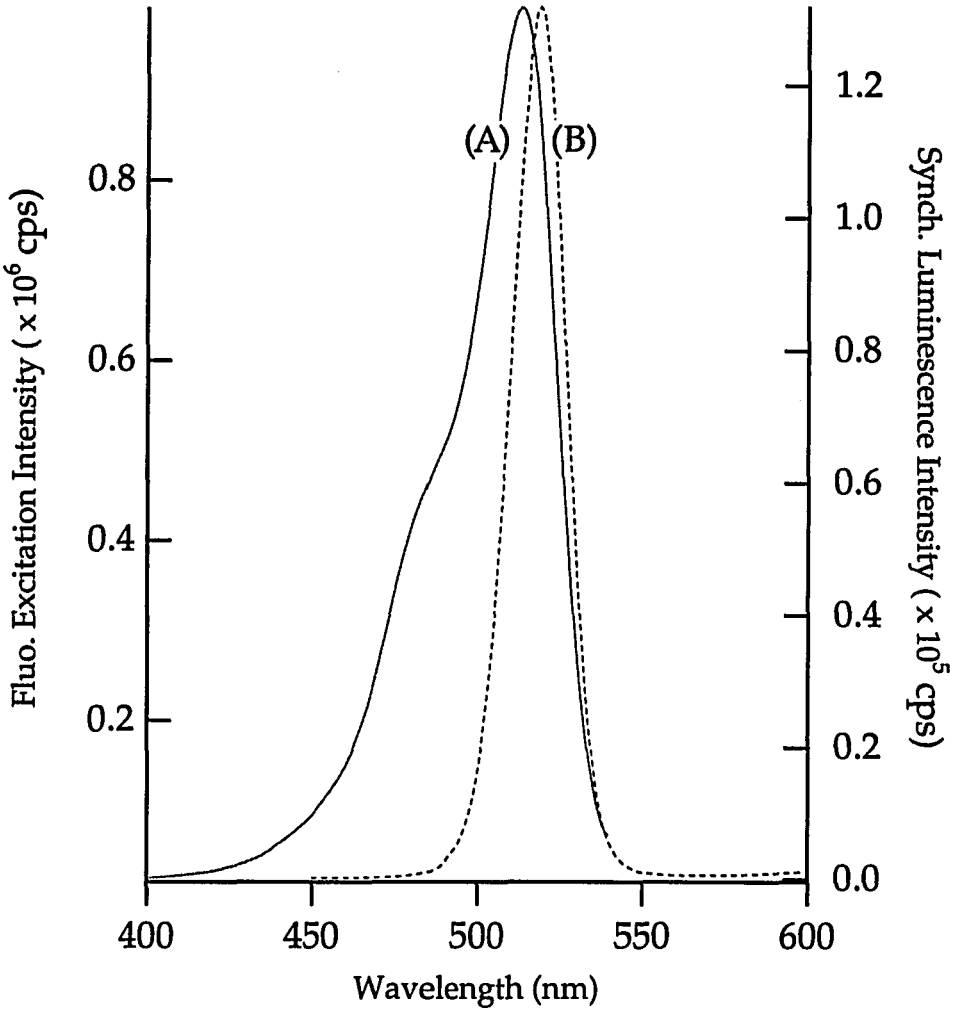

Figure 2.4. The fluorescence excitation (A) and synchronized luminescence (B) spectra of 1 x 10^{-6} M BIC in methanol.

Fluorescence lifetimes were measured with the phase-modulation method. For this method (9), the sample is excited with sinusoidally modulated radiation. Since there is a time lag between absorption and emission, emission is delayed in phase and demodulated relative to the incident light. The phase delay (ϕ) and demodulation factor (m) can be

experimentally measured. The phase and modulation apparent lifetimes, τ_p and τ_m, respectively, are defined as

$$\tau_p = \omega^{-1} \tan\phi \qquad (2.13)$$

$$\tau_m = \omega^{-1} \left(\frac{1}{m^2 - 1} \right)^{1/2} \qquad (2.14)$$

where ω is the modulation frequency.

Analysis and nonlinear least-squares fitting (Marquardt-Levenson minimization algorithm) were performed with software provided by Globals Unlimited (Urbana, IL). Phase-shift and demodulation measurements were obtained for modulation frequencies ranging from 10 to 250 MHz.

Frequency domain fluorescence intensity decay of the BIC monomer in methanol (1×10^{-6} M) at room temperature is shown in Figure 2.5. The excitation wavelength was 500 nm, and the phase shifts and modulations for the fluorescence intensities were measured by setting the emission monochromator at 530 nm with a 15 nm bandpass (5 mm slit width). The phase shifts and modulation measurements fit a single exponential decay-model with a $\chi^2 = 0.72$. The fluorescence lifetime of the BIC monomer in methanol at room temperature was found to be 47± 5 ps.

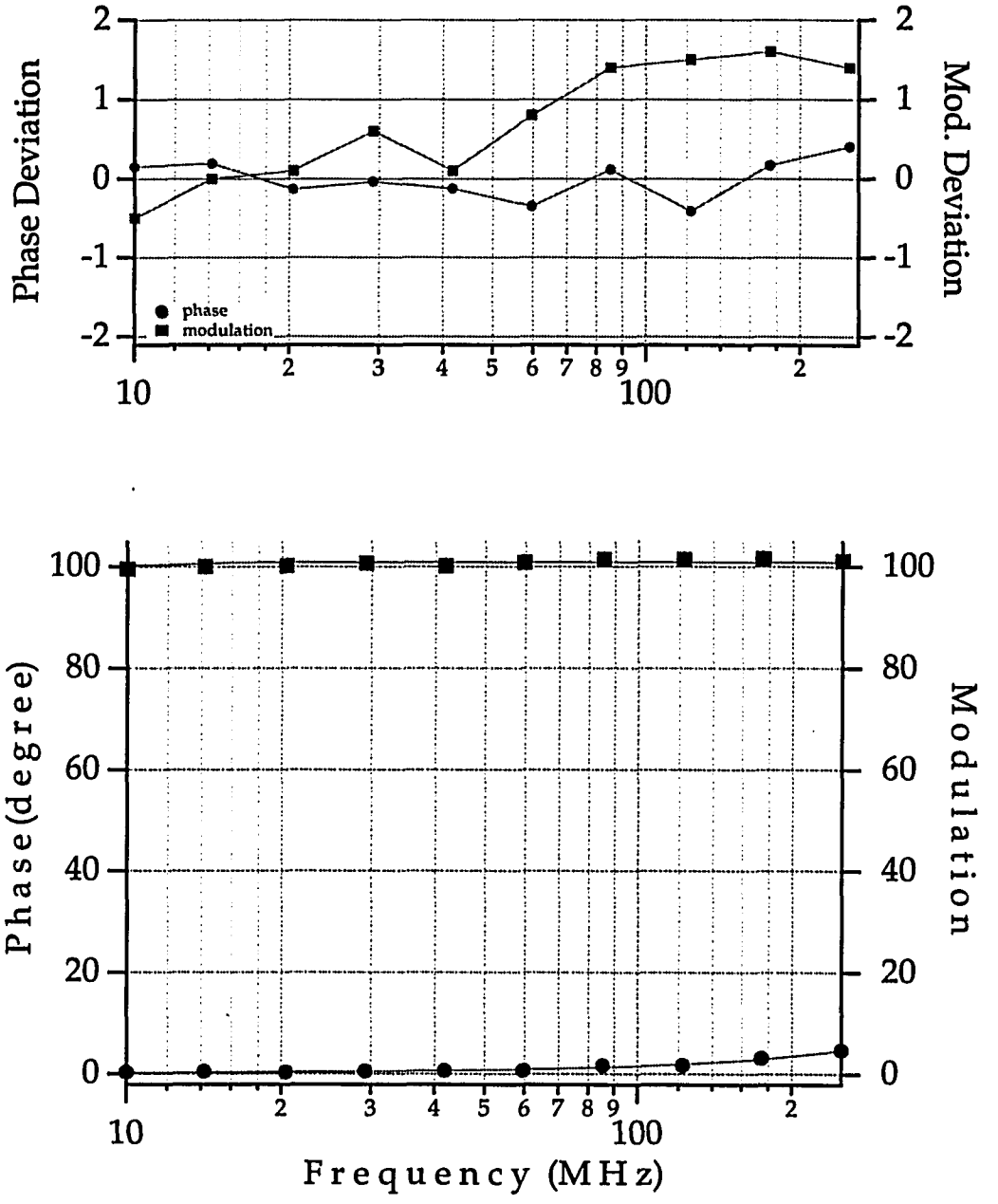

Figure 2.5. Frequency domain fluorescence intensity decay of 1 x 10^{-6} M BIC monomer in methanol at room temperature.

The fluorescence quantum yield was also measured by using equ. 2.8. In order to eliminate reabsorption effects very dilute solutions, about μM, were used for the measurements. The fluorescence standard,

Rhodamine 6G in ethanol, has known quantum yield of 0.90 (9). The fluorescence quantum yield of BIC in MeOH, excited at 480 nm, was determined to be 0.021 ± 0.002 by using equ. 3.

Phosphorescence lifetime of BIC in ethylene glycol/water glass at 77K were measured with the SPEX fluorolog-2 with a phosphorescence attachment. For excitation an xenon flashlamp with 3 μs pulse width was used. The sample was slowly immersed into a glass dewar. The phosphorescence spectrum maximum of BIC at 77 K was at 562 nm. The phosphorescence lifetime was also measured: a single exponential with 12 μs decay time. From these data, the intersystem crossing quantum yield may be estimated to be very low, i.e. < 0.001.

Upon substituting the measured values of fluorescence lifetime and quantum yield, one finds that $k_r = (0.53 \pm 0.06) \times 10^9\ s^{-1}$ and $k_{nr} = (24.5 \pm 0.06) \times 10^9\ s^{-1}$. This calculation indicates that, for BIC monomer in methanol, nonradiative relaxation is about 50 times faster than radiative relaxation.

The nonradiative rate can be represented as a sum of rates associated with different paths that serve to depopulate the excited-state,

$$k_{nr} = k_{ic} + k_{isc} + k_p + k_s$$

where k_{ic}, k_{isc}, k_p and k_s are the rate constants associated with internal conversion, intersystem crossing, photoisomerization, and solvent effects, respectively. The effects of various solvents on flourescence lifetime and rate constants can be seen in Table 2.1. In going from methanol to glycerol the fluorescence lifetime increases due to the higher viscosity of the solvent, suggesting solvent-dye interaction and solvent cage relaxation

Table 2.1. The photophysical properties of BIC in various solvents at room temperature.

	Solvents				
Parameters	MeOH	EtOH	DMSO	Ethylene Glycol	Glycerol
$\lambda_{abs,max}$ (nm)	515	517	524	519	520
$\Delta\nu_{abs}$ (cm^{-1}) [a]	798	781	753	770	480
$\lambda_{fluo,max}$ (nm)	527	529	536	531	533
$\Delta\nu_{fluo}$ (cm^{-1}) [b]	792	790	816	790	468
$\Delta\nu_{Stokes}$ (cm^{-1})	443	417	440	425	470
Φ_{fluo}	0.021 ± 0.002	0.029 ± 0.002	0.055 ± 0.002	0.075 ± 0.002	0.360 ± 0.002
τ_{fluo} (ps)	47 ± 5[c]	69 ± 5[d]	153 ± 10[e]	220 ± 15[f]	996 ± 15[g]
$k_r \times 10^9$ (s^{-1})	0.53 ± 0.06	0.41 ± 0.04	0.43 ± 0.03	0.35 ± 0.03	0.36 ± 0.01
$k_{nr} \times 10^9$ (s^{-1})	24.5 ± 0.06	13.9 ± 0.04	6.23 ± 0.03	4.20 ± 0.03	0.64 ± 0.01
Viscosity (cP)	0.55	1.08	1.99	26.1	1006
Dielectric Const.	32.7	24.6	46.7	37.7	42.5

Extinction coefficient = 2×10^5 M^{-1} cm^{-1} in MeOH.

(a) The bandwidth of the 0-0 transition is obtained by decomposed absorption spectra. **(b)** The bandwidth of the 0-0 transition is obtained by decomposed fluorescence spectra. **(c)** A single exponential decay with $\chi^2 = 0.72$. Excitation and emission wavelengths were 514 and 530 nm, respectively. **(d)** A single exponential decay with $\chi^2 = 1.20$. Excitation and emission wavelengths were 500 and 530 nm, respectively. **(e)** A single exponential decay with $\chi^2 = 1.19$. Excitation and emission wavelengths were 500 and 536 nm, respectively. **(f)** A single exponential decay with $\chi^2 = 1.12$. Excitation and emission wavelengths were 500 and 530 nm, respectively. **(g)** A double exponential decay: the shortest lifetime 211 ps with 4% of the emission and 0.99 ns with 96% of the emission; $\chi^2 = 0.80$. Excitation and emission wavelengths were 500 and 535 nm, respectively.

play an important role. However, there is no clear indication on dielectric constant dependence of fluorescence lifetime.

On the basis, in general, of extremely low intersystem crossing quantum yields (10,11) (production of triplet-states) and very short fluorescence lifetimes of cyanine dyes in low viscosity solvents (12,13), internal conversion to the ground-state has been proposed as the major deactivation pathway of the excited singlet state of cyanines. These studies indicate that the main factors controlling the rate of internal conversion are steric hindrance, molecular rigidity, and solvent viscosity (or some closely related solvent property). The results show that when relatively high viscosity solvents are used, such as ethylene glycol and glycerol, the fluorescence quantum yield and fluorescence lifetime increase due to restricted motion of BIC in the excited-state.

The strong dependence of the rate constant for internal conversion upon molecular rigidity (as, for example, affected by cross-linking between the heterocyclic rings) and solvent viscosity (11) suggests that twisting of the heterocyclic rings around the polymethine bridge takes place in the excited singlet state, and excitation into the first excited singlet state reduces the double-bond character of the polymethine bridge, thus allowing twisting. In the case of BIC, in higher viscosity the fluorescence lifetime and quantum yield of BIC increases as a result of restricted twisting. Therefore, we infer that, when BIC is photoexcited, benzimidazolyl rings twist around the polymethine bridge and adopt a different conformation in which the dihedral angle between the heterocyclic rings is increased, promoting interval conversion. The very short fluorescence lifetime of BIC in methanol indicates that the steric hindrance between the N-ethyl groups

and hydrogen atoms on the polymethine bridge are minimized in the new conformation.

We might note apparent differences in the results for BIC fluorescence lifetime and fluorescence quantum yield measurements performed by O'Brien et al. (11) and ourselves. In the former study, BIC chloride in methanol was used and a fluorescence lifetime of 550 ps and fluorescence quantum yield of 0.1 were obtained, while, in our study, BIC iodide in methanol was used and fluorescence lifetime of 47 ps and fluorescence quantum yield of 0.02 were measured. We acquired high-performance liquid chromatography (HPLC) of the BIC iodide and found the sample to be 99.99% pure. A very recent study on benzimidazolo-carbocyanine has proven that the interaction between the dye cation and iodide counterion forms an ion-pair and leads to enhancement of the internal conversion rate (14). We are left to attribute the difference between our finding and that of O'Brien et al. as due to heavy atom quenching by the iodide counterion.

2.3 Photophysical Properties of 3,3'-diethyl-9-phenyl-5,5'-dichloro-thiacarbocyanine chloride (DCTC)

The absorption and fluorescence spectra of DCTC in methanol are shown in Figure 2.6. They are typical for cyanine dyes. The Absorption spectrum consists of a band at ca. 566 nm (17668 cm^{-1}) and a shoulder at ca. 535 nm (18692 cm^{-1}). The extinction coefficient of DCTC in methanol is 2.5 x 10^5 $M^{-1}cm^{-1}$. The fluorescence band is at ca. 582 nm (17182 cm^{-1}) and relatively broader than the absorption spectrum. Fluoresecnce quantum

yield in methanol at 25°C is measured as 0.015 when excited at 520 nm. The meso-substituent effect on the fluorescence quantum yield is very clear: a few-fold decrease when compared to the unsubstituted analog: 3,3'-diethylthiacarbocyanine

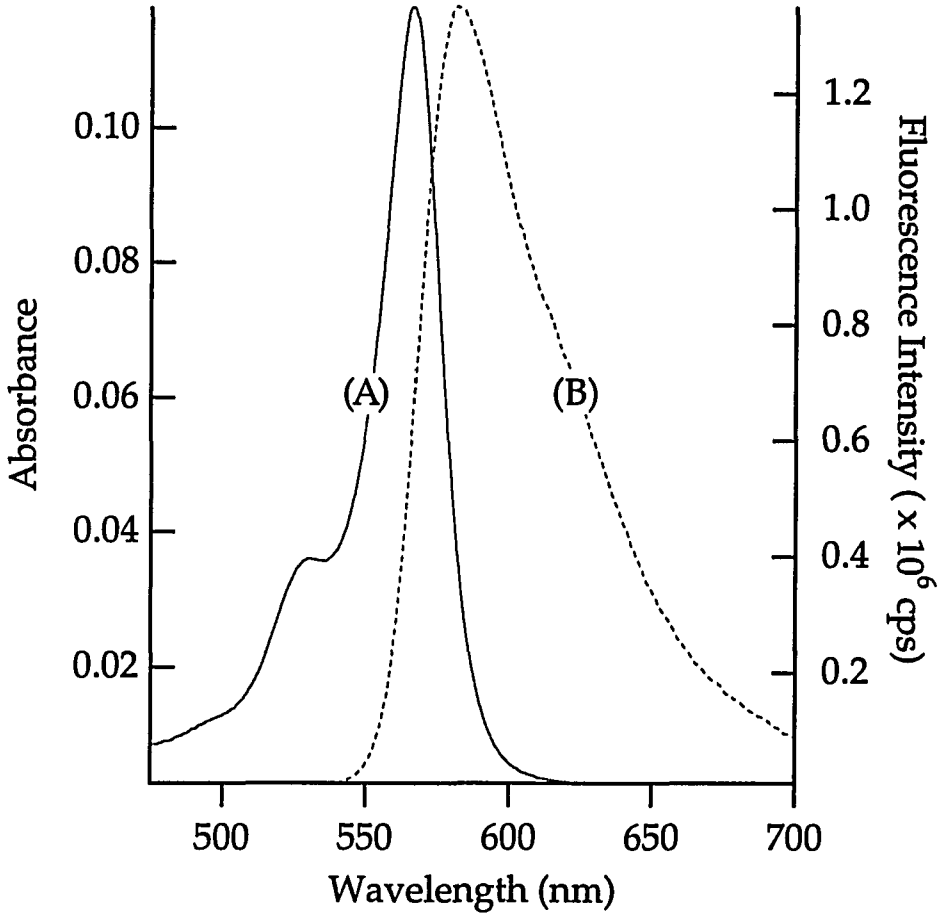

Figure 2.6. The absorption (A) and fluorescence (B) spectra of DCTC in methanol. Excitation wavelength for fluorescence is 520 nm.

chloride in ethanol at 25°C which has a fluorescence quantum yield of 0.07 (15,16). Krieg et al. (15) studied photophysical properties of 3,3'-dialkylthiacarbocyanine dyes in homogeneous solution. They found that photoisomerization and fluorescence were major deactivation channels of

the first excited singlet state, and intersystem crossing efficiency was very low. They also studied the effects of structural changes on photophysical parameters of dialkyl-thiacarbocyanine dyes in homogeneous solution and liposomes (17). They found a significant reduction in photoisomerization when a meso-substitution is introduced. However, internal conversion became the main deactivation pathway of the first excited singlet state.

Frequency domain fluorescence intensity decay of the DCTC in methanol (1×10^{-6} M) at room temperature is shown in Figure 2.7. The excitation wavelength was 550 nm, and the phase shifts and modulations for the fluorescence intensities were measured by setting the emission monochromator at 582 nm with a 30 nm bandpass (8 mm slit width). The phase shifts and modulation measurements fit a single exponential decay-model with a $\chi^2 = 1.6$. The fluorescence lifetime of the DCTC in methanol at room temperature was found to be 75 ± 5 ps.

The effects of viscous solvents on flourescence lifetime and rate constants can be seen in Table 2.2. In going from methanol to glycerol longer fluorescence lifetime are measured due to the higher viscosity of solvent, suggesting solvent-dye interaction restrict rotation of the end groups.

Phosphorescence lifetime of DCTC in ethylene glycol/water glass at 77K were measured. The phosphorescence spectrum maximum of DCTC at 77 K was at 610 nm. The phosphorescence lifetime was also measured: a single exponential with 15 μs decay time. From these data, the intersystem crossing quantum yield might be estimated to be very low, i.e. < 0.001.

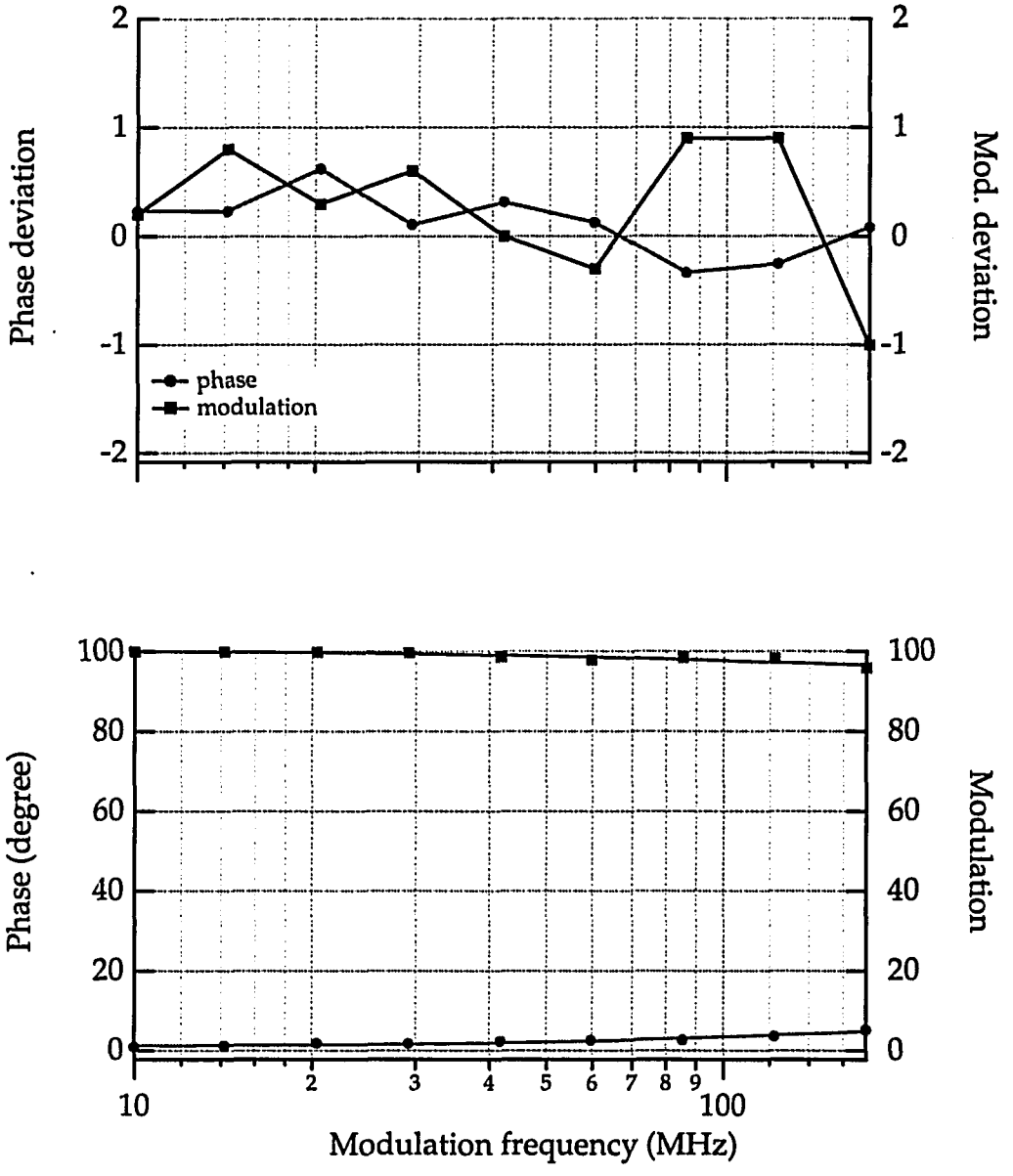

Figure 2.7. Frequency domain fluorescence intensity decay of 1×10^{-6} M DCTC monomer in methanol at room temperature.

Table 2.2. The photophysical properties of DCTC in various solvents at room temperature.

	Solvents		
Parameters	MeOH	Ethylene Glycol	Glycerol
$\lambda_{abs,\ max}$ (nm)	566	571	572
$\Delta\nu_{abs}$ (cm^{-1}) [a]	650	610	600
$\lambda_{fluo,\ max}$ (nm)	582	585	584
$\Delta\nu_{fluo}$(cm^{-1}) [b]	720	475	426
$\Delta\nu_{Stokes}$(cm^{-1})	485	419	359
Φ_{fluo}	0.015 ± 0.002	0.066 ± 0.002	0.105 ± 0.002
τ_{fluo} (ps)	74 ± 5 [c]	550 ± 15 [d]	2040 ± 15 [e]
$k_r \times 10^8$ (s^{-1})	2.0 ± 0.4	1.20 ± 0.06	0.53 ± 0.02
$k_{nr} \times 10^9$ (s^{-1})	1.31 ± 0.04	1.698 ± 0.006	0.446 ± 0.002

(a) The bandwidth of the 0-0 transition is obtained by decomposed absorption spectra. **(b)** The bandwidth of the 0-0 transition is obtained by decomposed fluorescence spectra. **(c)** A double exponential decay: the shortest lifetime 74 ps with 97% of the emission and 3.55 ns with 3% of the emission; $\chi^2 = 0.80$. Excitation and emission wavelengths were 525 and 590 nm, respectively. **(d)** A single exponential decay with $\chi^2 = 1.17$. Excitation and emission wavelengths were 550 and 585 nm, respectively. **(e)** A double exponential decay: the shortest lifetime: 764 ps with 5% of the emission and 2.04 ns with 95% of the emission; χ^2 =0.74. Excitation and emission wavelengths were 550 and 585 nm, respectively.

Many carbocyanine dyes photoisomerise upon excitation, indicating that the ground-state conformation undergoes significant changes in the excited-state. The low triplet state quantum yields for these dyes suggest

that photoisomerisation takes place via the excited singlet-state (10,19). Carbocyanine dyes are free to rotate and vibrate in low viscous solvents and have a high efficiency of internal conversion from the first excited singlet state. They exist in many planar and nonplanar conformations. The possible configurations are the all-trans, the 8,9-mono-cis, and the 2,8-mono-cis forms shown as in Figure 2.8. In general, it is expected that in the absence of steric effects the all-trans form would be the most stable. West et.al. (18) showed that 9-alkyl-substituted thiacarbocyanines exist in the all-trans and 8,9-mono-cis forms at -196 °C and at room temperature. The 2,8-mono-cis form was prohibited for 9-alkyl cyanines due to steric interactions between the N-alkyl and 9-alkyl substitutents. O'Brien et. al. showed that the 8,9-mono-cis form is non-fluorescent. Since the 2,8-mono-cis form cannot exist due to steric repulsions the DCTC may exist in the all-trans and 8,9-mono-cis forms. The very low value of fluorescence quantum yield for DCTC in methanol may indicate that DCTC exist mainly in the non-fluorescent 8,9-mono-cis form, and thus, in very small extent the fluoresecent all-trans form may exist in the excited-state; or possible, would be reverted to the 8,9-mono-cis form very rapidly, i.e., photoisomerisation.

The solvent viscosity dependence of the non-radiative rate constant indicates that a large angular displacement between the planes of the two end group should take place. Excitation results in a reduction ofthe double bond character of the polymethine chain to allow such an angular displacement between the end groups. In this new conformation, the repulsive steric effects are balanced by the weaken rigidity of the polymethine chain. The loss of resonance stabilization within the

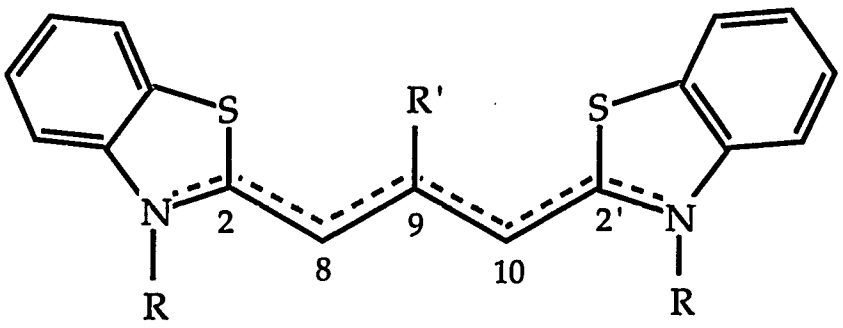

All-trans

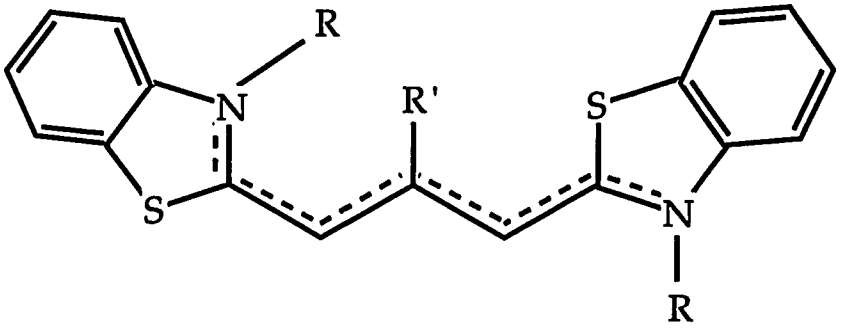

2,8 mono-cis

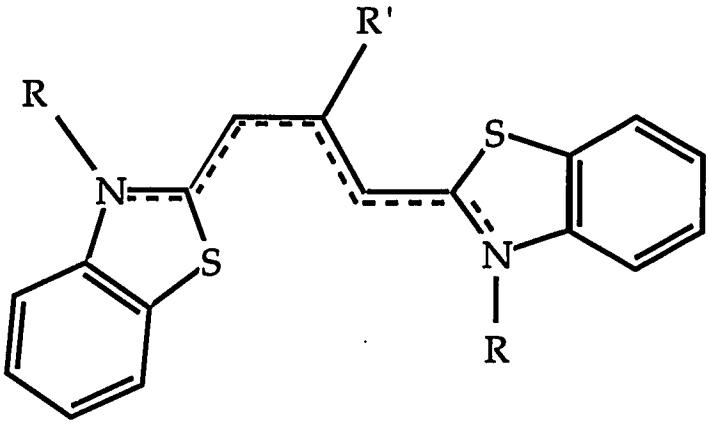

8,9 mono-cis

Figure 2.8. The chemical structures of photoisomers.

polymethine chain increase the ground-state potential energy while in the excited-state the restrictions of the resonance stabilizations are reduced due to the angular displacement between the end groups, the potential energy barrier might be insignificant. Thus photoisomers will rapidly revert to the normal isomer.

The Fermi golden rule relates the internal conversion rate to the elctronic structure of a molecule by the expression (2.13)

$$k_{ic} = h\rho_e\beta_e\sum\langle\phi_v|\phi_i\rangle \qquad (2.13)$$

where ρ_e is the density of states, β_e is the electronic factor for the radiationless transitions and $\sum\langle\phi_v|\phi_i\rangle$ is the Franck-Condon factor, describing the overlap of the continuum of vibrational states ϕ_v and ϕ_i. The Franck-Condon factor determines the rate of internal conversion to the ground-state. Siebrand et. al. (20) showed that the rate of the internal conversions increase rapidly as the molecular conformations approaches a dihedral angle of 90°, the angle between the end groups. The zero-point energy gap is also determined by the dihedral angle. The initial rate of the internal conversion will be set by the ground-state conformation of the dye. However, in low viscosity solvents, the end groups will start to rotate toward to equilibrium conformation within the excited-state lifetime. The very short lifetimes indicate that the excited-state molecule would not attain the equilibrium conformation before returning to the ground-state. The longer lifetimes suggest that the excited-state molecule can reach the equilibrium conformation and forms photoisomer. In higher viscosity solvents, the fluorescence lifetimes and quantum yields increase

dramatically which may be attributed to the stabilization of the excited-state in the ground-state conformation by the solvent restricted rotation of the end groups around the polymethine chain.

The conclusion of this study is that internal conversion and photoisomerization are the main deactivation channels of the first excited state of DCTC at room temperature.

2.4 Photophysical Properties of 3,3'-dimethyl-9-phenyl-5,5'-dibenzo-thiacarbocyanine chloride (DBTC)

The absorption and fluorescence spectra of DBTC in methanol are shown in Figure 2.9. Absorption spectrum consists of a band at ca. 596 nm (16778 cm^{-1}) and a shoulder at ca. 560 nm (17857 cm^{-1}). The extinction coefficient is 2.3 x 10^5 $M^{-1}cm^{-1}$. The fluorescence band is at ca. 620 nm (16129 cm^{-1}) and relatively broader than the absorption spectrum.

Fluorescence quantum yield in methanol at 25°C is measured as 0.006 when excited at 550 nm. Similar to DCTC, introduction phenyl group onto the meso-position decreases the fluorescence quantum yield: an eighteen-fold decrease when compared to the unsubstituted analog: 3,3'-diethyl-thiacarbocyanine chloride in ethanol at 25°C, the fluorescence quantum yield is 0.07 (15,16).

Frequency domain fluorescence intensity decay of the DBTC in methanol (1 x 10^{-6} M) at room temperature is shown in Figure 2.10. The excitation wavelength was 595 nm, and the phase shifts and modulations for the fluorescence intensities were measured by setting the emission

monochromator at 620 nm with a 30 nm bandpass (8 mm slit width). The phase shifts and modulation measurements fit a single exponential decay-model with a $\chi^2 = 0.6$. The fluorescence lifetime of the DBTC in methanol at room temperature was found to be 55 ± 5 ps.

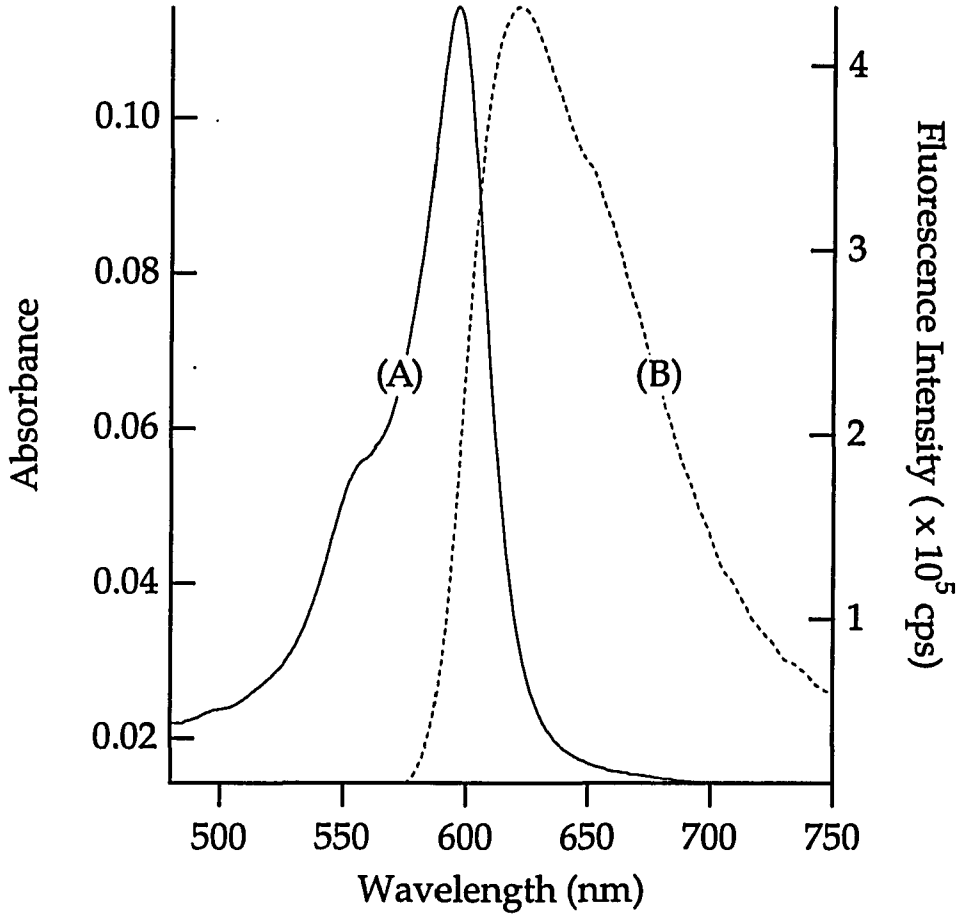

Figure 2.9. The absorption (A) and fluorescence (B) spectra of DBTC in methanol. Excitation wavelength for fluorescence is 550 nm.

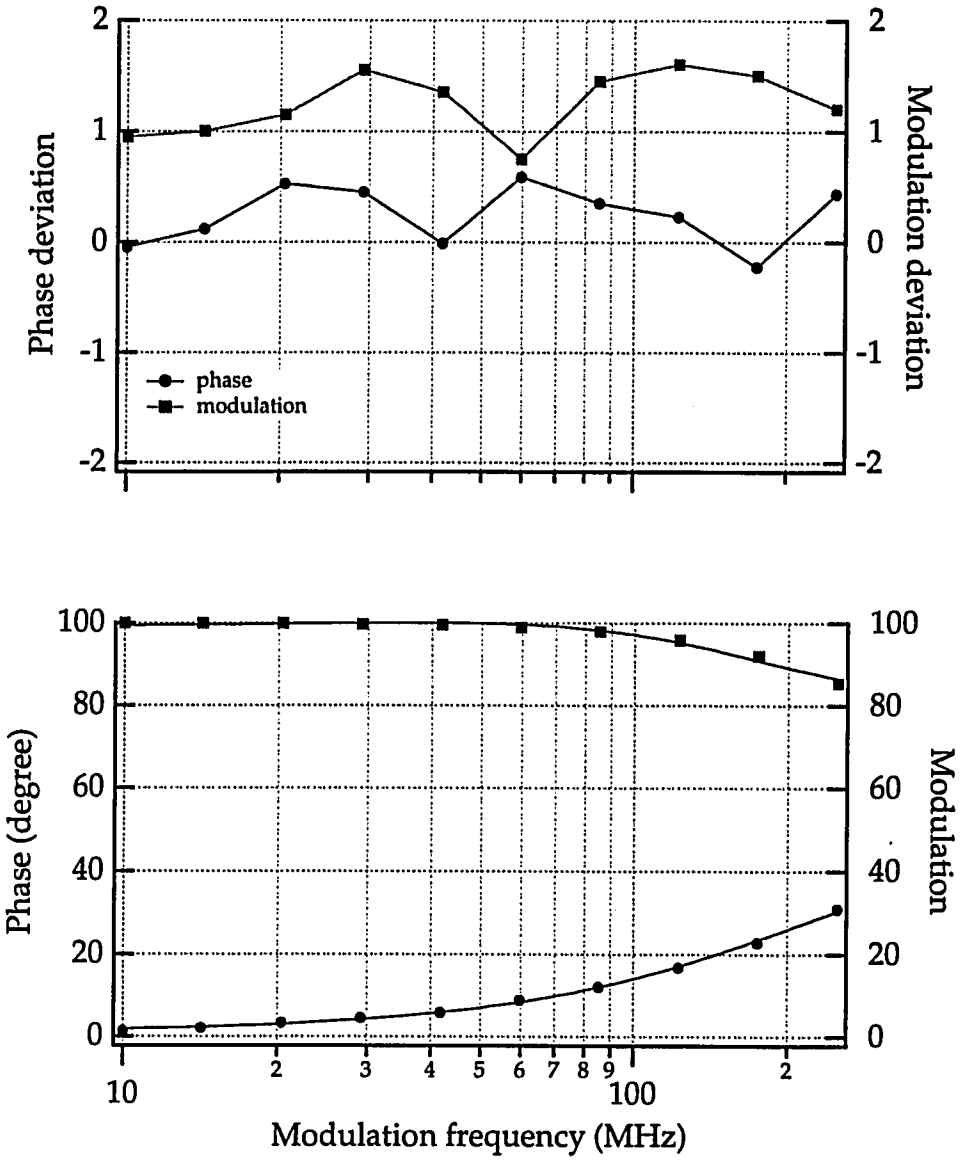

Figure 2.7. Frequency domain fluorescence intensity decay of 1×10^{-6} M DBTC monomer in methanol at room temperature.

The effects of viscous solvents on fluorescence lifetime and rate constants can be seen in Table 2.3.

Table 2.3. The photophysical properties of DBTC in various solvents at room temperature.

	Solvents		
Parameters	MeOH	Ethylene Glycol	Glycerol
$\lambda_{abs,max}$ (nm)	596	571	572
$\Delta\nu_{abs}$ (cm^{-1}) [a]	721	610	600
$\lambda_{fluo,max}$ (nm)	620	585	584
$\Delta\nu_{fluo}$(cm^{-1}) [b]	843	475	426
$\Delta\nu_{Stokes}$(cm^{-1})	647	419	359
Φ_{fluo}	0.006 ± 0.002	0.027 ± 0.002	0.042 ± 0.002
τ_{fluo} (ps)	55 ± 5 [c]	387 ± 15 [d]	1994 ± 15 [e]
$k_r \times 10^8$ (s^{-1})	1.09 ± 0.4	0.70 ± 0.07	0.21 ± 0.01
$k_{nr} \times 10^{10}$ (s^{-1})	1.80 ± 0.7	0.25 ± 0.03	0.048 ± 0.003

(a) The bandwidth of the 0-0 transition is obtained by decomposed absorption spectra. **(b)** The bandwidth of the 0-0 transition is obtained by decomposed fluorescence spectra. **(c)** A single exponential decay with $\chi 2 = 0.90$. Excitation and emission wavelengths were 595 and 620 nm, respectively. **(d)** A single exponential decay with $\chi 2 = 1.05$. Excitation and emission wavelengths were 590 and 623 nm, respectively. **(e)** A double exponential decay: the shortest lifetime 632 ps with 5% of the emission and 1.99 ns with 95% of the emission; $\chi 2 = 1.20$. Excitation and emission wavelengths were 590 and 620 nm, respectively.

A similiar discussions as made for DCTC is valid for DBTC. Additionally the steric interactions between 9-phenly and N-methly groups should be somewhat increased because of the observed red-shift in absorption and lowered fluorescence lifetime and quantum yield. To reduce steric repulsions an increase in the dihedral angle between the end groups is necessary which produces an increase in the ground-state potential energy and decrease in the excited-state potential energy. Thus, photoisomerisation is possible however, the shorter fluorescence lifetime suggests photoisomers will rapidly revert to the non-fluorescent form: the 8,9-mono-cis form.

The results indicate that the main deactivation channels for DBTC are internal conversion and photoisomerization.

REFERENCES

1. Birks, J. B., In "Photophysics of Aromatic Molecules", Wiley-Interscience, New York, 1971.

2. Strickler, S. J.; Berg, R. B., J. Chem. Phys. 1962, 37, 814.

3. Akins, D. L. J. Phys. Chem. 1985, 98, 13476.

4. Dorn, H.-P.; Muller, A; Chem. Phys. Lett 1986, 130, 426.

5. Gray, W. E; Brewer, W.R; Bird, G. R. Photo. Sci. Eng. 1970, 14, 316.

6. Zuckerman, B. Photo. Sci. Eng. 1967, 11, 156.

7. Smith, D. L.; Luss, H. R. Acta Crystallogr., Sec. B 1972, 28, 2793.

8. Lakowicz, J. R. In "Principles of Fluorescence Spectroscopy". Plenum Press: New York, 1983.

9. Schäfer, F.P. In "Dye Lasers." 3rd Edition Springer-Verlag: Heidelberg, 1990.

10. Buettner, A. V. J. Chem. Phys. 1967, 46, 1398.

11. O'Brien, D. F. ; Kelly, T. M.; Costa, L. F. Photo. Sci. Eng. 1974, 18, 76.

12. Tredwell, C. J.; Keary, C. M. Chem. Phys. 1979, 46, 307.

13. Velsko, S. P.; Fleming, G. R. Chem. Phys. 1982, 65, 59.

14. Murphy, S.; Sauerwein, B.; Drickamer, H. G.; Schuster, G. B. J. Phys. Chem. 1994, 98, 13476.

15. Krieg, M.; Redmond, R. W. Photochem. Photobiol. 1993, 57, 472.

16. Kuzmin, V.A; Darmanyan, A. P. Chem Phys. Lett., 1978, 47, 123.

17. Krieg, M.; Bilitz, J. M., Srichai, M. B.; Redmond, R. W. Biochim. Biophys. Acta. 1994, 1199, 149.

18. West, W.; Pearce, S.; Grum, F. J. Phys.Chem. 1967, 71, 1316.

19. Chibisov, A. K. J. Photochem. 1976/77, 6, 199.

20. Siebrand, W; Williams, D. F. J. Chem. Phys. 1968, 49, 1860.

CHAPTER 3

STRUCTURE AND EXCITED-STATE DYNAMICS OF J-AGGREGATED 2,2'-CYANINE ADSORBED ONTO A VESICLE SURFACE

In this chapter, I will discuss the aggregation behavior, structure and excited-state dynamics of 2,2'-cyanine iodide adsorbed onto a phospholipid vesicle surfaces formed in aqueous solutions containing L-α-dimyristoylphosphatidylcholine (DMPC) and dicetyl phosphate (DCP) (see Figure 3.1 for structures). Raman spectroscopy was used to study the structure of J-aggregate. Steady-state and picosecond phase-modulation fluorescence spectroscopy were utilized to study excited-state dynamics. The results of spectrophotometric titration and fluorescence quantum yield measurements are also discussed.

3.1. Introduction

Aggregated molecules play crucial roles in nature and have important technological applications. Aggregates are found in biological systems where they function to convert optical radiation into chemical energy and promote charge transfer reactions (1). Dye aggregates have been used as spectral sensitizers (principally for silver halide

semiconductor materials) (2), as organic photoconductors (3), and, recently, much interest has centered on their nonlinear optical susceptibilities (4,5), since aggregated molecules with enhanced nonlinear responses find utility as materials for use in nonlinear optical devices (6-8).

Aggregation of cyanine dyes was first reported by Jelley (9) and Scheibe (10), in 1936, who found that concentrated aqueous solutions of 1,1'-diethyl-2,2'-cyanine exhibit an absorption which is not present in dilute solution and is red-shifted and narrowed relative to monomer absorption bands, the so-called J-band attributed to aggregated molecules. Many other cyanine dyes exhibit similar spectral properties.

In terms of excited-state dynamics, recently, superradiance was observed for 1,1'-diethyl-2,2'-cyanine (also referred to as pseudoisocyanine, PIC) in ethylene glycol/water glass at low temperature (11,12), and adsorbed onto an AgBr surface at room temperature (13). The occurrence of superradiance for the dye aggregates suggests the concept of an effective coherence size for the emitting species (14-16): molecules which define the coherence size are considered to be strongly coupled and respond in phase to optical radiation. As a result, the radiative decay rate is increased by a factor dependent on the effective coherence size, and, often, enhanced nonlinear optical response is found.

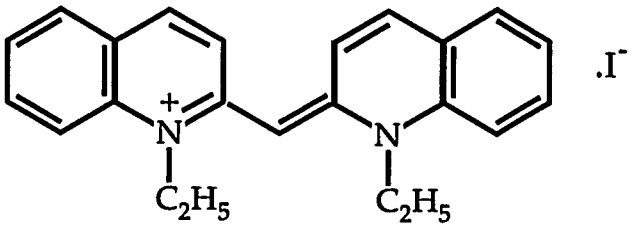

1,1'-diethyl-2,2'-Cyanine iodide

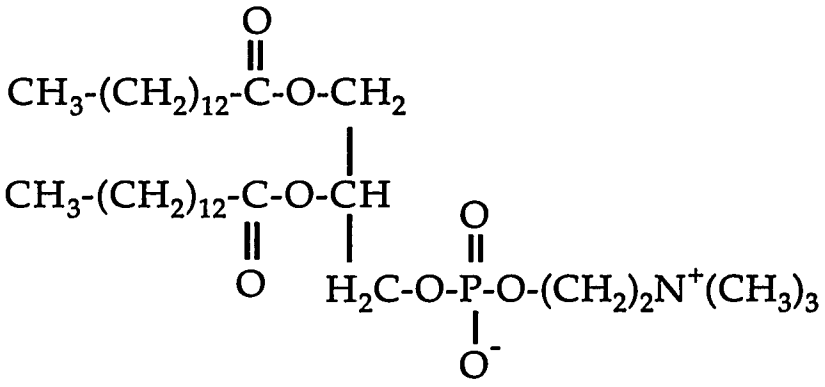

L-α-Dimyrisatoylphosphatidycholine(DMPC)

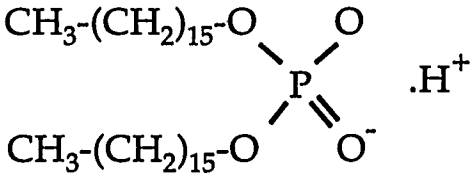

Diacetyl Phosphate (DCP)

Figure 3.1. The chemical structures of 2,2'-cyanine iodide, L-α-dimyristoyl phosphatidylcholine (DMPC) and dicetyl phosphate (DCP).

Raman scattering studies of aggregated 1,1'-diethyl-2,2'-cyanine iodide (hereinafter referred to as 2,2'-cyanine) on silver electrodes (17-24) have been utilized to gain insight into the structures of aggregates on metallic surfaces. More recently, cyanines have also been shown to aggregate on phospholipid vesicle surfaces (25). The structure, alignment, and photodynamics of cyanine dyes on such surfaces can provide reference type information for cyanines adsorbed onto metallic and semiconductor surfaces, and, also, might represent model systems for investigating electron transfer structures for chromophores intercalated into lipids (26).

Using a spectrophotometric titration study to analyze the equilibrium between solution phase monomeric and adsorbed, aggregated 2,2'-cyanine, we determine the absorption extinction coefficient (ε_J) for aggregated dye, specifically, the so-called J-aggregate; average number (N) of dye molecules in the aggregate; and the intrinsic binding constant (K(0)).

We also report measurements of photophysical parameters of J-aggregated 2,2'-cyanine adsorbed onto the vesicle surface. Steady-state and phase-modulation, fluorescence spectroscopies are used for this study, and support the presence of two aggregate conformers, heretofore referred to by us as cis- and trans-aggregates (26), for which the relative orientations of ethyl groups attached to the nitrogen heteronuclei of the monomer, either on the same or opposite side of the molecular plane, defined cis- and trans-, respectively. More recently (27), however, we understand the

cis/trans makeup of aggregates in terms of a somewhat different picture. Our new understanding derives from current photophysical studies in our laboratory for cyanine dyes at "low" concentrations, where dimers and other H-type aggregates are found to occur. We have, in agreement with others, ascertained that, in general, stereoisomers of the monomeric species exist, with the dominant stereoisomer being the so-called all-trans species and the stereoisomer of lower concentration being referred to as the mono-cis isomer (28-36). Henceforth in this chapter, the designations trans- and cis-aggregate will refer to aggregates composed of the trans- and mono-cis- configurational stereoisomers, respectively. Figure 3.2 shows the trans- and mono-cis- configurational stereoisomers.

(a) The mono-cis-isomer

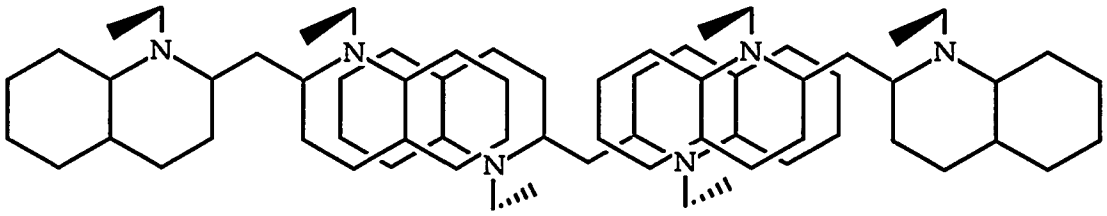

(b) The trans-isomer

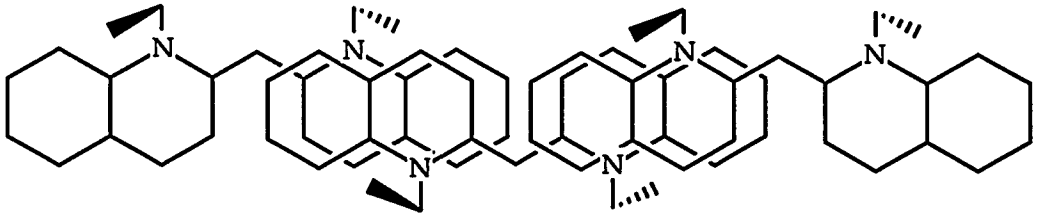

Figure 3.2. The mono-cis- (a) and trans- configurational (b) stereoisomers of the J-aggregate.

3.2 Experimental

2,2'-cyanine was purchased from Aldrich Chemical Company and the phospholipids from Sigma Chemical Company. All compounds were used without further purification and all experiments were conducted at room temperature.

Dye solutions were prepared using distilled and deionized water. pH values were adjusted by addition of 0.1 N NaOH. Vesicle solutions were made following a recipe given in the Ref. 25, briefly: the chloroform solutions of DMPC and DCP were slowly evaporated at 50-70° C to remove solvent; thin films were hydrated with distilled and deionized water at 70° C and sonicated in a bath type sonicator for 1-2 minutes to obtain homogeneous solutions. The pH of the vesicle solutions prepared by this method was ca. 3.0, and not further adjusted. The vesicle size was measured using a photon correlation spectrometer, and the average diameter was found to be ca. 400 nm (37).

Raman Apparatus: Tunable, continuous wave (cw) laser radiation was obtained from both a Coherent dye laser, model CR-599 with R6G as the laser dye, and a Coherent Ti:Sapphire laser, model CR-899. The pump laser was a 20-Watt, cw, Coherent Innova 200 argon-ion laser—approximately 3-Watts was used to pump the CR-599, while the full power could be utilized, when necessary, to pump the Ti:Sapphire. Raman

scattering of samples contained in quartz cells was excited with either 610 or 712 nm radiation. Raman spectra were recorded using a SPEX 1877, 0.6 m triple-spectrometer coupled to a SPEX SpectrumOne charge-coupled-device (CCD), cooled with liquid nitrogen to 140° K. The spectrometer and detector were interfaced to a SPEX DM-3000 computer controller. Reported Raman spectra, in general, correspond to 8 scans with a 10 s integration period per scan, and have been refined by background subtraction—by exporting data to analysis software (IgorPro) from Wavematrix (Lake Oswego, Oregon). Additionally, all reported Raman spectra have a resolution of ca. 2 cm^{-1}.

Absorption and Fluorescence Apparatus: Absorption spectra were recorded using a Perkin-Elmer Lambda 19, UV-vis/NIR spectrometer. Steady-state fluorescence, fluorescence excitation and synchronously scanned luminescence spectra were acquired using a SPEX Fluorolog-τ2 spectrofluorometer. Principal components of the Fluorolog-τ2 are the following: a 450 W xenon incandescent lamp coupled to both a single grating excitation and an emission spectrometer; a Pockels cell which modulates the excitation light from 0.5 MHz to 300 MHz for lifetime studies (see below); a T-box sampling module, including an automated, four-position sample changer; and two Hamamatsu model R928-P photomultiplier tubes, one used as a reference detector, and operated in the direct-current acquisition mode, and the other operated in the photon-

counting acquisition mode. Scanning of excitation, emission, or both simultaneously are under computer control (SPEX DM3000F software run on a SPEX-486 PC). All data are stored and analyzed using vendor software.

Quantum Yields: The fluorescence quantum yields were determined relative to rhodamine 6G in ethanol (Φ = 0.90) as the reference (38). The reference and sample were prepared optically dense (optical density near 2) at the excitation wavelength 525 nm, and greater than 2 at 582 nm for the J-aggregate solution. Front-face illumination (with an incident angle of ca. 22.5° relative to the normal) was used. In our measurements we used a 1 cm cell, with "complete" absorption occurring within 1 or 2 mm near the front surface of the cell. The contributions to the total absorption due to the cis- and trans-aggregates were determined by decomposing the absorption spectrum (such as that shown in Part B of Figure 3.2) when both species are present. For quantum yield as well as fluorescence lifetime measurements, solution conditions which gave rise to two aggregate bands were chosen. Self-absorption and reemission corrections were applied to the measured spectra. The corrections required for wavelength response of the emission monochromator-photomultiplier combination were made with correction factors supplied by the vendor. The slit widths for the excitation and emission monochromators was set to 0.5 mm ($\approx$ 2 nm).

Fluorescence Lifetimes: Absorption and steady-state fluorescence measurements that were ancillary to lifetime measurements were conducted with the same apparatus used for the spectrophotometric titration studies mentioned earlier. The SPEX Fluorolog-τ2 spectrofluorometer, which uses the phase-modulation technique, was used for the determination of fluorescence lifetimes. When configured for lifetime measurements, radiation from a cw xenon incandescent light source (or laser) is directed to a Pockels cell: in our experiments we used front-face illumination and radiation at 550 nm, with a bandpass of ca. 4 nm (resulting from a 1 mm entrance slit width of the excitation spectrometer). Approximately 8% of modulated excitation light from the Pockels cell is directed to the reference detector and the remainder to the sample. To measure the fluorescence lifetime of 2,2'-cyanine aggregates, a reference standard, glycogen, as well as the sample are required. The fluorescence lifetime determination is made through an analysis which utilizes the relative phase shift and relative demodulation of the sample compared to that of the reference.

3.3 Aggregation Enhanced Raman Scattering (AERS)

In order to acquire information about the structure of the aggregate adsorbed on vesicle surface, Raman spectra of 2,2'-cyanine have been taken. According to absorption spectrum the excitation at 610 nm is

expected to project out aggregates scattering because it is near resonance with the J-band. Figure 3.3 shows Raman spectra of 2,2'-cyanine in the aggregate (A) and as monomer in water (B) excited with 610 nm excitation. By comparing, we deduce that the enhancement in relative Raman intensities of the aggregated dye comes from aggregation and near resonance contribution which are predicted from the theory (17). Morever, excitation at 712 nm corresponds to the off-resonance scattering for both species, e.g., aggregates and monomer (part C and D of Figure 3.3). For 712 nm excitation, a Raman spectra are observed with decreased signal, might be due to smaller Raman scattering cross section. Enhancement in relative Raman intensities of the Raman spectrum of aggregates excited at 712 nm can be explained in terms of aggregation since there is no near-resonance contribution. Variations of the relative intensities in the Raman spectrum in the different environments, e.g., in water and/or methanol solutions, and on vesicle surface indicate that the spectrum is due to molecules in more than one chemical condition. Three intense band at 1350, 1370, and 1388 cm^{-1} appear to vary independently with environment. This observation suggests that the molecules in different environment are in at least three structurally different situations. The attribution to the composition of the band at 1388 cm^{-1} comes from an earlier report from our laboratory which stated that the band at 1388 cm^{-1} was assigned to the polycrystalline species (22). The bands at 1350, and 1370

cm^{-1} were assigned to the trans and cis isomers in the aggregate (20). The Raman spectrum of the aggregates is subtracted from the Raman spectrum of monomer to compare the band positions. Upon comparison of the Raman spectra of aggregated 2,2'-cyanine adsorbed on vesicle surface with those obtained from the dye in water and/or methanol, we deduce that bands are not shifted upon adsorption, however relative intensity differences exist.

The Raman bands observed in the high frequency region (>1000 cm^{-1}) can be assigned to symmetric ring breathing vibrations and in-plane deformation as well as bridge stretching and bending modes. These bands have been suggested by Mejean and Forel (60) based upon normal-coordinate calculations assuming C_2 molecular symmetry. They found that all of the Raman bands are due to in-plane vibrations, and polarized in solution measurements. The Raman scattering of 2,2'-cyanine in methanol was also investigated by Pace and Pace (61). They reported that the observed bands in the region 1200-1700 cm^{-1} are strongly polarized due to symmetrical vibrational modes. Additionally, they discussed the nature of some bands and resonance enhancements in terms of Albrecht's theory. The bands at 1361 and 1380 cm^{-1} were assigned to the ring stretching modes of the cyanine molecule, 1397 cm^{-1} to the C-H stretching mode of the quinoline due to

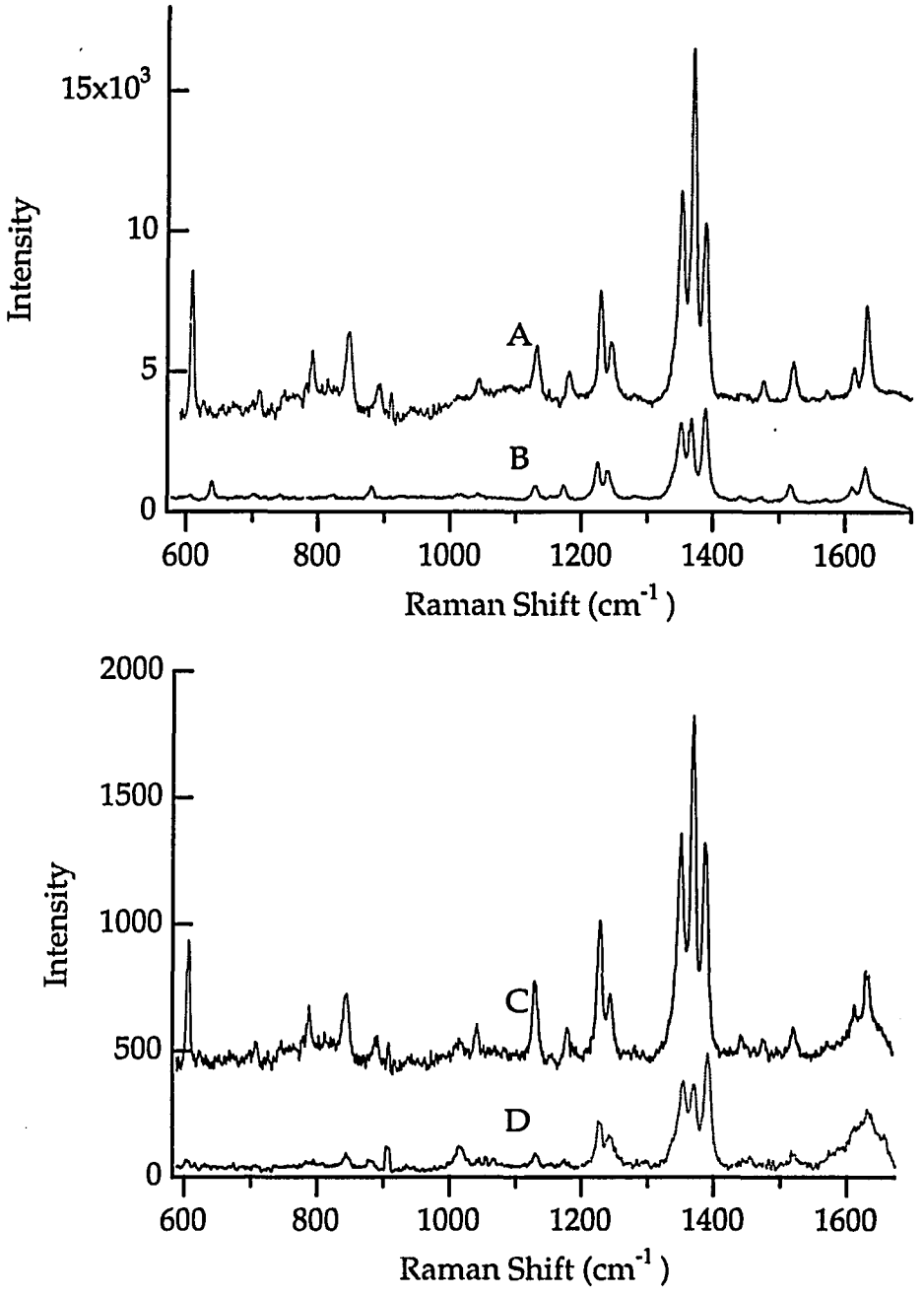

Figure 3.3. Raman spectra of 2,2'-cyanine in the absence (B and D) and presence (A and C) of vesicle. Concentration of the dye 0.05 mM, pH= 10; vesicle concentration 0.36 mM; pH=3. (Dye : vesicle) = 2:1. Excitation wavelengths are 610 nm for the spectra A and B, and 710 nm for C and D.

resonance enhancement and 1639 cm^{-1} to the symmetric stretching mode of the conjugated bridge, C-C=C, between the quinolinic end groups of the cyanine molecule. We made the vibrational mode assignments by considering symmetry and polarization of the bands in the region from 1000 to 1700 cm^{-1}. They are mainly C-C ring breathing and C-H in plane deformation modes and C-C=C conjugated bridge plane bendings and stretching modes as well. Most of the frequencies attributed to J-aggregate and monomeric materials do not differ significantly, as is to be expected. The structures, shown in Figure 3.2, advanced for J-aggregated 2,2'-cyanine incorporates the face to face association between quinoline rings which has been seen to be present on the silver electrode surface (19). Therefore, We adopt this pictures to explain the J-aggregate structures adsorbed onto vesicle surface since the feature of Raman bands, i.e., the band frequencies and their intensities, are quite similar that of those adsorbed on a silver electrode.

Our conclusion is that the Raman spectrum of aggregated 2,2'-cyanine adsorbed on vesicle surface consists of randomly mixed two configurational isomer of aggregates (the trans and cis) on vesicle surface, and polycyrstalline and monomer molecules as well. The electrostatic interactions may take place however no chemical interactions occur, i.e. covalent and/or hydrogen bonding occur between dye molecules and surface molecules of vesicle.

3.4 Steady-State Spectroscopic Studies

Figure 3.4 shows absorption spectra of 2,2'-cyanine in the absence (Part A) and presence (Parts B and C) of vesicle solution, as well as the "quasi-resonance" fluorescence spectrum (Part D, also in the presence of vesicle solution), in which the fluorescence band nearly overlaps the absorption band. The absorption spectrum of 2,2'-cyanine in the absence of vesicle solution (Part A) consists of a vibronic progression with the band at ca. 524 nm corresponding to the 0←0 band (bandwidth 1100 cm^{-1}), the band at ca. 490 nm corresponding to the 1←0 band (bandwidth 1550 cm^{-1}), and the shoulder at ca. 454 nm corresponding to the 2←0 band (estimated bandwidth of 1800 cm^{-1}).

Addition of vesicle solution to the dye solution promote aggregation of the dye, as indicated by a color change from orange to pink. Based upon experimental conditions, such as the concentrations of the dye and vesicle solutions, the solution pH, viscosity and temperature, and the surface potential of the vesicle, we obtain, in general, two different absorption spectra: one has two red-shifted bands (see Part B) located at ca. 572 and 582 nm and the other has only one red-shifted band (see Part C) located at ca. 582 nm. The experimental solution composition conditions which typically led to the occurrence of spectra containing one red-shifted band spectrum were dye concentration, 5×10^{-5} M ; vesicle concentration, 1.6 x

10^{-3} M; and a volume ratio of dye to vesicle of 2:1. Typical experimental conditions which led to the existence of two red-shifted bands were dye concentration, 1 x 10^{-4} M; vesicle concentration, 2 x 10^{-5} M; and a volume ratio of dye to vesicle of 1:1. When the volume ratio of the latter dye/vesicle solution was varied the relative absorbances of the two red-shifted bands were changed, as well as that of the monomer (data not shown here). The two red-shifted bands, termed the J-bands, are attributed to adsorption by aggregated molecules consisting of mono-cis monomers (at 572 nm) and all-trans monomer (at 582 nm). This assignment is also supported by Raman spectra of J-aggregates adsorbed onto a vesicle surface (26).

It might be noted that the optical absorption spectrum of the J-aggregate of 2,2'-cyanine has been theoretically calculated using excitonic transitions, and the narrow bandwidth of the J-band was shown to result from motional narrowing (39). Furthermore, two vibronic bands of the aggregate, for low temperature systems, have been found at 495 and 535 nm (40,41). For the present study, we assume that the aggregate vibronic bands are of much lower intensity than those absorption bands due to the monomer, and, as a result, do not measurably alter relative absorbance determinations for aggregate and monomer.

Part D of Figure 3.4 shows the quasi-resonance fluorescence spectrum of the J- aggregate, with a band centered at 585 nm, when excited

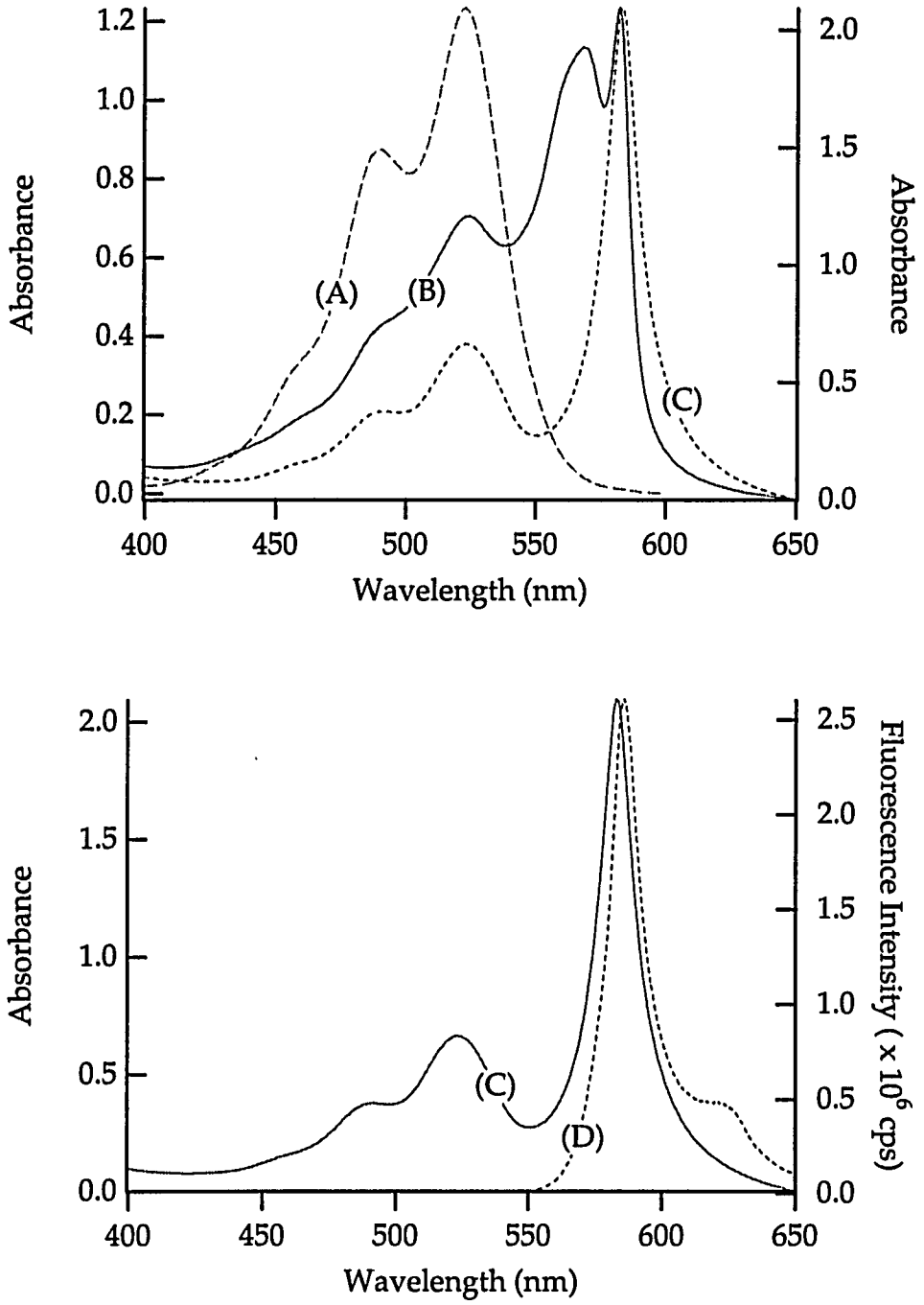

Figure 3.4. Absorption spectra of 2,2'-cyanine in the absence (A) and presence (B and C) of vesicle solution, as well as the "quasi-resonance" fluorescence spectrum (D).

at 550 nm. The fluorescence maximum is shifted to the red by ca. 3 nm when compared to the absorption due to the J-band (see Parts C and D of Fig. 3.4). We have also studied the dependence of the position of the fluorescence intensity maximum on excitation wavelength (not shown), and found it invariant, leading to the conclusion that the fluorescence originates from the lower levels of the LUMO excited state—the lower band edge levels are presumably populated by nonradiative relaxations. It is to be noted that monomer dye molecules in water alone (concentration of ca. 10^{-5}, pH = 11) do not fluoresce (42).

Parts A and B, respectively, of Figure 3.5 show fluorescence excitation and synchronized emission spectra of the aggregate. For the fluorescence excitation spectrum the excitation range is from 400 to 600 nm with detection on the shoulder of the low energy side of the J-band at 605 nm (with a bandpass of 0.4 nm throughout the range). The excitation spectrum reveals bands at 572 and 585 nm, which are attributed to structurally different aggregates, namely, the cis- and trans-aggregates, respectively. In addition, weaker bands at ca. 450, 480, 520, and 540 nm are present, and presumably are due to vibronic transitions of the aggregates. The synchronized emission spectrum of the aggregate, with 3 nm offset between the excitation and emission spectrometers (of the SPEX Fluorolog) throughout the range from 400 to 650 nm, reveals bands at ca. 575 and 585 nm. Again, these two bands are assigned to the putative cis- and trans-aggregates, respectively. We find that the relative intensity of

these latter bands differ from that found in the fluorescence excitation spectrum. In the fluorescence excitation spectrum the 572-nm band is

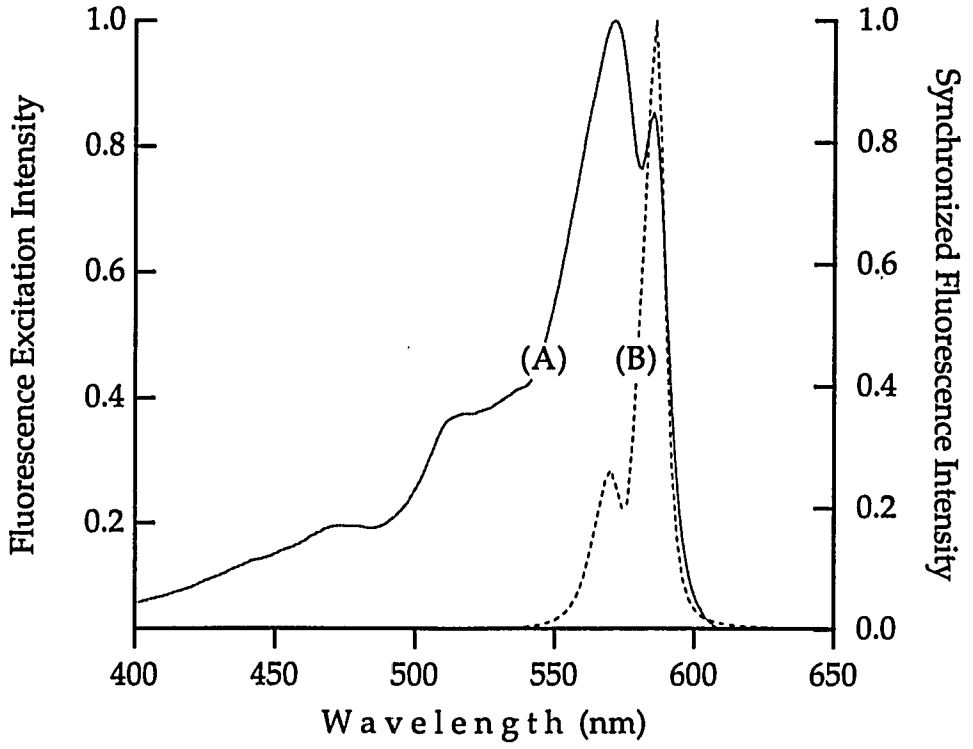

Figure 3.5. Fluorescence excitation (A) and synchronized emission (B) spectra of the J-aggregated 2,2'-cyanine adsorbed onto vesicle surface. Spectra are normalized to their maximum intensity.

more intense than the 585-nm band, while in the synchronized emission spectrum the 575-nm band is less intense that the 585-nm band. We presume that this variation in relative intensities for the two J-bands signals energy transfer from the higher energy cis- aggregate to the lower energy trans- aggregate. The higher ratio of the 572-nm band to the 585-nm band in the fluorescence excitation spectrum occurs because during

the lifetime of the emission energy moves from the cis- to the trans-aggregate and contributes to intensity at the detection wavelength of 605 nm. The cis-aggregate, thus, is deduced to have a greater relative concentration in the ground state than does the trans-aggregate. The fact that the synchronized emission spectrum reveals an inverse relationship between the relative intensity of the bands is interpreted as indicating a greater relative concentration of the trans- to the cis-aggregate in the excited state: a determination arrived at since an offset of 3 nm means that the intensity will track the concentration of the particular aggregate, and possibly will have only a minimal contribution from the wing or shoulder of a nearby emission band. The deduction concerning relative populations of the two ground and excited states of the aggregate is the same reached by de Boer et al. (41) from a contrasting of fluorescence excitation and extinction measurements.

3.5 Spectrophotometric Titration

Absorption titrations were performed to obtain the intrinsic binding constant, K(0), the effective extinction coefficient of aggregate, ε_J, and the average number of monomer molecules in the aggregate, N. We chose the experimental conditions that led to the presence of only one J-band in the absorption spectrum (the 582-nm trans-aggregate band), thus indicating the predominance of one J-aggregate species. Various solutions

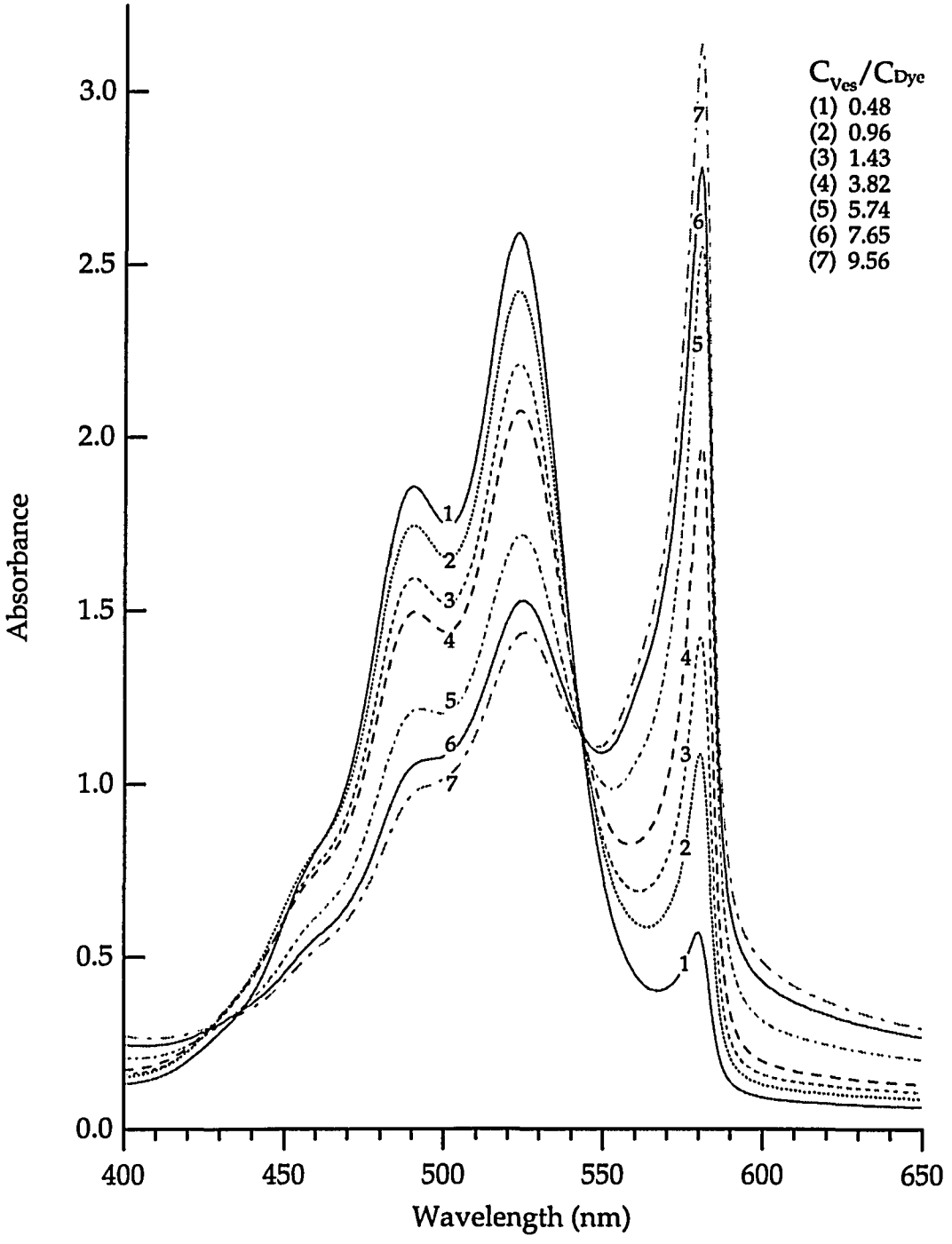

Figure 3.6. A series of absorption spectra of 2,2'-cyanine titrated with vesicle. C_{Ves}/C_{Dye}, the total vesicle monomer concentration to the ratio of aggregate concentration. 0.05 mM 2,2'-cyanine, 0.05 to 1.20 ml, titrated with 2 ml of 1.6 mM vesicle.

were prepared by keeping the volume of the dye solution constant (2 mL) while varying the volume of the added vesicle solution (0.05 - 1.20 mL). The corresponding concentrations for both dye and vesicle monomer were calculated. A series of absorption spectra, as shown in Figure 3.5, reveals that the absorbance at 524 nm decreases as the absorbance at 582 nm increases, and, in addition, an isobestic point is observed at 545 nm.

These findings are suggestive of a chemical equilibrium between dye monomers and aggregates, such as represented by the following relationships which are used for analysis of our measurements:

$$M + V \overset{k_e}{\rightleftharpoons} J, \tag{3.1}$$

which allows the equilibrium constant k_e to be calculated from the expression,

$$k_e = \frac{C_J}{(C_V - C_J)C_M}. \tag{3.2}$$

In the above expressions, M represents dye monomers, J represents aggregated dye, and V represents the vesicle, which has binding sites for dye monomers. Additionally, k_e is the equilibrium constant, and the concentrations of free dye monomer, aggregated dye, and total vesicle monomer are represented by C_M, C_J, and C_V, respectively. We also, for later use, represent the total added dye concentration by C_T.

One approach we use in our analyses for the aforementioned parameters is to define $r = C_J/C_V$, the ratio of aggregate concentration to the total vesicle monomer concentration, and to note that the intrinsic binding constant is given by the expression:

$$K(0) = \lim_{r\to 0} k_e = \lim_{r\to 0} \frac{C_J}{(C_V - C_J)C_M} = \frac{C_J}{C_V C_M} \qquad (3.3)$$

where K(0) is the intrinsic binding constant.

For our studies we measured absorbancies for both the monomer (ε_M) and the aggregate (ε_J), thus leading to concentrations being expressed in terms of extinction coefficients. Our measured value of ca. 7×10^4 M^{-1} cm^{-1} for the extinction coefficient of the monomer agrees with the value reported in the literature (43). The extinction coefficient of adsorbed aggregate is determined by extrapolating the measured absorbancies to conditions of complete binding, and is discussed below.

For the analysis, we define ε_{ap} as the apparent extinction coefficient at a given wavelength for a mixture of aggregated and monomeric dye

$$A = \varepsilon_{ap} C_T, \qquad (3.4)$$

where A is the absorbance (with path length set equal to 1). Combining the relation

$$A = \varepsilon_J C_J + \varepsilon_M C_M \tag{3.5}$$

with equ. (3.4), we obtain equ. (3.6),

$$C_J = \frac{(\varepsilon_{ap} - \varepsilon_M)}{(\varepsilon_J - \varepsilon_M)} C_T \ . \tag{3.6}$$

Upon inserting equ. (3.6) into equ. (3.3), we obtain

$$\frac{C_V}{(\varepsilon_{ap} - \varepsilon_M)} = \frac{C_V}{(\varepsilon_J - \varepsilon_M)} + \frac{1}{(\varepsilon_J - \varepsilon_M)\, K(0)} \ , \tag{3.7}$$

an equation originally derived by Schmechel and Crothers (44), which makes the assumption that the species bound to the substrate is the aggregate, and that the average number of monomers coupled to form the aggregate is N.

The absorbance of 2,2'-cyanine at 582 nm for different concentrations of vesicle monomer, but fixed total concentration of dye, plotted according to equ. (3.7) is shown in Figure 3.7. The intrinsic binding constant K(0) and the absorption extinction coefficient of the aggregate ε_J, determined from the slope and intercept of the resultant linear plot, are $(9.6 \pm 0.5) \times 10^3\ M^{-1}$ and $(2.3 \pm 0.2) \times 10^5\ M^{-1}\ cm^{-1}$, respectively.

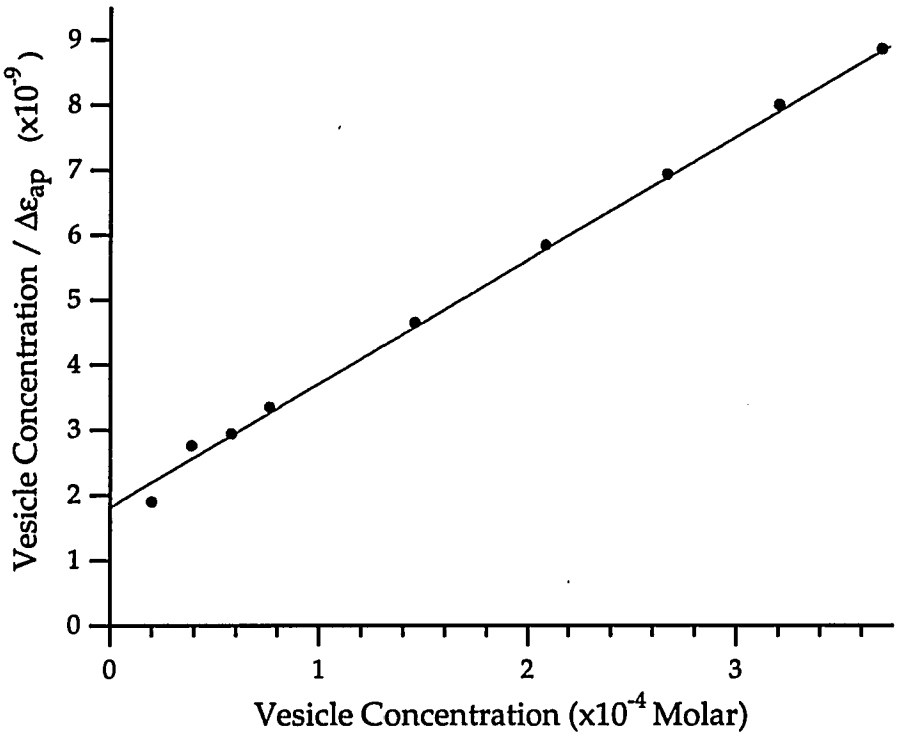

Figure 3.7. The "Scatchard" binding plot of the J-aggregates.

We next performed a curve fit to the same data as used above, in order to determine N, the average number of monomers in the aggregate. This analysis utilizes equ. (3.8), derived by combining the Scatchard equation and the mass action law. We assume that there is one "binding" site per head group of the vesicle. The Scatchard equation has the form:

$$r = \frac{C_J}{C_V} = \frac{KC_M}{1 + KC_M} \quad . \tag{3.8}$$

Now upon substituting $C_M = C_T - NC_J$, one obtains

$$KN(C_J)^2 - (1 + KC_T + NKC_V)C_J + KC_TC_V = 0, \tag{3.9}$$

which gives

$$C_J = \frac{1}{2\,K(0)\,N} \times$$

$$\{(1+K(0)C_T+NK(0)C_V)+\sqrt{\{(1+K(0)C_T+NK(0)C_V)^2-4K(0)^2C_TC_V\}}\} \quad (3.10)$$

In order to obtain the absorbance A_J, both sides of equ. (3.10) are multiplied by ε_J. Values of K(0) and ε_J from the linear fit above are taken as known parameters, A_J is defined as the absorbance at 582 nm, and C_V and C_T are calculated from the known total concentration of added vesicle and dye, respectively. Using the measured values of A_J for a known C_V and C_T allows N to be determination.

Upon fitting the absorbance data to the above equation (see Figure 3.8), we find that $N = 10 \pm 1$.

3.6 Fluorescence Dynamics

Early measurements of the fluorescence lifetime of J-aggregates formed in solution or on glass gave very short lifetimes (45-49), on the order of picoseconds, since the high excitation intensities used resulted in exciton annihilation.

Sundström et al. (50) performed experiments on J-aggregates of 2,2'-cyanine in homogeneous aqueous solution at room temperature and

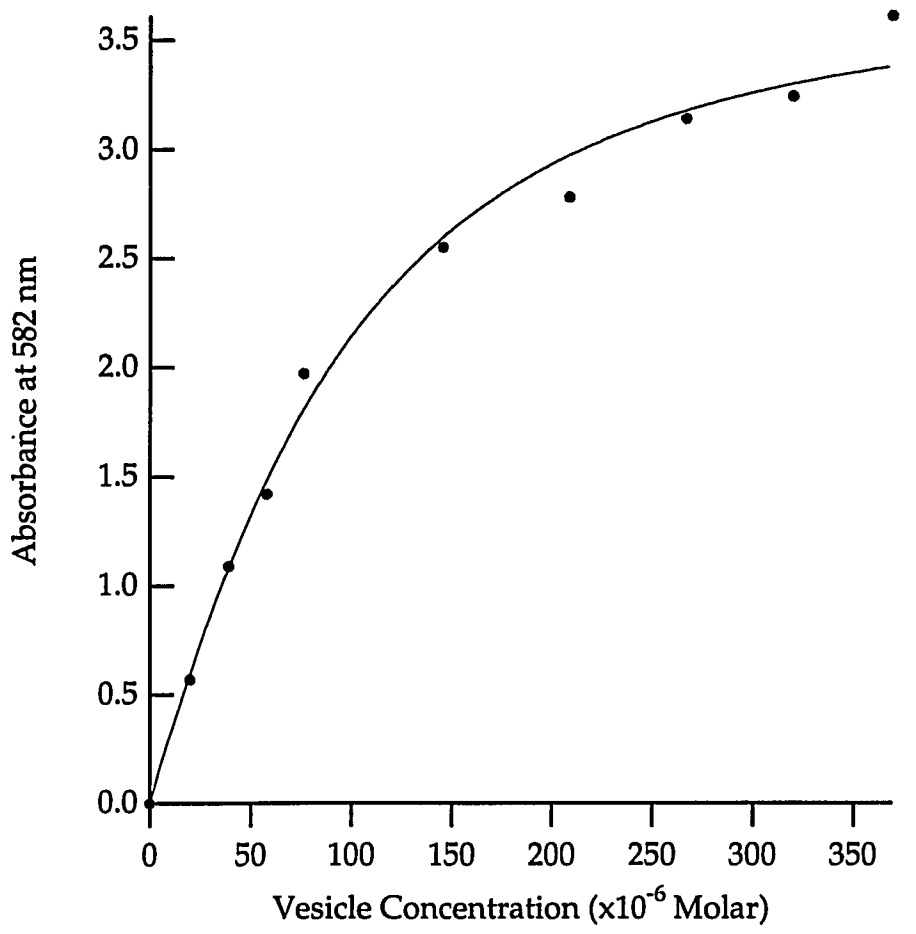

Figure 3.7. The modified "Scatchard" type binding plot of the J-aggregate.

determined that both the lifetime and the fluorescence yield were strongly dependent on excitation pulse intensity; a single exponential lifetime of about 400 ps was measured at low excitation intensity. Other time-dependent studies that avoided the excitation pulse intensity problem were conducted by Wiersma et al. (11,12,41,51,52) who utilized J-aggregates of 2,2'-cyanine formed in an ethylene glycol/water glass at low temperature, and ascertained that the low-temperature fluorescence lifetime was 70 psec. In these latter studies, the measured lifetime was

found to be independent of temperature up to 50 K, and temperature dependent (increasing with temperature) above 50 K; they further concluded that molecular superradiance (due to disordered molecular aggregates) is the dominant deactivation process.

Other, recent investigations provide information on fluorescence dynamics for 2,2'-cyanine. For example, Muenter et al. (13) reported the dependence of fluorescence lifetime and relative quantum yield on temperature and aggregate size for the J-aggregates of 2,2'-cyanine on AgBr surface, and showed that the dominant process controlling the dynamics was energy transfer to a defect state—a dimer structure was suggested. This nonradiative process was postulated to lead at room temperature to a strong diminution in fluorescence yield with increasing concentration.

Dorn and Müller (53) measured a lifetime of 8.2 ps for a Langmuir-Blodgett monolayer of 2,2'-cyanine J-aggregate at room temperature, and a value of 5.5 ps at 143 K; they interpreted the decrease in lifetime as evidence for superradiance enhancement.

Additionally, Fidder et al. (12) have shown for a Langmuir-Blodgett monolayer of 2,2'-cyanine J-aggregate at 1.5 K that the fluorescence lifetime of the initial decay process was 10 ps— a slower, secondary decay was not evaluated. These latter authors attributed the nonexponentiality of the decay to a combination of exciton transport and radiative decay. The structure of J-aggregates in a Langmuir-Blodgett monolayer was deduced

to be quasi two-dimensional and more delocalized than one dimensional aggregates formed in frozen glass.

In this laboratory we used the phase-modulation method to determine fluorescence lifetimes. In this method (54), the sample is excited with light whose intensity is sinusoidally modulated. Since there is a time lag between absorption and emission, emission is delayed in phase and demodulated relative to the incident light. The phase delay (ϕ) and demodulation factor (m) can be experimentally measured and used to determine the fluorescence lifetime of the aggregate. The phase and modulation apparent lifetimes, τ_p and τ_m, respectively, are defined as

$$\tau_p = \omega^{-1} \tan \phi \tag{3.11}$$

$$\tau_m = \omega^{-1} \left(\frac{1}{m^2 - 1} \right)^{1/2} \tag{3.12}$$

where ω is the modulation frequency.

Analysis and nonlinear least-squares fitting (Marquardt-Levenson minimization algorithm) were performed with software provided by Globals Unlimited (Urbana, IL). Phase-shift and demodulation measurements were obtained for modulation frequency ranging from 20 to 250 MHz.

Frequency domain fluorescence intensity decay of the putative trans- and cis-aggregates of 2,2'-cyanine adsorbed onto a vesicle surface at room temperature is shown in Figure 3.9. The excitation wavelength was 550 nm and the phase shifts for the fluorescence intensities for the cis- and trans-aggregates were measured separately by setting the emission monochromator at appropriate detection wavelengths, 575 and 585 nm, respectively. Both measurements fit single exponential decay models with low χ^2 values: the fluorescence lifetime of the cis-aggregate was found to be 110 ± 20 ps, with a χ^2 = 1.06; the trans-aggregate's fluorescence lifetime was found to be 340 ± 20 ps, with χ^2 = 0.87.

The fluorescence quantum yield measurements were carried out under the conditions mentioned in the experimental section. Fluorescence quantum yields were determined by using the relationship (55),

$$Q_J = Q_S \frac{A_J}{A_S} \frac{(1-10^{-OD_S})}{(1-10^{-OD_J})} \frac{n_J^2}{n_S^2} \qquad (3.13)$$

where, for our system, J and s specify the J-aggregate and the standard, respectively; A is the integrated area under the corrected fluorescence spectrum; n is the refractive index of the solution; and OD is the optical density at excitation wavelengths used: 525, 560, and 570 nm.

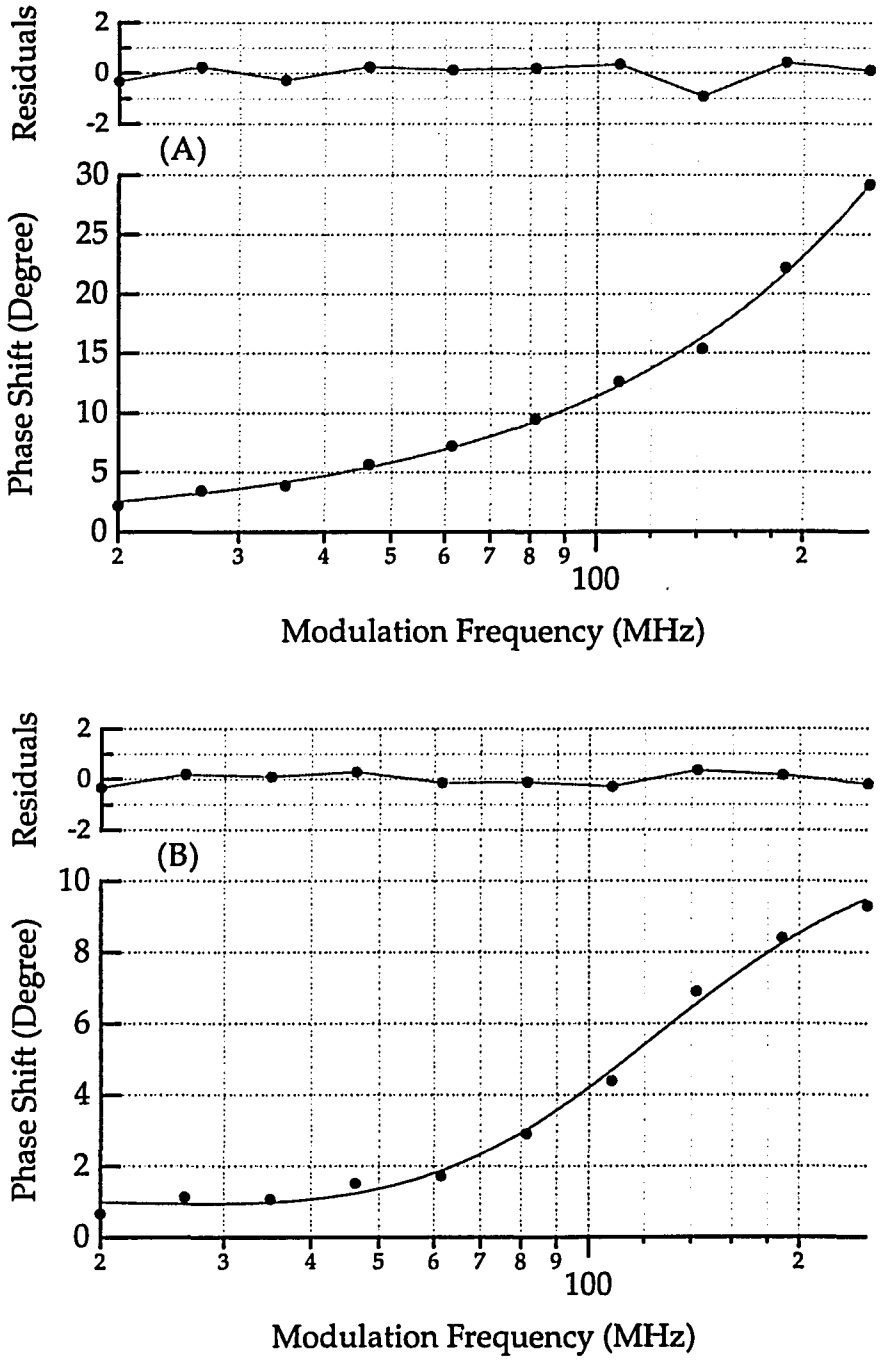

Figure 3.9. Frequency domain fluorescence intensity decay of (A) the trans-aggregate, a single exponential decay with χ^2 = 1.06; and (B) cis-aggregate, a single exponential decay with χ^2 = 0.87 aggregates of 2,2'-cyanine adsorbed onto a vesicle surface at room temperature.

Fluorescence quantum yields were found to be 0.28 ± 0.03 for the trans-, and 0.04 ± 0.01 for the cis-aggregate, respectively—with the possible error in the determination reflecting the range in the respective measurement when several different excitation wavelengths, between 560 and 570 nm, were use. (Note that for the cis-isomer, the synchronized emission spectrum was used.)

Since in quantum yield measurements reabsorption and reemission errors are important when there is significant overlap of the absorption and emission spectra, the correction equation for radiation trapping derived by Melhuish (56) was applied to our measurements. As a result, the measured fluorescence quantum yield Q was related to the true fluorescence quantum yield Φ by the expression

$$Q = \frac{\Phi}{1-\kappa'\Phi}\left\{\int f(\lambda')\frac{\alpha_\lambda}{\alpha_\lambda+\alpha_{\lambda'}}d\lambda' + (1-\kappa')\right\}, \qquad (3.14)$$

here $\alpha_\lambda = \varepsilon(\lambda)c\ell$, $f(\lambda')$ is the fluorescence intensity at the emission wavelength λ', α_λ and $\alpha_{\lambda'}$ are the absorbancies at the excitation and emission wavelengths, and κ', the reemission probability, is approximated by being defined for emission following the initial self-absorption process, and set equal to $\int f(\lambda')[1-10^{-\varepsilon(\lambda')c\ell}]d\lambda'$. The integration in equ. 3.14 covers a range defined by the measurable fluorescence intensities, while α_λ and $\alpha_{\lambda'}$

are obtained from the absorption spectrum of the J-aggregate, decomposed in terms of overlapping contributions. The integral κ' is found to be equal to 0.66 for the spectral range from 560 to 620 nm. The integral in equ. 3.14 is approximately 1/2 since α_λ and $\alpha_{\lambda'}$ are essentially equal. Hence, the true fluorescence quantum yield for the J-aggregate is essentially equal to

$$\Phi \approx \frac{6Q}{4Q+5} \tag{3.15}$$

which, for the cis- and trans- aggregates, give the values 0.05 ± 0.01 and 0.28 ± 0.03, respectively, for Φ^C and Φ^T. As a result, within the experimental uncertainty, the quantum yields remain unchanged.

Measured fluorescence lifetimes were also corrected for the reabsorption and reemission error. In order to obtain the true fluorescence lifetimes, we used the equation derived by Birks (57)

$$\tau_m = \frac{\tau}{(1-\kappa')} \tag{3.16}$$

where τ_m is the measured fluorescence lifetime, and τ is the true fluorescence lifetime. The true fluorescence lifetimes for the trans- and cis- aggregates, using equ. 3.16 and the errors in the τ_m's, are calculated to be 115 ± 7 and 40 ± 7 ps, respectively.

Fluorescence lifetime and quantum yield are related to the radiative rate constant k_r and nonradiative rate constant k_{nr} by the photophysical equations:

$$k_r = \frac{\phi_f}{\tau_f} \tag{3.17}$$

$$k_{nr} = \frac{1-\phi_f}{\tau_f} \tag{3.18}$$

Upon substituting the measured values of fluorescence lifetimes and quantum yields, one finds that for the trans-aggregate $k_r = (2.4 \pm 0.3) \times 10^9\ s^{-1}$ and $k_{nr} = (6.3 \pm 0.3) \times 10^9\ s^{-1}$. We deduce, in this case, that the nonradiative process is exciton transport (electronic energy transfer): each exciton created travels within the aggregate before being captured by a local potential minimum (luminescent center), suggesting the concept of coherence size, i.e., the length (or area) of the molecules strongly coupled to each other and responding in phase to the external optical field. The radiative rate suggests some alignment of molecules in a single aggregate, thus supporting the concept of a coherence dimension. The implicit disorder might be attributed to variations in orientation of the remaining molecules in an aggregate. A consequence of this assumption, as suggested by other, is that the physical size of a single aggregate would differ from the coherent size. The coherence size, in fact, has been deduced to be equal to the ratio of the J-aggregate's and monomer's

radiative rate constants. This ratio is found to be 8 for the trans-aggregate, with the monomer radiative rate constant calculated by the data taken from Ref. 42. We interpret our results as indicating superradiant emission of the trans-aggregate adsorbed onto a vesicle surface at room temperature.

The radiative and nonradiative decay rates for the cis-aggregate are calculated to be $(1.3 \pm 0.1) \times 10^9\ s^{-1}$ and $(2.4 \pm 0.1) \times 10^{10}\ s^{-1}$, respectively. In this case, the nonradiative processes would be exciton transport: energy transfer, for example, to the trans-aggregate or a defect state. The strong overlap of the absorption spectrum of the cis-aggregate and the emission spectrum of the trans-aggregate, about 40% of the normalized spectra (not shown here), suggests a large cross-section for energy transfer. Energy transfer, indeed, is likely to emanate from an electromagnetic coupling between the cis-aggregate (energy donor) and the trans-aggregate (energy acceptor) (58, 59), both aggregates being coupled to the lattice, and weakly coupled to each other. We estimate that the energy transfer rate is of the same order of magnitude as the fluorescence lifetime, that is $\approx$ 100 ps. Thus, the ratio of the nonradiative to radiative decay rate for the cis-aggregate (about 19), indicates that nonradiative processes are of principal importance in determining excited-state dynamics. It is also to be noted that the ratio of the radiative rate constants for the cis-aggregate to that of the monomer is calculated to be 4, indicating weaker superradiance than the trans-aggregate. Hence, upon comparison of this result with that of

the trans-aggregate, we observe that superradiance is greater for the lower energy aggregate configuration.

The photophysical properties of the J-aggregates adsorbed on a vesicle surface and those for the monomer are tabulated in table 3.1.

It is to be noted that Mukamel et al. (14-16) have provided a theoretical relationships connecting superradiance, exciton-phonon coupling, coherence size, etc. The coherence size is found to depend on the coupling strength, the phonon bandwidth, the aggregate temperature, and the aggregate's physical size, for small aggregates whose size is much smaller than the optical wavelength. Our results indicate that the exciton-phonon coupling strength for the cis-aggregate (compared to that of the trans-aggregate) should be larger due to its smaller coherence size. This latter finding has been theoretical suggested by Spano et al. (16), and confirms the suggestion by Muenter et al. (13) that microscopic structure is related to superradiance.

In the case of J-aggregates formed in solution at low temperature (11,12), more intense superradiance is observed, with ca. 100 molecules apparently coupled, while J-aggregates on a AgBr surface at room temperature (13) shows weaker superradiance with ca. 2 molecules responding in phase to the external optical field. For our system, though two structurally different J-aggregates are formed on the vesicle surface,

Table 3.1. The photophysical properties of the J-aggregates adsorbed on a vesicle surface and those for the monomer.

Parameters	Monomer	Cis-aggregate	Trans-aggregate
$\lambda_{abs,max}$ (nm)	524[a]	572[b]	582[a]
$\lambda_{fluo,max}$ (nm)	570[d]	575[c]	585[e]
$\Delta\nu_{abs}$ (cm^{-1})	1100[a]	1000[b]	300[a,b]
$\Delta\nu_{fluo}$ (cm^{-1})	2400[d]	325[c]	400[e]
ϕ_{fluo}	0.026[d]	0.05 ± 0.01[c]	0.28 ± 0.03[e]
τ_{fluo} (ps)	94 ± 5[d]	40 ± 7[f]	115 ± 7[g]
τ_o (ps)	3700 ± 100[d]	800 ± 300	410 ± 70
$k_r \times 10^9$ (s^{-1})	0.3	1.3 ± 0.1	2.4 ± 0.3
$k_{nr} \times 10^9$ (s^{-1})	10	24 ± 1	6.3 ± 0.3
Coherence size	—	4 ± 1	8 ± 1

(a) Absorption (b) Fluoresecence excitation (c) Synchronized luminescence (d) Taken from Ref. 42 (e) Fluorescence (f) A single exponential decay: $\chi^2 = 1.06$. (g) A single exponential decay: $\chi^2 = 0.87$.

the trans-aggregate exhibits greater superradiance and more coupled molecules than reported for the AgBr system, but less superradiance than found for the frozen glass system.

It might be noted, that the dynamics parameters which we have measured correlate with other studies reported from this laboratory in which a silver electrode was used as the substrate. We have suggested that the measured widths of the Raman excitation profiles of the two low

frequency Raman exciton-phonon modes located at 232 and 278 cm^{-1} (with room temperature peak intensities occurring at 575.5 and 577.5 nm, respectively), can be rationalized in terms of the relative energies of two aggregates [24]: the halfwidths of the excitation profiles of the trans- and cis-aggregate were found to be 434 ± 25 and 321 ± 20 cm^{-1} for the 232- and 278-cm^{-1} bands, respectively, with the widths reflecting the strengths of the dipole-dipole coupling in the excitonic state (i.e., the trans-aggregate has a larger dipole-dipole interaction energy, hence a larger spacing between sublevels, resulting in a wider excitation profile). In addition, the relative widths of the 232- and 278-cm^{-1} exciton-phonon Raman bands were rationalized using dephasing rate arguments: the dephasing of the higher energy 278-cm^{-1} band (assigned to the cis-aggregate) is faster since the spacing between sublevels is less, and dephasing depopulates the k=1 state from which transitions are allowed, leading to a narrower profile for the cis-aggregate. These earlier finding, indeed, are consistent with the cis-aggregate having a smaller coherence size, lower superradiance, and a shorter fluorescence lifetime than the trans-aggregate.

We conclude from the accumulated information that superradiance and energy transfer are the principal determinants of excited-state dynamics.

REFERENCES

1. Feher, G.; Okumura, M. Y. In "The Photosynthetic Bacteria"; Clayton, K.; Sistrom, W.F., Ed.; Plenum: New York, 1978.

2. Gilman, P. B. Photo. Sci. Eng. 1974, 18, 418.

3. Borsenberger, P. M.; Chowdry, A.; Hoesterey, D. C.; W. Mey J. Appl. Phys. 1978, 44, 5555.

4. Hanamura, E. Phys. Rev. B. 1988, 37, 1273.

5. Sasaki, F.; Kobayashi, S. Appl. Phys. Lett. 1993, 63, 2887.

6. Wang, Y. Chem. Phys. Lett. 1986, 126, 209.

7. Wang, Y. J. Opt. Soc. Am. B. 1991, 8, 981.

8. Kobayashi, S. Mol. Crys. Liq. Crys. 1992, 217, 77.

9. Jelley, E. Nature, 1936, 138, 1009.

10. Scheibe, G. Angew. Chem. 1936, 49, 563.

11. Fidder, H.; Knoster, J.; Wiersma, D. A. Chem. Phys. Lett. 1990, 171, 529.

12. Fidder, H.; Terpstra, J.; Wiersma, D. A. J. Chem. Phys. 1991, 94, 6895.

13. Muenter, A. A.; Brumbaugh, D. V.; Apolito, J.; Horn, L. A.; Spano, F. C.; Mukamel, S. J. Phys. Chem. 1992, 96, 2783.

14. Grad, J.; Hernandez, G; Mukamel, S. Phys. Rev. A. 1988, 37, 3835.

15. Spano, F. C.; Mukamel, S. J. Chem. Phys. 1989, 91, 683.

16. Spano, F. C.; Kuklinski, J. R.; Mukamel, S. J. Chem. Phys. 1991, 94, 7534.

17. Akins, D. L. J. Phys. Chem. 1986, 90, 1530.

18. Akins, D. L.; Lombardi, J. R. Chem. Phys. Lett. 1987, 136, 495.

19. Akins, D. L.; Akpabli, C. K.; Li, X. J. Phys. Chem. 1989, 93, 1977.

20. Akins, D. L.; Macklin, J. W. J. Phys. Chem. 1989, 93, 5999.

21. Akins, D. L.; Macklin, J. W.; Parker, L. A.; Zhu, H. -R. Chem. Phys. Lett. 1990, 169, 564.

22. Akins, D. L.; Macklin, J. W.; Zhu, H. -R. J. Phys. Chem. 1991, 95, 793.

23. Akins, D. L.; Zhu, H. -R. Langmuir 1992, 8, 546.

24. Akins, D. L.; Zhuang, Y. H.; Zhu, H. -R.; Liu, J. Q. J. Phys. Chem. 1994, 98, 1068.

25. Sato, T.; Yonezewa, Y., Hada, H. J. Phys. Chem. 1989, 93, 14.

26. Akins, D. L., Ozcelik, S.; Liu, J. Q. Pittsburgh Conference, 1994, Abstract # 936.

27. Ozcelik, S.; Akins, D. L. "Photophysics of Cyanine Dyes: I. Steady-State Spectroscopy and Fluorescence Lifetime of Monomeric Benzimidazolocarbocyanine," submitted to J. Phys. Chem., 1995.

28. West, W.; Pearch, S. J. Phys. Chem. 1965, 69, 1894.

29. O'Brien, D. F.; Kelly, T. M.; Costa, L. F. Photo. Sci. Eng. 1974, 18, 76.

30. Knudtson, J. T.; Eyring, E. M. J. Phys. Chem. 1974, 78, 2355.

31. Tredwell, C. J.; Keary, C. M. Chem. Phys. 1979, 43, 307.

32. Sundström, V.; Gillbro, T. J. Chem. Phys. 1985, 83, 2733.

33. Murphy, S.; Sauerwein, B.; Drickamer, H. G.; Schuster, G. B. J. Phys. Chem. 1994, 98, 13476.

34. Aramendia, P. F.; Negri, R. M.; San Romàn, E. J. Phys. Chem. 1994, 98, 3165.

35. Awad, M. M.; McCarthy, P. K.; Blanchard, G. J. J. Phys. Chem. 1994, 98, 1454.

36. Åkesson, E.; Sundström, V.; Gillbro, T. Chem. Phys. 1986, 106, 269.

37. Measurement made at General Food of Fort Lee, NJ by Dr. Stephen Habif.

38. Schafer, F. P. In "Dye Lasers." Springer-Verlag: New York, 1989.

39. Knapp, E. W. Chem. Phys. 1984, 85, 73.

40. Misawa, K.; Ono, H.; Minoshima, K.; Kobayashi, T. J. Lumin. 1994, 60&61, 812.

41. De Boer, S.; Vink, K. J., Wiersma, D. A. Chem. Phys. Lett. 1987, 137, 99.

42. Dorn, H-. P.; Muller, A. Chem. Phys. Lett. 1986, 130, 426.

43. Brooker, L. G. S.; White, F. L.; Sprague, R. H.; Dent Jr., S. G.; Van Zandt, G. Chem Rev. 1947, 41, 325.

44. Schmechel, D. E. V.; Crothers, D. M. Biopolymers 1971, 10, 465.

45. Yu, Z. X.; Lu, P. Y.; Alfano, R. R. Chem. Phys. Lett. 1983, 79, 289.

46. Kopainsky, B.; Kaiser, W. Chem. Phys. Lett. 1982, 88, 357.

47. Rentsch, S. K.; Danielius, R. V.; Gadonas, R. A.; Piskarkas, A. Chem. Phys. Lett. 1981, 84, 446.

48. Brumbaugh, D. V.; Muenter, A. A.; Knox, W.; Mourau, G.; Wittmershaus, B.; J. Lumin. 1984, 31&32, 783.

49. Fink, F.; Klose, E.; Teuchner, K.; Dahne, S. Chem. Phys. Lett. 1977, 45, 548.

50. Sundström, V.; Gillbro, T.; Gadonas, R. A.; Piskarkas, A. J. Chem. Phys. 1988, 89, 2754.

51. De Boer, S.; Wiersma, D. A. Chem. Phys. 1989, 131, 135.

52. De Boer, S.; Wiersma, D. A. Chem. Phys. Lett. 1990, 165, 45.

53. Dorn, H-. P.; Muller, A. Appl. Phys. B. 1987, 43, 167.

54. Lakowicz, J. R. In "Principles of Fluorescence Spectroscopy." Plenum Press: New York, 1983.

55. Demas, J. N; Crosby, G. A. J. Phys. Chem. 1971, 75, 991.

56. Melhuish, W. H. J. Phys. Chem. 1961, 65, 229.

57. Birks, J. B.; In "Photophysics of Aromatic Molecules", p. 92, Wiley-Interscience, 1971.

58. Di Bartolo, B.; In "Energy Transfer Processes in Condensed Matter", NATO-ASI Series B: Physcis, Vol. 114, Plenum Press, 1983.

59. Agranovich, V. M.; Galanin, M. D. In "Electronic Excitation Energy Transfer in Condensed Matter." North-Holland Pub. Co., Amsterdam, 1982.

60. Mejean, M.; Forel, M.T. J.Raman Spect. 1977, 6, 117.

61. Pace, L. J.; Pace E. L. Spectrochim. Acta. 1980, 36A, 557.

CHAPTER 4

PICOSECOND EXCITON DYNAMICS OF 1,1',3,3'-TETRAETHYL-5,5',6,6'-TETRACHLORO-BENZIMIDAZOLOCARBOCYANINE AGGREGATES

In this chapter I will discuss excited-state dynamics and photophysics of 1,1',3,3'-tetraethyl-5,5',6,6'-tetrachlorobenzimidazolo carbocyanine (BIC) J-aggregates adsorbed on colloidal silica surface. In order to provide information on spectroscopy and dynamics of aggregates, other than PIC which is the cyanine mostly studied so far, BIC was used and the results are discussed. BIC has some advantages for study: the aggregation starts at low concentrations, i.e. 10^{-5}M comparing to PIC, 10^{-2}M ; and it is not sterically hindered in monomeric state and very close to a planar form. The chemical structure of BIC is shown in Figure 4.1.

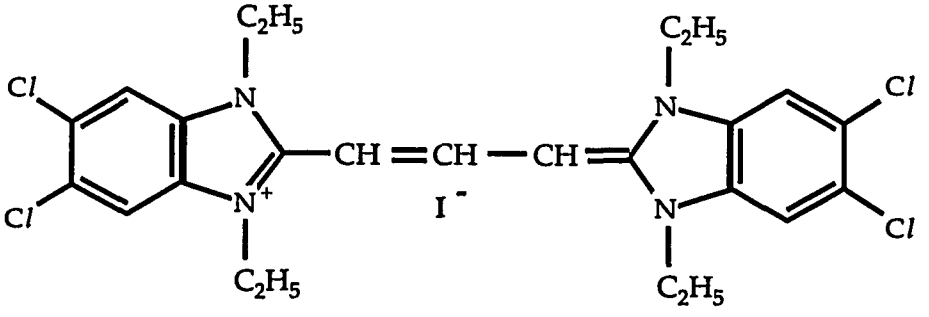

Figure 4.1. The chemical structure of (BIC).

4.1 Some Previous Studies on BIC J-Aggregates

Earlier studies on BIC J-aggregates started back to late 1960's with Zuckerman (1) who showed that BIC forms well ordered, multilayer J-aggregates reproducibily and easily. Gray et.al. examined the structure of J-aggregates adsorbed on single crystals of silver bromide. They used visible and IR absorption and found the IR band at 1475 cm^{-1} having relatively low intensity comparing to the powdered sample of crystalline dye dispersed in KBr. They identified the band at 1475 cm^{-1} as an antisymmetric C=C streching vibration of the conjugated polymethine chain with transition dipole lying in the short axis of molecule. The transition dipole of this band is perpendicular to the crystal surface, so the band disappears when light is incident normal to the crystal surface. They also noted that the IR absorption bands were sharp and showed no broadening and splitting as seen in IR bands of the powdered sample of crystalline dye dispersed in KBr, interpreted indicating one molecule per unit cell. The presence of one J-band at 593 nm indicated one molecule per unit cell. It has been pointed out (3) that for each absorption band of a monomeric dye there will be as many allowed absorption bands as there are molecules per aggregate unit cell.

X-ray crystallography of BIC/methanol (DYEM) and BIC/acetonitrile (DYEA) solvates were studied by Smith (4). They reported that the dye molecules pack plane to plane and end to end on edge in sheets parallel to

(100) axis. Adjacent lines of end to end dye molecules are shifted laterally to form a tilted brick-stone. DYEA crystallizes in the triclinic space group P1 with one molecule per unit cell. DYEM crystallizes in the triclinic space group $P2_1/c$ with four molecules per unit cell. In spite of extensive conjugation, the molecules are approximately planar and mean molecular planes make angles of 87.6° and 85.8° with the sheets for DYEM and DYEA, respectively.

In most of the studies sodium salt of BIC were used. Herz (5) studied that absorption dependence of BIC on electrolyte and methanol concentration in aqueous solution. Addition of KCl caused the intensity of the monomer band (M-band) at 514 nm to decrease while the J-band at 593 nm to increase. The extinction coefficient was calculated as 5×10^5 M^{-1} cm^{-1}. Resonance fluorescence with a half width 300 cm^{-1} was also reported. The existence of an equilibrium between monomer and J-aggregate is suggested. The number of monomer in the aggregate unit cell and equilibrium constant were 4 and 4.6×10^{16}, respectively.

Using a monomolecular film of 1,1'-diethyl-3,3'-dioctadecyl analog of BIC, O'Brien (6) found the J-band at 593 nm when a rigid layer of this dye is deposited on glass, polyethylene and/or AgBr. On the other hand, BIC gave a J-band in aqueous soluiton at 595 nm and a J-maximum at 575 nm at AgBr when it was adsorbed from solution rather than deposited as a preformed film. Clearly, a J-aggregate in solution and a J-aggregate on a

surface have different spectral properties. J-aggregates in solution vary with concentration while J-aggregates on surfaces vary with composition and surface properties of the substrate. It is apparent that these aggregates may differ in their spatial arrangement depending on whether they are free-standing in solution, part of a rigid monolayer or oriented by adsorption on AgBr.

The fluorescence lifetime of BIC J-aggregate in solution was measured by O'Brien et.al. (7) with time correlated single photon counting technique (TCSPC) and was found to be 0.960 ns, without details such as concentration, excitation and emission wavelengths, temperature, etc. Recently, Lindbrum et.al. (8) have carried out fluoresence lifetime measurements of sodium salt of BIC J-aggregates. The temperature dependence of fluoresence lifetime has been measured varied between 4 and 300K with different solvent mixtures and cooling procedures. At very low temperatures, the lifetime was nearly constant and single exponential with 80 ps; $50 < T < 300$K the fluoresence lifetime, varied 100 to 200 ps with either single or double exponentials depending on solvent mixture and cooling procedures, indicating that the microscopic environment of the J-aggregate determines the lifetime. At room temperature, the solvent dependence of the lifetime was also studied and it was found that the lifetime depends on linearly on the reciprocal viscosity.

Yoshihara and coworkers have conducted some very important experiments regarding excited state dynamics of sodium salt BIC J-aggregates. They measured the picosecond pump-probe absorption spectra of J-aggregates at high pump intensities, 10^{15} - 10^{16} photons/cm^2 (9). They observed a strong negative signal, the sum of a bleach due to depopulation of the ground-state and a stimulated emission due to population of the excited-state; and a positive signal which is excited-state absorption. A fast response faster than their time resolution 10 ps, and a slow response, 400 ps assigned to the lifetime of a single exciton on an aggregate were observed. At high excitation intensities, the excited-state dynamics was exciton-exciton annihilation processes. In their second study (10), they studied temperature dependence of superradiant emission of sodium salt BIC J-aggregates in ethylene glycol/water glass. They measured a lifetime which decreases with increasing temperature in the range of 20-60K, from 100 ps at 8K to 70 ps at 65K. Additionally, emission intensity monotonically decreased with increased temperature in the range 4-100K, indicating the existence of nonradiative decay channel. Possible mechanisms were discussed: internal conversion, nonradiative decay to another excited-state, or intra-aggregate electron transfer. Emission characteristics of sodium salt BIC J-aggregates in solution at room temperature was also reported by the same group (11). A blue shift and narrowing of emission spectrum were observed along with double exponential decay at high excitation intensities. These observations were

explained as one exciton emission and emission from two exciton to one exciton state. Reported one exciton lifetime was 110 ps and the two exciton lifetime was 30 ps.

Nabetani et.al (12) studied absorption and emission spectra of monolayer BIC iodide J-aggregates in the range from 4 to 300K. The main observations were: (a) an asymmetric absorption band due to asymmetry in density of states and an asymmetric oscillator strength around the k=0 exciton state; (b) when k=0 the high energy side is Lorentzian because of exciton-phonon scattering and the low energy side is governed by the probability distrubution of the disordered states; and (c) the peak position shifts to higher energy with decreased temperature due to diminished exciton-phonon coupling. Their conclusion was that two-dimensional (2D) J-aggregates on monolayers were formed in which coherent length of J-aggregate is expected to be larger than one-dimentional (1D) system.

J-aggregates of cyanines have been found on silver and silver halide colloids (19,20). The J-aggregate on colloidal surfaces has been attributed to the coupling of dye molecules in a brickstone arrangement (21). This model assumes that the molecules are lined up on their long edge in a close-packed array. J-aggregates of PIC on colloidal silica has been studied by Quitevis et. al. (22). They measured picosecond electronic energy relaxation dynamics and explained the results in terms of polariton model, an exciton-photon coupling(23).

4.2 Experimental

BIC was purchased from Accurate Chemical and Scientific Co., Westbury, New York. 40 wt% colloidal silica suspension in water, pH=9.7 was purchased from Aldrich Chemical Co., Milwaukee, WI. Other specifications, supplied by the manuacturer (Du Pont), of the silica colloid are 220 m^2/g of specific surface area, 12 nm of average diameter, 452 nm^2 of total surface area, 16 cP of viscosity. All chemicals were used without further purification, and all experiments were conducted at room temperature. All solvents used in this study are spectroscopic grade pure and purchased from Aldrich Chemical Co., Milwaukee, WI.

Absorption spectra were recorded using a Perkin-Elmer Lambda 19, UV-Vis/NIR spectrometer. Steady-state fluorescence, fluorescence excitation and synchronized luminescence spectra were acquired using a SPEX Fluorolog-τ2 spectrofluorometer. Details about Fluorolog-τ2 can be found in the experimental section of chapter 2.

The fluorescence lifetimes of BIC J-aggregate were measured with the HAMAMATSU C4256 picosecond fluorescence lifetime measurement system that is a two dimensional streak camera which enables simultaneous fluorescence lifetime measurement and time-resolved spectrophotometry. The excitation source for the streak camera was a COHERENT mode-locked Nd-YAG synchronously-pumped rhodamine 6G dye laser, producing 5 ps pulses at 76 MHz. The excitation intensity at

the sample was 20 mW (0.23 nJ/pulse). The front-face excitation was used. A 0.25-meter imaging spectrometer with a high pass filter and a CCD detector was used. The dispersion of the system is 0.445 nm/channel. There are 640 channels for the spatial axis of CCD detector. The total dispersion is 284.8 nm. The system resolution in time domain is 25 ps. The typical data collection time was 100 s. The fluorescence decay time were analyzed with the Hamamatsu U4790 fluorescence lifetime analysis software.

The SPEX Fluorolog-τ2 phase-modulation fluorometer was also used to measure fluorescence lifetimes. The details for Fluorolog-τ2 can be found in the experimental section of chapter 2. The phase shift and demodulation factor were obtained for intensity-modulation frequency range from 10 to 250 MHz. At a given frequency, an average of 5 repetitive signal with a 5 s collection time per signal generates the data. A glycogen solution or silica colloid itself, a light scatterer, was used as the lifetime reference. The data were analyzed with the Globals Unlimited software.

4.2 Spectral Properties of BIC Adsorbed on Colloidal Silica

The spectroscopy of molecules adsorbed on surfaces provides information concerning molecular interactions at solid-liquid interfaces. Colloids are convenient systems in order to study molecular interactions

on surfaces (13). We have chosen colloidal silica (SiO_2) due to the absence of either surface-enhanced optical properties (14) or electron transfer between adsorbed molecules and the surface molecules (15). Due to absence of photochemistry on silica surface, it may be a good reference system for energy and charge-transfer studies. Energy and charge-transfer photodynamics on colloidal silica have been studied because of applications to solar energy systems (16,17).

The physical properties of colloidal silica have been studied and documented (18). At pH > 6, the silanol (SiO^-) groups on the surface are ionized and negatively charged; and an electrical double layer is formed. The number of ionized sites at pH= 9.8 which is binding sites per particle are 60-65 (18). A laser flash-photolysis method was employed (24) to estimate number of binding site per particle. By this method, the number of binding site at pH= 9 was estimated to be 32.

In order to prepare adsorbed monomer, 1 mL of 10 μM BIC/MeOH was added into 4mL of 40 wt% colloidal silica suspension in water, pH=9.7. After mixing the dye with colloid; absorption, fluoresence excitation and fluorescence spectra of the sample was taken to observe the formation of adsorbed monomer, as shown in Figure 4.1. In order to prepare J-aggregate, 1 mL of either 0.1 mM or 1 mM BIC/MeOH was added into 4mL of 40 wt% colloidal silica suspension in water, pH=9.7.

The strong electrostatic interactions between cationic BIC and negatively charged silica colloids led to aggregation of BIC molecules on the silica surface. At low BIC concentration, about 10 μM, a red-shifted broad absorption band is observed along with similiar fluorescence excitation spectrum, as shown in Figure 4.2. Figure 4.2 also shows fluorescence spectrum. These spectra are similiar to the monomeric BIC spectra in methanol; i.e., the band shape but not the maximum: a red-shifted broad absorption band ca. at 562 nm and a red-shifted sharp fluorescence band ca. at 568nm. These data suggest an adsorbed monomer The shape and location of the band maxima of the adsorbed dye molecules depend on their structure, surface concentration (adsorbed dye concentration) and nature of substrate (5). Dyes are adsorbed, at low concentrations, as isolated molecules in a flat orientation; this arrangement allows maximum interaction between the delocalized π-electrons of the dye and the substrate. This is the case for the lowest BIC, concentration, 10 μM, used in this study. With increasing surface formation on the silica surface. There are two possibilities: (a) isolated BIC molecules might be vertically adsorbed on their long edge with respect to the surface, or (b) isolated BIC molecules might be adsorbed on their molecular plane (in a flat orientation) with respect to the surface. The equilibrium, assuming one-on-one binding, between BIC molecule and the silica surface may be expressed as

$BIC + SiO_2 \longrightarrow BIC \bullet SiO_2$.

The aggregate formation is observed upon addition of the higher BIC/MeOH to silica colloidal suspension. Figure 4.3 shows the absorption, excitation and fluorescence spectra of the BIC J-aggregate adsorbed onto

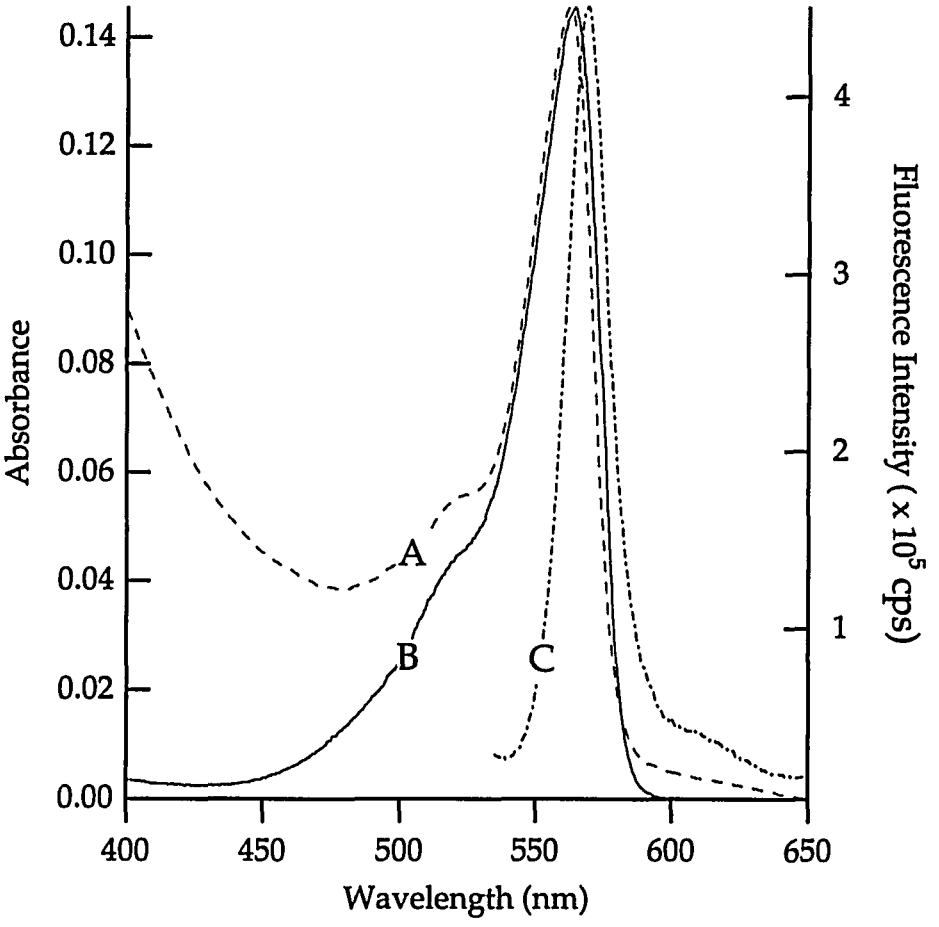

Figure 4.2. Absorption (A), fluorescence (C) and its excitation (B) spectra. 1 mL of 10 μM BIC/MeOH was added into 4mL of 40 wt% colloidal silica suspension in water, pH=9.7. Excited at ca. 550 nm for fluorescence and detected at ca. 585 nm for fluorescence.

negatively charged silica colloid surface. The monomeric dye has characteristic absorption maximum at 514 nm in methanol. In the colloidal silica suspension, two new bands observed while monomer band disappeared. Upon addition of the higher concentrated BIC/MeOH, 100 μM; a residual band at 584.5 nm is observed along with the dominant band at 562 nm in the absorption spectrum (see Figure 4.3). The new band ca. at 584.5 nm is assigned to the J-aggregate. Morever, dramatic changes are observed in fluoresence excitation and fluorescence spectra as is seen in Figure 4.3. In fluorescence spectrum two bands are observed ca. at 568 and 593 nm and assigned to the adsorbed monomer and the J-aggregate fluorescence, respectively. In fluorescence excitation spectrum three bands are observed at 500, 568 and 593 nm. The band at 500 nm indicates H-type aggregate is also formed, even though it is not observed in the corresponding absorption spectrum. The bands ca. at 568 and 593 nm are due to adsorbed monomer and the J-aggregate, repectively. The H-type aggregate generally consists of a dimer unit whereas the J-type aggregate for BIC containing a tetramer unit (5). Dimerization (formation the H-type aggregate) and aggregation (formation the J-type aggregate) take place simultaneously. Based upon these assumptions, the equilibrium between BIC molecules and the silica surface may be expressed as

$$2\ BIC + SiO_2 \longrightarrow (BIC)_2 \bullet SiO_2$$

$$4\ BIC + SiO_2 \longrightarrow (BIC)_4 \bullet SiO_2.$$

At the highest BIC concentration used in this study, 1mM, the H-type and J-type aggregation are observed in the absorption, fluorescence excitation and fluorescence spectra (Figure 4.4). In fluorescence spectrum, one sharp band ca. at 593.5 nm and a shoulder ca. at 630 nm were observed. While the J-band is located at ca. 584.5 nm in the absorption spectrum, it is located at ca. 591 nm in the fluorescence excitation sprctrum. The difference may be related to structure of the J-aggregate in the excited-state. Bird et al. advanced experimental and theoretical evidence for a new model of aggregation on silver colloid surfaces (26). They proposed that the planar molecules pack together at the closest possible interplanar distance and

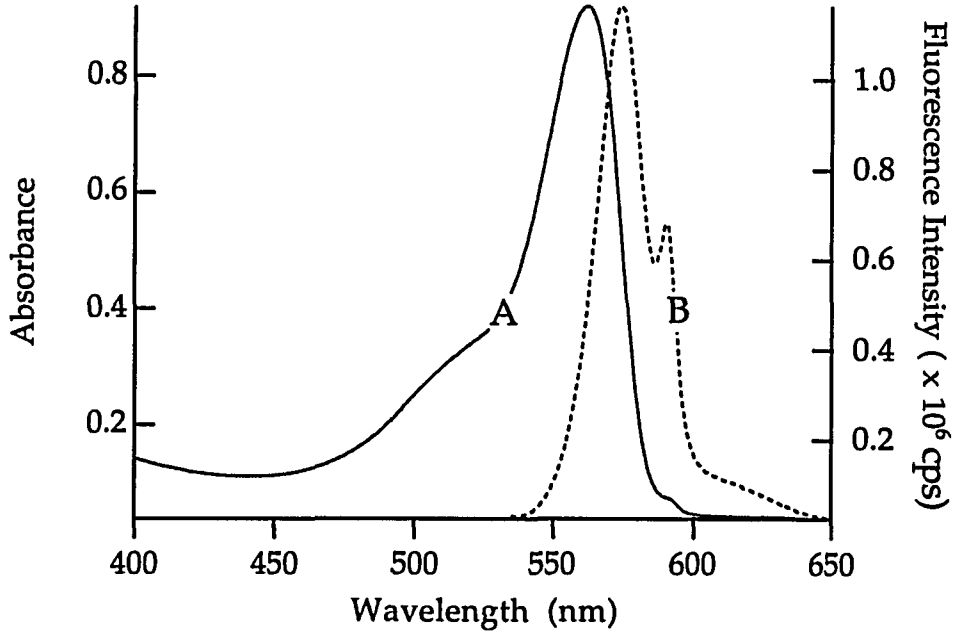

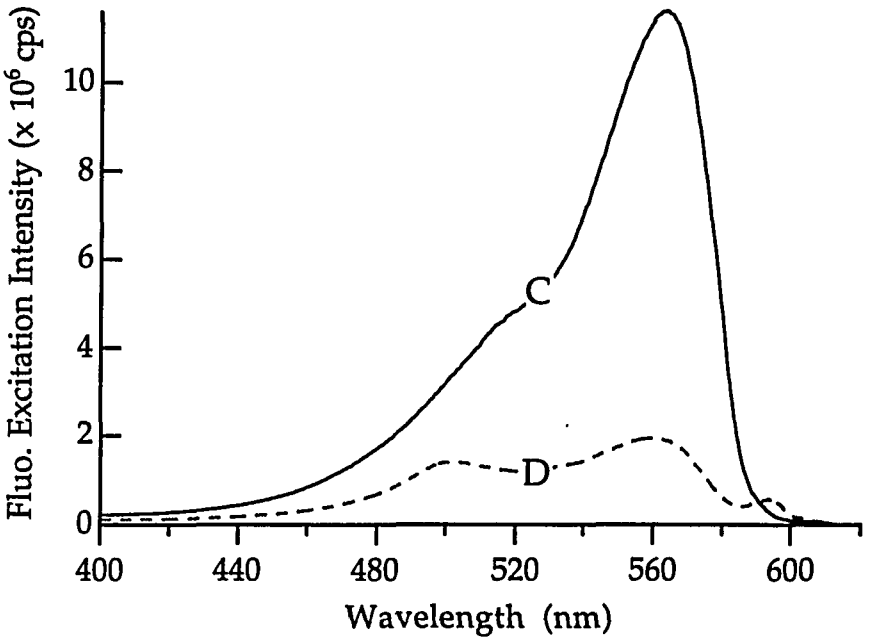

Figure 4.3. Absorption (A), fluorescence (B) and its excitation (C and D) spectra of 1 mL of 100 μM BIC/MeOH added into 4mL of 40 wt% colloidal silica suspension in water, pH=9.7. Excited at ca. 550 nm for fluorescence and its excitation detected at 580 nm (C) and at 595 nm (D).

adsorb with their long edge contacting the surface. The adjacent molecules of the aggregate may be displaced with respect to one another and they may also be tilted with respect to the surface, remaining parallel to one another throughout but overlapping less and less as the displacement and inclination increase. The new feature was the use of a theory of coupled concentration, the cases for 100 μM and 1000 μM BIC in this study, lateral dye-dye interactions play important role and ultimately cause the flat dye molecules to stand on their long edge in a closed-packed

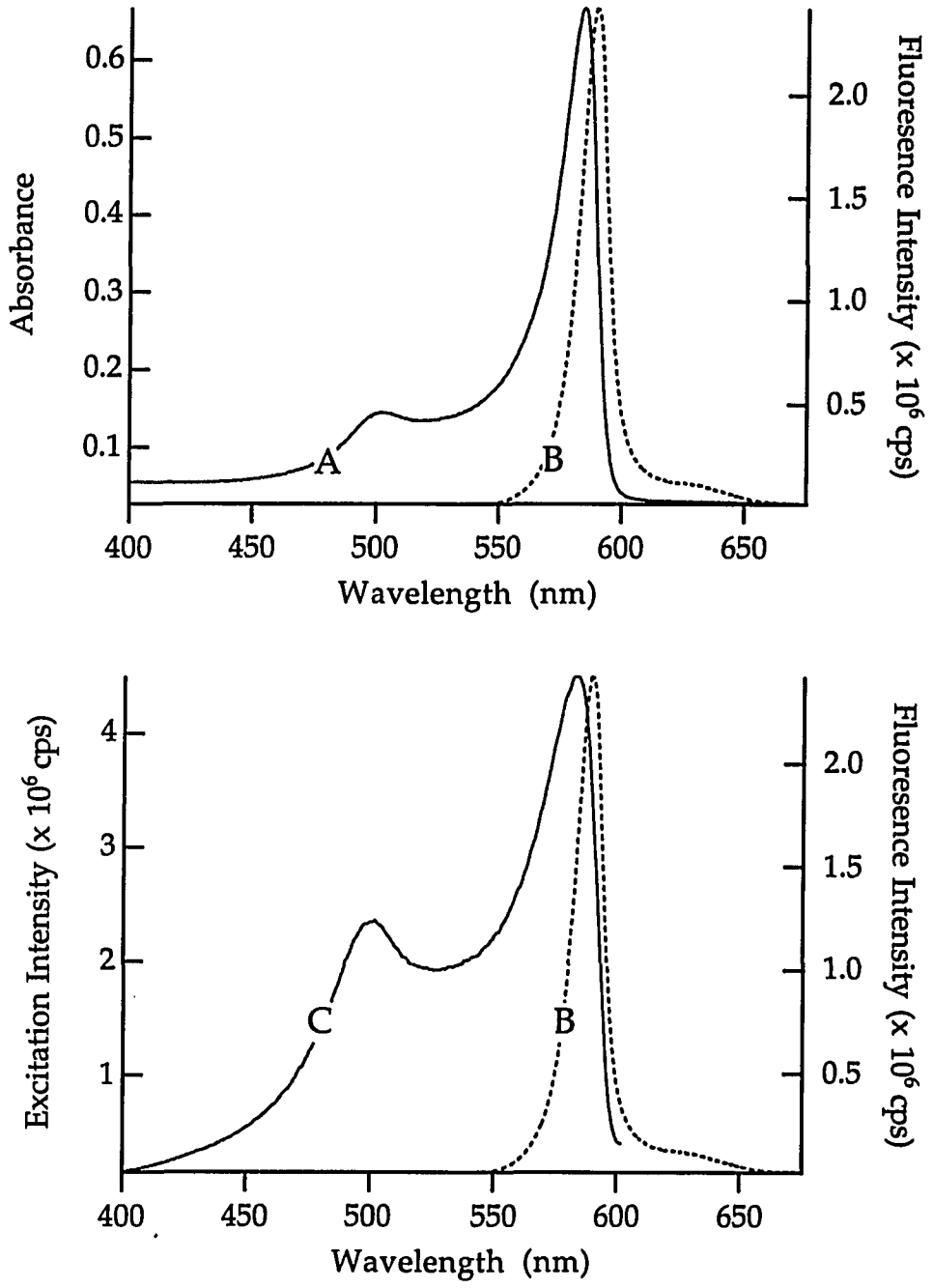

Figure 4.4. The absorption (A), fluorescence (B) and its excitation (C) spectra of the BIC J-aggregates adsorbed onto silica surface. 1 mL of 1 mM BIC/MeOH was added into 4mL of 40 wt% colloidal silica suspension in water, pH=9.7.

array. This change in orientation is accompanied by formation of the dye vertically adsorbed on their long edge, i.e. adsorbed monomer; and H-type and J-type aggregates on the surface.

4.3 Structures of BIC Aggregates Adsorbed on Silica Surface

Models of aggregate structures have generally been advanced theoretically and spectroscopically due to difficulty to grow good single crystal (25). Scheibe and co-workers studied PIC J-aggregates adsorbed on mica surface and concluded that the dye cations were adsorbed edge-on in closed packed monolayers. They postulated two possible epitaxial arrangements of the aggregates on the surface; the ladder and the staircase forms. Bird and co-workers point transition dipoles. The theoretical calculations of Norland and Ames (27) predict that the absorption maxima for all such aggregates will be red shifted with respect to their respective monomer absorption maxima and that the least inclined of these aggregates having least separation and greatest interaction between adjacent chromophores should absorb farthest to the red. Therefore, it is expected to find the lesser tilted dye aggregate on a surface the longer absorption maximum. Additionally, free-standing aggregates in homogeneous solution may be more red shifted.

Structures for the H-type and J-type aggregates may also be proposed based on the exciton theory (28,29). The theory predicts that the basic

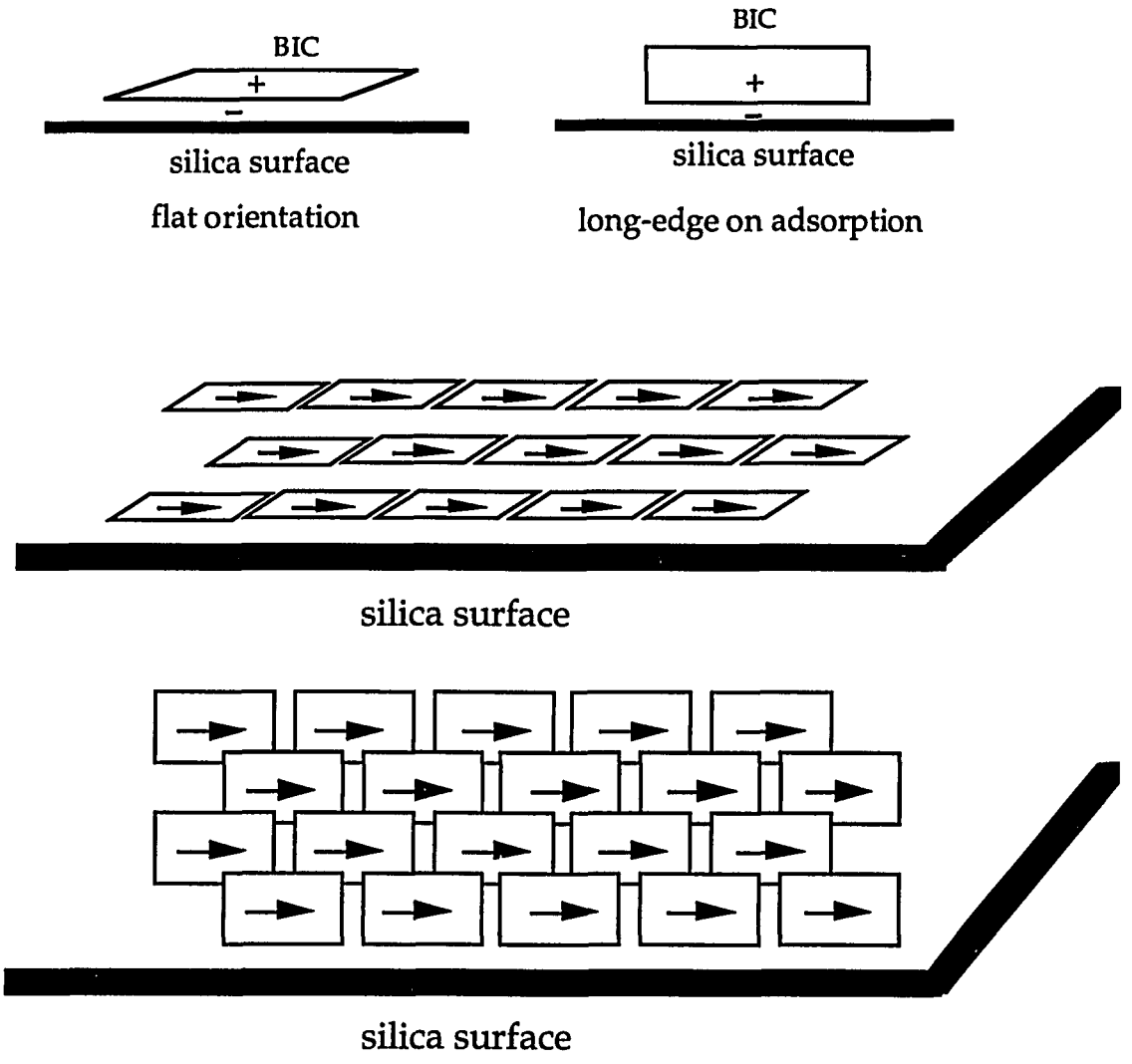

Figure 4.5 The possible structures of BIC aggregates adsorbed on silica surface. The head-to-tail orientation makes J-aggregates while coplanar inclined form favors H-aggregates.

structure of all aggregates is the same but the stacking angle is small, <54° in J-aggregates while it approaches 90° in H-aggregates. The presence of the N,N-diethyl groups of BIC which protrude perpendicular to the plane of the molecule forces the molecules to line up off center from one another at an acute angle. This structure favors J-aggregation. The N,N-

diethyl groups also prevent the molecules from sliding past one another. Hovewer, if the molecules are free to slide out of the arrangenment and line up face to face, H-aggregate will form. Based on the absorption, fluorescence and its excitation spectra, the "proposed" structures for BIC aggregates adsorbed onto silica surface are depicted in Figure 4.5.

4.4 Excited-State Dynamics of BIC J-Aggregates Adsorbed on Silica Surface

In order to obtain information about excited-state dynamics of BIC J-aggregates adsorbed on silica surface, fluorescence lifetimes were measured and picosecond time-resolved fluorescence spectra were obtained.

(A) Fluorescence Lifetime Measurements: Fluorescence lifetime measurements of BIC monomers and J-aggregates adsorbed on colloidal silica surface have been carried out at room temperature with phase-modulation method and with a streak camera. Morever, the lifetime of the absorbed monomer was measured with phase-modulation method.

Samples were prepared as follows briefly: adsorbed monomer, 1 mL of 10 μM BIC/MeOH was added into 4mL of 40 wt% colloidal silica suspension in water, pH=9.7; and J-aggregate, 1 mL of 1 mM BIC/MeOH was added into 4mL of 40 wt% colloidal silica suspension in water, pH=9.7.

The fluorescence lifetime of absorbed monomer was measured with the SPEX fluorolog τ2 phase-modulation fluorometer. The absorbance at 562 nm was 0.09. A 3 mm cell was used, providing 1.5 mm for both excitation and emission path length and right angle excitation was used. Under these conditions, we assume that reabsorption and reemission effects are not considerable . Excitation and emission wavelengths were 550 and 570 nm, respectively. The phase shift and demodulation factor were obtained for intensity-modulation frequency range from 10 to 250 MHz. At a given frequency, an average of 25 repetitive signal acquired to generate the data. A glycogen solution, a light scatterer, was used as the lifetime reference. The data were analyzed with the Globals Unlimited software.

A double exponential decay model was used to fit the data with χ^2 = 1.4. The fluorescence lifetime results are 51 ps with 95 % of the emission, and 705 ps with 5%. The value of 51 ps is very close to the 47 ps, monomer lifetime in methanol. This suggests that BIC monomer in the excited-state does not dramatically change either its structure or energy deactivation pathways. No interactions between silica surface and adsorbed BIC molecules take place because the electronic transitions of silica occur in the ultraviolet range. The longer-lifetime component, 705 ps, indicates a new state formed in the excited-state. This latter state could be an "excimer" or "J-aggregate" itself. Refocusing on adsorbed monomer; the steady-state

fluorescence spectrum of the adsorbed monomer is different than the monomer in methanol: no shoulder was seen, suggesting reduced vibrational transitions. Additionally, the bandwidth of its fluorescence spectrum is clearly narrower than that of monomer in methanol. As is explained in the spectral properties section, BIC molecules may be absorbed in flat orientation on the surface.

The conclusion of this part is that adsorbed BIC molecules do not interact with silica surface and do not change their excited-state structure and energy deactivation channels.

The fluorescence lifetimes of BIC J-aggregate were measured with the Hamamatsu C4256 streak camera. The excitation source for the streak camera was a Coherent mode-locked Nd-YAG synchronously-pumped rhodamine 6G dye laser, producing 5 ps pulses at 76 MHz. The excitation intensity at the sample was 20 mW. The front-face excitation was used. The excitation wavelength was 568 nm. Fluorescence was monitored in the range from 418 to 706 nm with picosecond time resolution. The system resolution was measured as 25 ps before experiments

Figure 4.6 shows the fluorescence decays of BIC J-aggregate adsorbed on colloidal silica surface excited at 568 nm and monitored at varied wavelength ranges. Three different regions were selected from the fluorescence image because they have different image pattern. The data were analyzed by Hamamatsu U4290 fluorescence analysis software. The

quality of fit is judged by the χ^2-test. The results are tabulated in table 4.1. The fluorescence lifetimes indicate fluorescence wavelength dependence. In the region from 580 to 586 nm, the higher-energy side of the fluorescence band peak, has evidenly the shortest decay time. A slower components with a lower percentages in this region is also observed. The lifetimes in the region from 588 to 602 nm, the fluorescence peak region, are longer than those at the higher energy side. Shorter lifetimes again are observed at the lower energy side, from 605 to 640 nm. These results clearly show that the aggregate lifetime varies with fluorescence wavelength, suggesting that excited-state dynamics of BIC J-aggregates depends on coherent aggregate size: delocalized exciton size. The lifetime of the higher energy state is determined 53 ps. As will be clear in the next section (picosecond time-resolved fluorescence spectra), this state is assigned as "repulsive" biexciton state because exciton-exciton interactions take place and form two states: a "repulsive" biexciton and an "attractive" biexciton state. The "repulsive" biexciton state is blue shifted and its lifetime is the shortest one among the three excited states, one-exciton and biexciton states, formed by interacting excitons, i.e. J-aggregates. The "attractive" biexciton state has fluorescence lifetime of 73 ps and red shifted relative to the one-exciton state. Apparently, the biexciton states have different structure and interactions leading to different exciton dynamics.

Table 4.1. The fluorescence lifetime analysis of BIC J-aggregates adsorbed on to silica surface, at room temperature.

$\Delta\lambda_{fluo}$(nm)	τ_1 (ps)	A_1 (%)	τ_2 (ps)	A_2 (%)	τ_3 (ps)	A_3 (%)	χ^2
580-586	—	—	52.6 ± 0.3	81	285 ± 1.4	19	1.03
	25.3 ± 0.2	75	176.7 ± 1.4	22	885 ± 5.7	3	0.95
588-602	81.9 ± 0.7	80	854 ± 8.0	20	—	—	0.92
	75.5 ± 0.7	81	581 ± 5.7	18	5558 ± 23	1	0.91
605-640	—	—	73.0 ± 0.4	93	732 ± 4	7	1.02
	38.1 ± 0.4	73	149 ± 1.4	24	1150 ± 12	3	0.93

1 mL of 1.0 x 10^{-3} M BIC/MeOH was added into 4 mL of 40 wt% silica suspension. Coherent 700 series dye laser pumped by Nd:YAG laser. Excitation wavelength 568 nm and excitation power 20 mW at sample = 2 x 10^{10} photons/cm^2 pulse. FWHM = 25 ps in 1.0 ns sweep rate, 2.44 ps/channel 480 channel on time axis, 1.173 ns. Spectrometer 10 μm slit width, 50 lines/mm, 0.445 nm/channel 640 channel on spectral axis, 284.8 nm.

The one exciton state lifetime is estimated to be 854 ps. Since exciton-exciton interactions take place it is difficult to determine the lifetime of the one-exciton state. However, it is expected that the one-exciton state lifetime should be longer than that of monomer lifetime because the narrower the fluorescence bandwidth the longer the lifetime.

Another important result from these measurements is the origin of the decay: non-exponential decay, because two or three exponential decay

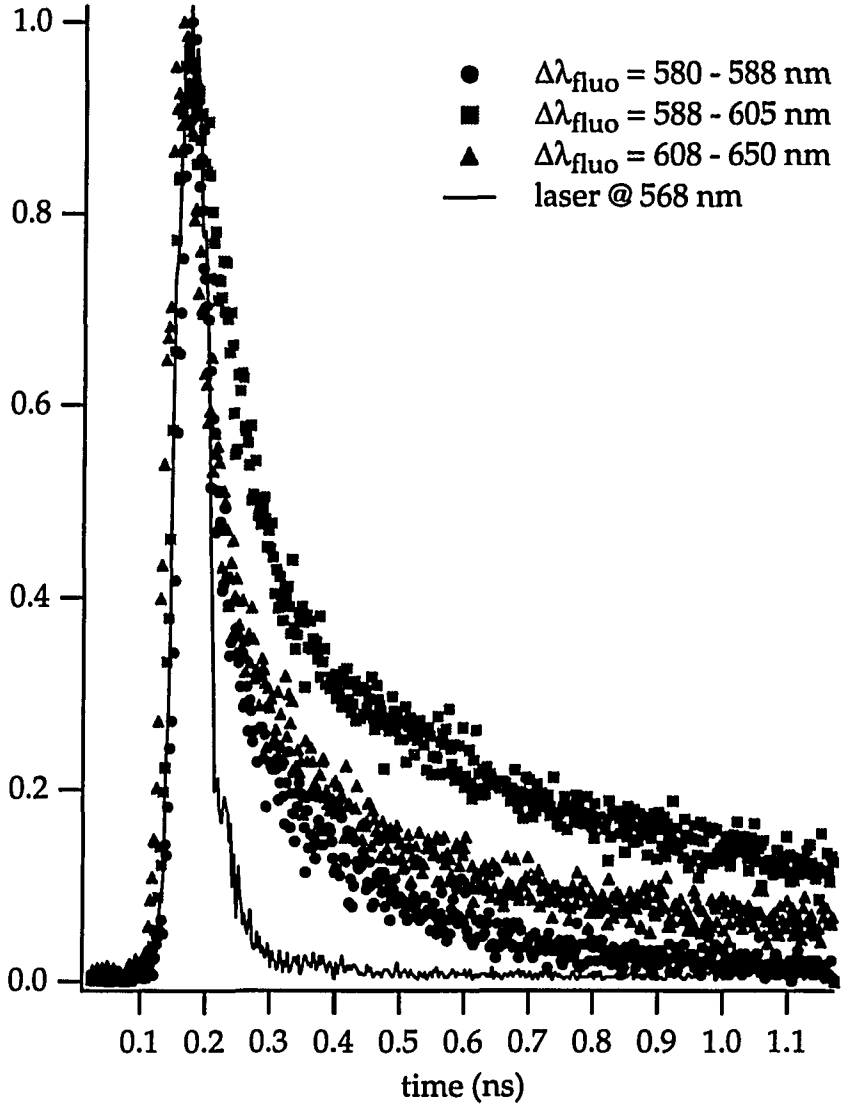

Figure 4.6 The fluorescence decays of BIC J-aggregates on silica surface.

model succesfully fit to the data. The excitation intensity is enough to produce an excited-state concentration causing exciton-exciton interactions: exciton annihilation (9, 11, 30-32). The major deactivation processes are believed to be singlet-singlet annihilation (33) and singlet-

triplet annihilation (34) that is considered to be negligible. Singlet-singlet exciton annihilation reaction can be expressed by the following equation:

$$S_1 + S_1 \xrightarrow{\gamma} S_n^* + S_0 \qquad (4.1)$$

where S_n^* is excited singlet state ($n \geq 1$) and γ is bimolecular rate constant. The process in equ. 4.1 lead to disappearance of one exciton. The excited singlet state S_n^* can either convert internally to S_1 and then decay back to the ground state with emission

$$S_n^* \rightarrow S_1 \rightarrow S_0 + h\upsilon, \qquad (4.2)$$

or it can ionize:

$$S_n^* \rightarrow e^- + h^+. \qquad (4.3)$$

The ionization process is generally less efficient than the electronic deactivation, so it is not considered here. Other annihilation processes involving triplets are possible and will not be considered here due to less efficiency .

The exciton photodynamics in the presence of annihilation have been modeled (30-33, 35-38) and will be discussed below.

Binary Collision of Excitons. This theory was applied to the exciton dynamics of PIC J-aggregates in aqueous solution (31). The theory is

characterized by the following assumptions: (a) the domain over which the excitons migrate is assumed to be sufficiently large such that the exciton density remains constant, (b) the exciton migration rate is assumed to be faster than the single-exciton decay rate; therefore a random distribution of excitons is maintained over the domain. The exciton decay rate is described by the differential equation

$$\frac{d[S_1]}{dt} = -k[S_1] - \gamma[S_1]^2. \qquad (4.4)$$

where $[S_1]$ is the exciton concentration, k is the single-exciton decay rate and γ is the exciton annihilation rate.

Exciton Migration in Reduced Dimensions. Assumptions for this theory are: (a) exciton migration is confined to the one- or two-dimensional domain; (b) exciton migrates through long range dipole-dipole interactions or via diffusion, i.e. hopping like motion. The exciton decay rate is given by the following equation

$$\frac{d[S_1]}{dt} = -k[S_1] - \frac{\gamma}{2}t^{-h}[S_1]^2 \qquad (4.5)$$

where $[S_1]$ is the exciton concentration, k is the single-exciton decay rate and h=1-d/2, is related to the dimensionality, d; $1 \le d < 2$. The values of h vary depending upon the dimensionality of the exciton motion. This model is applied to triplet excitons in fractal dimensions (37,38) and one

dimensional exciton annihilation in colloidal phthalocyanine (36). The results of latter study are: (a) exciton transfer between different molecular species was suggested to explain the exciton dynamics ≤ 1 ps regime; (b) exciton decay was found to be dominated by singlet-singlet annihilation with a $t^{-1/2}$ time dependence, which suggested a one-dimensional exciton diffusion; (b) intermolecular exciton hopping time of 0.2 - 1 ps was determined.

Very recently, the result of a temperature dependent fluorescence study of BIC aggregates embedded in poly(vinyl alcohol) was that the effective dimensionality was fractal with d=1.8 (39). Another result of this study was that a self-trapped exciton state, a red-shifted emission with 330 ps at 4K, formed.

Exciton Migration in Restricted Domains. Theory of exciton annihilation in confined domians, developed for photosynthetic systems, assumes that; (a) Exciton is randomly distributed over domian and energy transfer time is sufficiently smaller than the characteristic exciton annihilation time; (b) the depletion of ground-state is considered to be negligible; (c) the exciton coherence time is extremly short so that random hopping like motion of exciton describes the energy transfer processes. No assumptions concerning the dimensions of the domains were made in this theory.

At sufficiently low excitation intensities only one exciton is created per domain. When several excitons are created simultaneously in a given domain, exciton-exciton annihilation processes are possible. It is assumed that excitons in different domains cannot interact with each other. When initial exciton density is not large enough, e.g. 1 exciton per 10 molecules , exciton-exciton annihilation is considered to be negligible. The major deactivation process is believed to be singlet-singlet annihilation. Singlet-triplet annihilation is considered to be negligible. Singlet-singlet annihilation leads to disapperance of one exciton (Equ. 4.6) or both excitons (Equ. 4.7)

$$S_1 + S_1 \xrightarrow{\gamma(1)} S_n^* \rightarrow S_1 + S_0 \tag{4.6}$$

$$S_1 + S_1 \xrightarrow{\gamma(2)} S_n^* \rightarrow \begin{matrix} T_1 + S_0 \\ S_0 + S_0 \\ T_1 + T_1 \end{matrix} \tag{4.7}$$

where $\gamma(1)$ and $\gamma(2)$ is the appropriate annihilation rate constants and T_1 is the lowest triplet state. The exciton decay rate equation is given

$$\frac{d[S_1]}{dt} = -k[S_1] - \left(\gamma(2) + \frac{\gamma(1)}{2}\right)[S_1]^2 \tag{4.8}$$

where $[S_1]$ is the exciton concentration, k is the single-exciton decay rate. This model was applied to PIC J-aggregates in aqueous solutions (30). The

results of the study are: (a) both the fluorescence lifetime and quantum yield are strongly dependent on excitation pulse intensity; (b) at low excitation intensities, 10^{10} photons/cm^2. pulse, a single exponential lifetime of 400 ps and at higher intensities nonexponential decay were observed; (c) observed intensity dependence of excited-state dynamics was attributed to the exciton-exciton annihilation; (d) the exciton transport over the domain was described as a hopping motion; (e) the domian over which excitons move freely is 50 - 20,000 monomer units.

The fluorescence intensity decay of BIC J-aggregates adsorbed onto silica surface is obtained solving the rate equation numerically. The equation is

$$\frac{d[S_1]}{dt} = \alpha I - k[S_1] - \frac{\gamma(1)}{2}[S_1]^2 \qquad (4.9)$$

here α is absorption cross-section, 2.8 x 10^{-13} cm^2, I is excitation intensity, 2x10^{10} photons/cm^2 sec. $\gamma(1)$is used and $\gamma(2)$ is considered to be negligible. The excitation pulse is assumed to be gaussian. The annihilation rate constant is estimated to be 10^{12} sec^{-1}. This suggests exciton-exciton annihilation is very strong for BIC J-aggregates. It indicates that even for low excitation intensities used, highly concentrated excited-states are created.

B) Picosecond Time-Resolved Fluorescence Spectra of BIC J-Aggregates

Picosecond time-resolved fluorescence spectra of BIC J-aggregates adsorbed onto silica surface have been measured at room temperature. The streak camera was used to obtain time-resolved fluorescence spectra. Figure 4.7 shows the time-resolved spectra. The sample is freshly prepared in the same way described in the experimental section.

The time origin, t = 0 ps, corresponds to the pulse starting time of the laser. However, it is chosen because of the physical fact: exciton generation starts when the first photon collides with aggregates.

The time-resolved spectra show three distinctive bands located at ca. 585, 596 and 625 nm. The assignment of these bands will be discussed with their time evolution. The band at ca. 625 nm appears dominant at early times, from 0 to 10 ps regime. The band at ca. 596 nm in the early regime (till 25 ps) is weaker than the band at 625 nm. Both bands, at 596 and 625 nm, are also seen in the steady-state spectrum (see Fig. 4.4); while the 596 nm band was assigned to the 0-0 transition of the J-aggregate, the assigment of the band at 625 nm is made tentatively to the vibronic transitions of the J-aggregate. In the time-resolved fluorescence spectra, the 596 nm becomes dominant from 25 to 1000 ps while the band at 625 nm becomes weaker as time evolves and totally disappears about 400 ps after laser excitation. The band at 596 nm is assigned to the one-exciton state. The band at 585 nm appears with delay: about 40 ps after laser

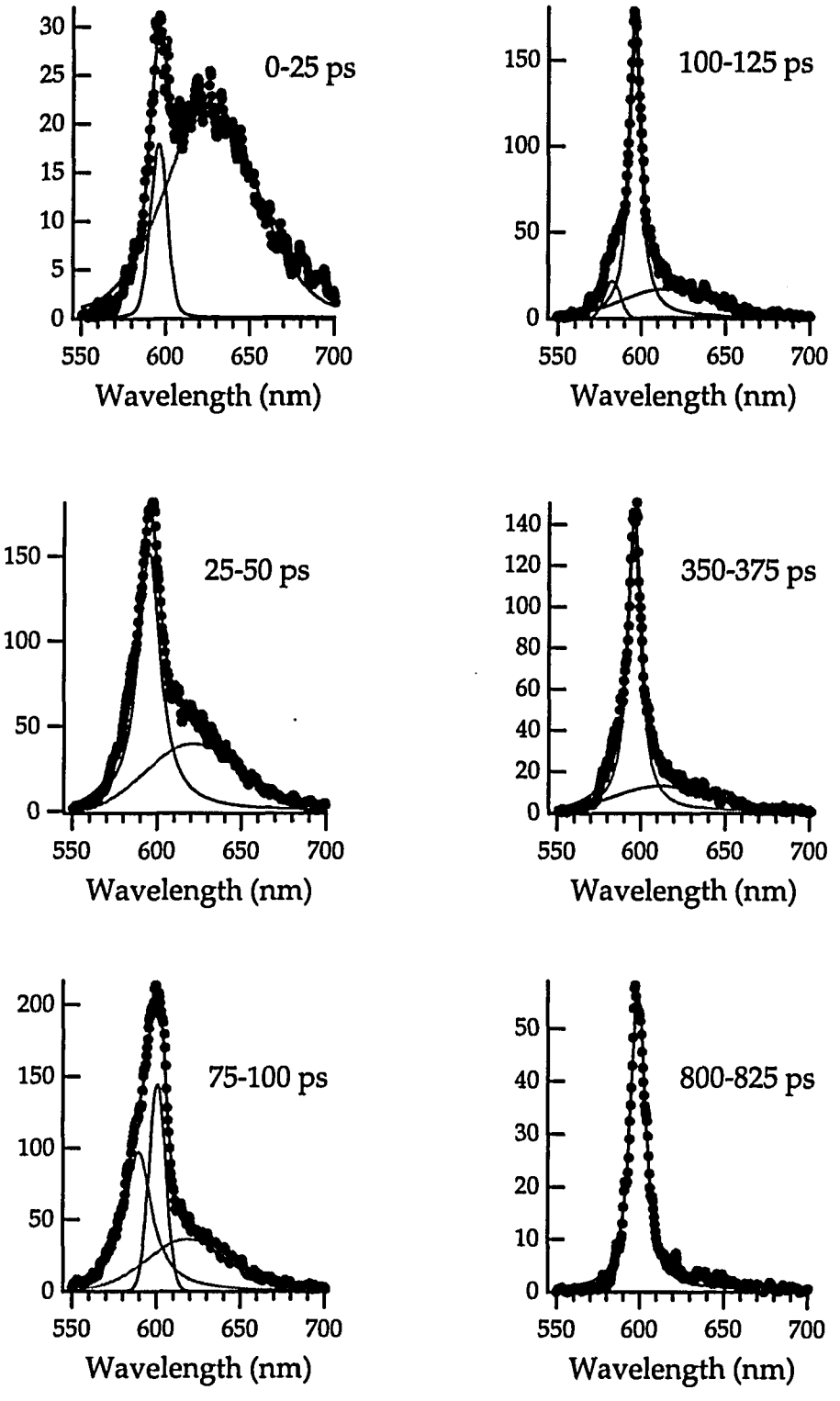

Figure 4.7 The picosecond time-resolved fluorescence spectra of BIC J-aggregates.

excitation. Apparently, the formation of this band takes time, suggesting an excited-state reaction is necessary to create a new specie in the excited-state. At the beginning, exciton are created very fast, probably in femtosecond: generation starts when the first photon arrives to the sample. When two exciton come close to each other exciton-exciton interactions then take place. As a result of the interaction, new states in addition to the one-exciton state are created: a "repulsive" and "attractive" states. To create these states, at least two excitons should interact through dipole-dipole coupling, diffusion or collision. Since two excitons, at least, are required to form the states they might be named "repulsive" biexciton, a blue-shifted state relative to the one-exciton state, and "attractive" biexciton state, a red-shifted state relative to the one-exciton state. These photophysical processes can be summarized as follows:

$S_0 + h\nu_{exc} \rightarrow E^*$ exciton formation

$E^* + E^* \rightarrow (E^* \cdots E^*)$ exciton-exciton interaction

$(E^* \cdots E^*) \rightarrow B_r^* + B_a^*$ "repulsive" and "attractive" biexciton formation

$E^* \rightarrow h\nu_{fluo}(596nm)$ one-exciton (J-aggregate) fluorescence

$B_r^* \rightarrow h\nu_{fluo}(585nm)$ "repulsive" biexciton fluorescence

$B_a^* \rightarrow h\nu_{fluo}(625nm)$ "attractive" biexciton fluorescence

where S_0 is ground state, E^* is one-exciton (Jaggregate) state, B_r^* and B_a^* are repulsive and attractive biexciton states, respectively.

The band at 596 nm is assigned to the one-exciton state. This state forms fast, i.e. it follows laser excitation without any delay, indicating laser pulse limited formation. Therefore, its formation time should be in femtosecond. It decays within 850 ps, as is expected because of the narrower the bandwidth the longer the lifetime of the state. However, there is another component, an induced form of the one-exciton state with decay time of 80 ps due to exciton annihilation. The lifetime of the one-exciton state is sufficiently long to build up exciton concentration leading to interactions through dipole-dipole coupling or diffusion. Binary collision of excitons is unlikely because it should create a state that absorb (emit) around 300 nm which is not observed. Therefore, dipolar interactions or exciton diffusion remain as interaction mechanisms.

The evidence of formation of biexciton states is clearly seen from the picosecond time-resolved fluorescence spectra: a shoulder at the higher energy side appears as time evolves and vanishes completely 150 ps after laser excitation. The higher energy state is therefore assigned to the "repulsive" biexciton state. When the time-resolved spectra is decomposed the "repulsive" biexciton state band position is found at ca. 585 nm. The formation of this state takes 40 ps and decays within 53 ps due to its repulsive nature. A red-shifted band relative to the one-exciton

band appear in the spectrum at the very beginning: this lower-energy state is assigned to the "attractive" biexciton state located at ca. 625 nm. The "attractive" biexciton state forms very fast, less than the time resolution of our system, 25 ps, and then decays within 73 ps. The lower energy band for J-aggregates have been assigned as being remnant monomer fluorescence (40) and/or a sandwich dimer fluorescence adsorbed on silver colloid surface(41). The lifetime of the sandwich dimer was also reported as 10 ps; and assigned as trap state quenching superradiance. The higher energy band for J-aggregates have been assigned to biexciton state (42,43) and a transition from two-exciton state to one-exciton state (11,44-46).

Assuming dipolar interaction occurs, the dipole-dipole coupling, i.e. the energy needed for the exciton-exciton reaction could be estimated. The dipole-dipole coupling constant for the "repulsive" biexciton is about +315 cm^{-1}; and for the "attractive" biexciton -780 cm^{-1}. Since the room temperature thermal energy is about 210 cm^{-1} thermal excitation is unlikely to create biexcitons.

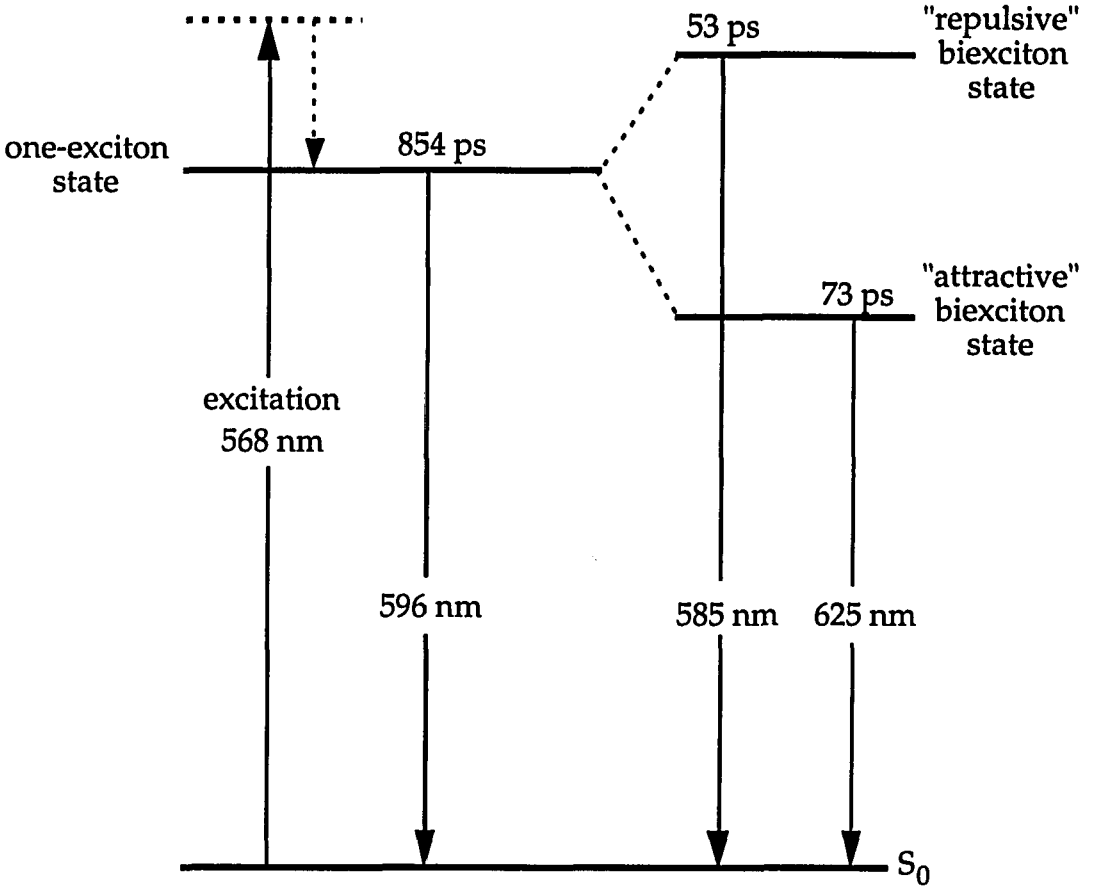

Figure 4.8. The kinetic model for BIC J-aggregates adsorbed on silica surface.

Two important processes have been ignored in this model: exciton-phonon interactions and excitonic relaxations. Exciton-phonon interactions have been invoked as the mechanism for exciton localization in J-aggregates. Exciton relaxation could lead to a time-dependent decrease in exciton size.

In conclusion; the exction dynamics can be summarized as follows: following laser excitation, excitons are created probably in femtosecond,

forming the one-exciton state. Exciton-exciton interactions then take place and form two states in addition to the one-exciton state: a "repulsive" and "attractive" state. To create these states, at least two excitons should interact through dipole-dipole coupling. They may be named as "repulsive" biexciton, a blue-shifted state relative to the one-exciton state, and "attractive" biexciton state, a red-shifted state relative to the one-exciton state. The kinetic model for explaning the exciton dynamics is depicted in Figure 4.8.

REFERENCES

1. Zuckerman, B. Photo. Sci. Eng. 1967, 11, 156.

2. Gray, W. E; Brewer, W.R; Bird, G. R. Photo. Sci. Eng. 1970, 14, 316.

3. Hochstrasser, R. M.; Kasha, M Photochem. Photobiol. 1964, 3, 317.

4. Smith, D. L.; Luss, H. R. Acta Crystallogr., Sec. B 1972, 28, 2793.

5. Herz, A. H Photo. Sci. Eng. 1974, 18, 323.

6. O'Brien, D. F. Photo. Sci. Eng. 1973, 17, 226.

7. O'Brien, D. F. ; Kelly, T. M.; Costa, L. F. Photo. Sci. Eng. 1974, 18, 76.

8. Lindbrum, M; Glismann, A.; Moll, J.; Daehne, S. Chem. Phys. 1993, 178, 423.

9. Johnson, A. E.; Kumazaki, S.; Yoshihara, K. Chem. Phys. Lett. 1993, 211, 511.

10. Kamalov, V. F.; Struganova, I. A.; Tani, T., Y.; Yoshihara, K. Chem. Phys. Lett. 1994, 220, 257.

11. Kamalov, V. F.; Struganova, I. A.; Koyama, Y.; Yoshihara, K. Chem. Phys. Lett. 1994, 226, 132.

12. Nabetani, A.; Tomioka, A.; Tamaru, H.; Miyano, K J. Chem. Phys, 1995, 102, 5109.

13. Thomas, J. K. J. Phys. Chem., 1987, 91, 267.

14. Weitz, D. A; Garoff, S.; Gersten, J. I.; Nitzan, A. J. J. Chem. Phys. 1983, 78, 5324.

15. Fox, M. A. Acc. Chem. Res. 1983, 16, 314.

16. Laane, C.; Willner, I.; Calvin, M. Proc. Natl. Acad. Sci., 1981, 78, 5928.

17. Willner, I.; Laane, C.; Otvos, J. W.; Calvin, M. In Inorganic Reactions in Organized Media; Holt., S. L., Ed.; American Chemical Society, Washington, DC, 1982, ACS Semp. Series No. 177, pp 71-95.

18. Iler, R. K. The Chemistry of Silica, 2nd edition; Wiley: New York, 1979.

19. Herz, A. Adv. Colloid. Interfac. Sci., 1977, 8, 237.

20. Herz, A.; Danner, R. P., Janusonis, G. A. In Adsorption from Aqueous Solution; Gould, R. F.; Ed.; American Chemical Society, Washington, DC, 1968, ACS Semp. Series No. 79, pp 173-197.

21. Czikklely, V. Forsterling, H. D.; Kuhn, H. Chem Phys. Lett., 1970, 6, 207.

22. Quitevis, E. L.; Horng, M-L.; Chen, S-Y. J. Phys. Chem., 1988, 92, 256.

23. Philpott, M. R. J. Chem. Phys., 1975, 63, 485.

24. Kamat, P. V.; Ford, W. E. J.Phys. Chem. 1989, 93, 1405.

25. Smith, D. L. Photo. Sci. Eng. 1974, 18, 309.

26. Emerson, E. S; Conlin, M. A.; Rosenoff, A. E.; Norland, K. S.; Rodriguez, H.; Chin, D.; Bird, G. R. J.Phys. Chem. 1967, 71, 2396.

27. Norland, K. S; Ames, A. E Photo. Sci. Eng. 1970, 14, 295.

28. McRae, E.; Kasha, M. J. Chem. Phys. 1958, 28, 721.

29. Kasha, M. In Physical Processes in Radiation Biology. Academic Press, New York, 1964.

30. Sundstrom, V.; Gillbro, T.; Gadonas, R. A.; Piskarkas, A. J. Chem. Phys., 1988, 89, 2754.

31. Brumbaugh, D. V.; Muenter, A. A.; Knox, W.; Mourou, G; Wittmershaus, B. J. Lumin., 1984, 31 and 32, 783.

32. Reid, P.; Higgins D. A.; Barbara, P. J. Phys. Chem., 1996, 100, 3892.

33. Paillotion, G.; Swenberg, E.; Breton, J.; Geactinov, N. E. Biophys. J., 1979, 25, 513.

34. Pope, M. and Swenberg, E. In Electronic Processes in Organic Crytals. p158-161.

35. Dexheimer, S. L.; Vareka, W. A.; Mittleman, D., Zettl, A.; Shank, C. V. Chem. Phys. Lett., 1995, 235, 552.

36. Gulbinas, V.; Chachisvilis, M.; Persson, A.; Svanberg, S.; Sundstrom, V. J. Phys. Chem., 1994, 98, 8118.

37. Kopelman, R.; Parus, S.; Prasad, J. Phys. Rev. Lett., 1986, 56, 1742.

38. Klymko, P. W.; Kopelman, R. J. Phys. Chem. 1983, 87, 4565.

39. Kamalov, V; Yoshihara, K. Time-resolved vibrational spectroscopy VII, p 28, 1995.

40. De Boer, S.; Wiersma, D. A. Chem. Phys. 1987, 131, 135.

41. Muenter, A. A.; Brumbaugh, D. V.; Apolito, J.; Horn, L. A.; Spano, F. C.; Mukamel, S. J. Phys. Chem. 1992, 2783.

42. Spano, F. C. Chem. Phys. Lett., 1995, 234, 29.

43. Gagel, R.; Gadonas, R.; Laubereau, A. Chem Phys. Lett. 1994, 217, 228.

44. Fidder, H; Knoester, J.; Wiersma, D. A. J. Chem. Phys. 1993, 98, 6554.

45. Minoshima, K.; Taiji, M.; Misawa, K.; Kobayashi, T. Chem. Phys. Lett. 1994, 218, 67.

46. Durrant, J. D.; Knoester, J.; Wiersma, D. A. Chem. Phys. Lett. 1994, 222, 450.

CHAPTER 5

SPECTROSCOPY AND EXCITED-STATE DYNAMICS OF THIACARBOCYANINE J-AGGREGATES

Spectroscopy and fluorescence dynamics of 3,3'-dimethyl-9-phenyl-5,5'-dibenzothiacarbocyanine chloride (DBTC) J-aggregates are studied. The J-aggregates are formed in homogeneous solution and on silica surface: the difference between the J-aggregates in different environment will be discussed in terms of electronic structure and exciton dynamics. The chemical structure of DBTC is shown below.

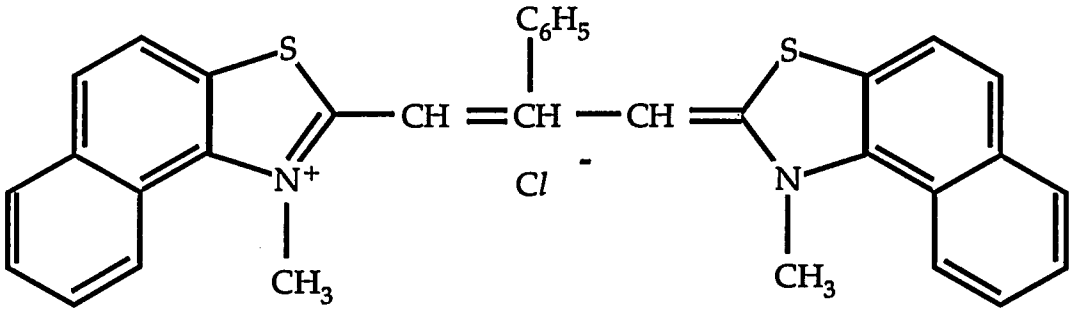

3,3'-dimethyl-9-phenyl-5,5'-dibenzo-thiacarbocyanine chloride (DBTC)

The body of literature for DBTC studied here is concentrated on some spectroscopic and mostly exciton energy transfer between J-aggregates in monolayers and adsorbed on vesicle surfaces (1-9). As

regards exciton dynamics some studies for analog dyes are found (10-14). Exciton dynamics is found being varied based on aggregate system: electron transfer to substrate, exciton-exciton annihilation and energy-dependent exciton-phonon scattering.

5.1 Experimental

The DBTC were purchased from Nippon Kanko Shikiso Co. Ltd., Okayama, Japan. 40 wt% colloidal silica suspension in water, pH=9.7 was purchased from Aldrich Chemical Co., Milwaukee, WI. Other specifications, supplied by the manuacturer (Du Pont), of the silica colloid are 220 m^2/g of specific surface area, 12 nm of average diameter, 452 nm^2 of total surface area, 16 cP of viscosity. All chemicals were used without further purification, and all experiments were conducted at room temperature. All solvents used in this study were spectroscopic grade pure and purchased from Aldrich Chemical Co., Milwaukee, WI.

Absorption spectra were recorded using a Perkin-Elmer Lambda 19, UV-Vis/NIR spectrometer. Steady-state fluorescence, fluorescence excitation and synchronized luminescence spectra were acquired using a SPEX Fluorolog-τ2 spectrofluorometer.

The fluorescence lifetimes of DBTC J-aggregates were measured with the HAMAMATSU C4256 picosecond fluorescence lifetime

measurement system. The heart of the system is a two dimensional streak camera which enables simultaneous fluorescence lifetime measurement and time-resolved spectrophotometry. The excitation source for the streak camera was a COHERENT mode-locked Nd-YAG synchronously-pumped Kiton-Red dye laser, producing 5 ps pulses at 76 MHz. The time resolution of the system in singlet-shot operation was 20 ps. A CCD equiped 0.25-meter imaging spectrometer with a high pass filter was used for lifetime and time-resolved fluorescence measurements. The typical data collection time was 100 s. The fluorescence decay times were analyzed with the Hamamatsu U4790 fluorescence lifetime analysis software.

5.2 Steady-State Spectroscopy of DBTC J-Aggregates

(A) J-Aggregates in homogeneous solutions

Figure 5.1 shows the absorption and fluorescence spectra of DBTC J-aggregate in homogeneous solution and monomer absorption spectrum as a reference. The J-aggregate forms upon mixing the dye solution with water (1 ml of 1.0×10^{-3} M DBTC/MeOH added into 4 ml of water containing 0.01 M KCl). A red-shifted, relatively narrow band located at ca. 700 nm and a shoulder at ca. 600 and another band at 548 nm appeared in the absorption spectrum. The red-shifted band at ca. 700 nm is assigned to the 0-0 transition of the J-aggregate (J-band). The shoulder and the other band are tentatively assigned to the vibronic transitions. Another

possibility for them would be transitions of the monomer whose preserved its individuality. But, this latter assignment seems unlikely because the band at 548 nm is blue shifted and the shoulder is red shifted relative to the monomer in MeOH solution. The band at 548 nm might be also assigned to H-aggregate or H-dimer. At this moment, these latter two will be assigned to the vibronic transitions of the J-aggregate.

The J-aggregate bandwidth is 470 cm^{-1} and is broad relative to the bandwidths of PIC and BIC J-aggregates, as discussed in the earlier chapters.

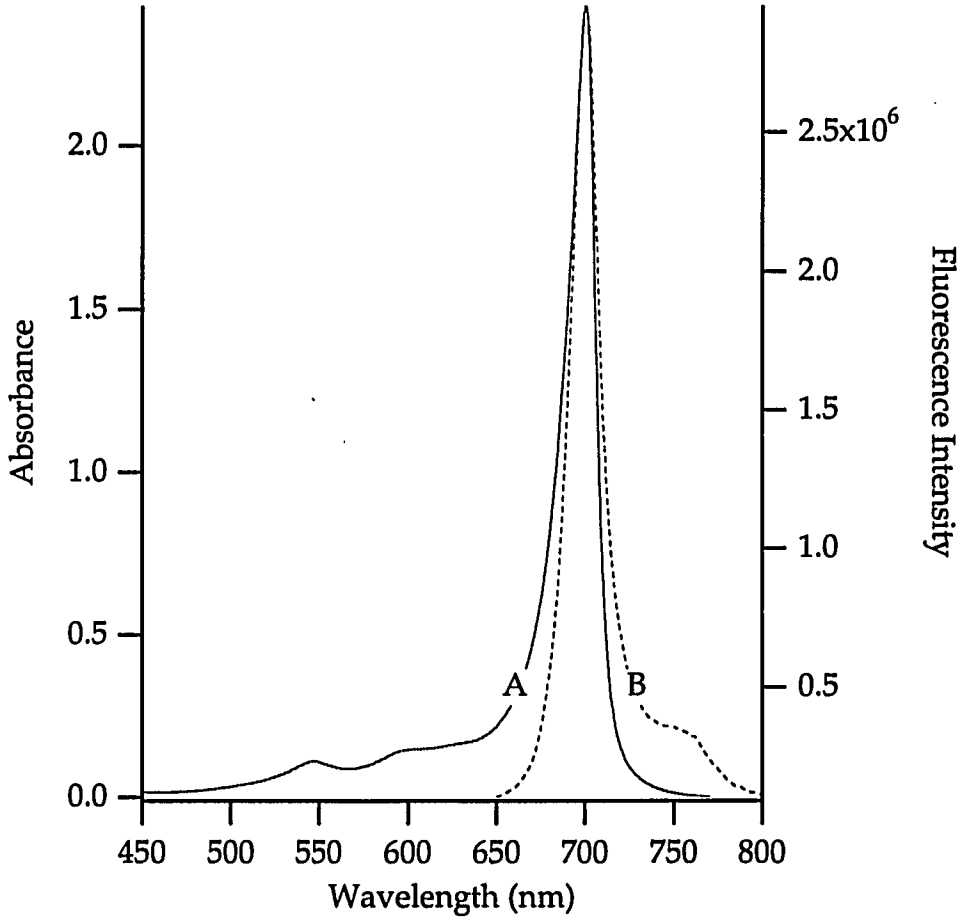

Figure 5.1. Absorption (A) and fluorescence (B) spectra of DBTC J-aggregate formed in homogeneous solution.

This indicates that the phenyl group attached in the meso position plays an important role and effects the J-aggregate structure. The narrowness results from the delocalized exciton states of the aggregate. The narrower the band the stronger the interactions in the aggregate which implies that the monomer units in the aggregate are well aligned; leading to longer delocalization length. However, in this case the J-band is relatively broad; suggesting smaller delocalization of excitons because of the phenyl substituent. The phenyl group protrudes to the molecular plane to reduce hindrance between phenyl and the thiazole groups (3). Since the phenyl is a bulky substituent, the hindrance is likely between the nearest-neighbor monomer units in the J-aggregate. The distance will increase to reduce the hindrance between the monomers in the aggregate. Since the distance is related to the intermolecular interactions and exciton delocalization, it is reasonable to expect decreasing interactions that causes smaller delocalization, i.e., broader bandwidth.

The fluorescence band of DBTC J-aggregate in homogeneous solution is at ca. 700 nm. The fluorescence band is not shifted relative to the absorption spectrum, this is a "resonance fluorescence". The fluorescence bandwidth is about 490 cm^{-1}. The maximum of the fluorescence band and its bandwidth do not change with excitation wavelengths, from 500 to 650 nm; additionally no Stokes shift. These

observations indicates excitonic relaxations does not occurs in the exciton states of aggregate. Morever, they suggest that the aggregate structure in the excited-state should be same that of the ground-state structure. The observations also suggest that the relaxed exciton size and the size of the exciton immediately following excitation, i.e., the size of the created exciton, are the same. As a result, the exciton can be identified as "free exciton" which moves fast in the delocalized aggregate domain. By definition, free-exciton luminescence involves initial electronic states which may be very similiar, or close in energy to, the states responsible for absorption (15).

Additionaly, a shoulder at ca. 750 nm appears in the fluorescence spectrum of the J-aggregate, see Figure 5.1. Since vibronic transitions are observed in the absorption spectrum, it is believed that they could be related to the vibronic transitions in the aggregate; from the lowest excitonic level, k=0, to the vibrational levels of the ground state. It is true, the lifetime of this emission should be a few picosecond.

(B) J-Aggregates adsorbed on silica surface

Figure 5.2 shows the absorption and fluorescence spectra of DBTC J-aggregate adsorbed on silica surfaces at room temperature. The spectral properties of the adsorbed J-aggregate is remarkably changed: suggesting structurally different aggregate formed on the surface. Aggregation takes place immediately when the dye solution and silica colloid mixed. Upon

aggregation, a red-shifted band at ca. 675 nm is observed in the absorption spectrum. The red-shifted band is assigned to the formation of J-aggregates adsorbed on silica surface (J_a-band). The shoulder is presumably related to vibronic transition as discussed above. The J_a-band is very broad, 1230 cm^{-1}, comparing to the bandwidth of J-aggregate in homogeneous solution. This broadness implies that structurally different aggregates would be formed on the surface. The dimension or length of aggregate should be small in which monomer units are coupled; leading to smaller aggregate size. Upon comparison, the J_a-band is less red-shifted and broader than the J-band for the aggregates in homogeneous solution. These observations lead to a conclusion that structurally different aggregates adsorbed on the silica surface could be formed and weakly interact while the aggregates formed in homogeneous solutions are strongly coupled and possible, one type of aggregate may exists. It is expected that dynamics of the J-aggregate in homogeneous solution and adsorbed on the surface should be different: faster fluorescence decay times may be anticipated for the J-aggregate in homogeneous solution.

The J-aggregate fluorescence spectrum has one band at ca. 691 and and a shoulder at ca. 750 nm. The fluorescence spectrum shows no excitation wavelength dependency. However, there is a Stokes shift: 350 cm^{-1}. This Stokes-shift indicates the aggregate structure in the excited-state should be changed comparing to the ground-state structure. This

observation suggests that the relaxed exciton size is substantially different from the exciton size created immediately upon excitation. It is likely that excitonic relaxations take place in the exciton states of the J-aggregate adsorbed on silica surface. If the nonradiative relaxations are dominant then very short decay times are expected.

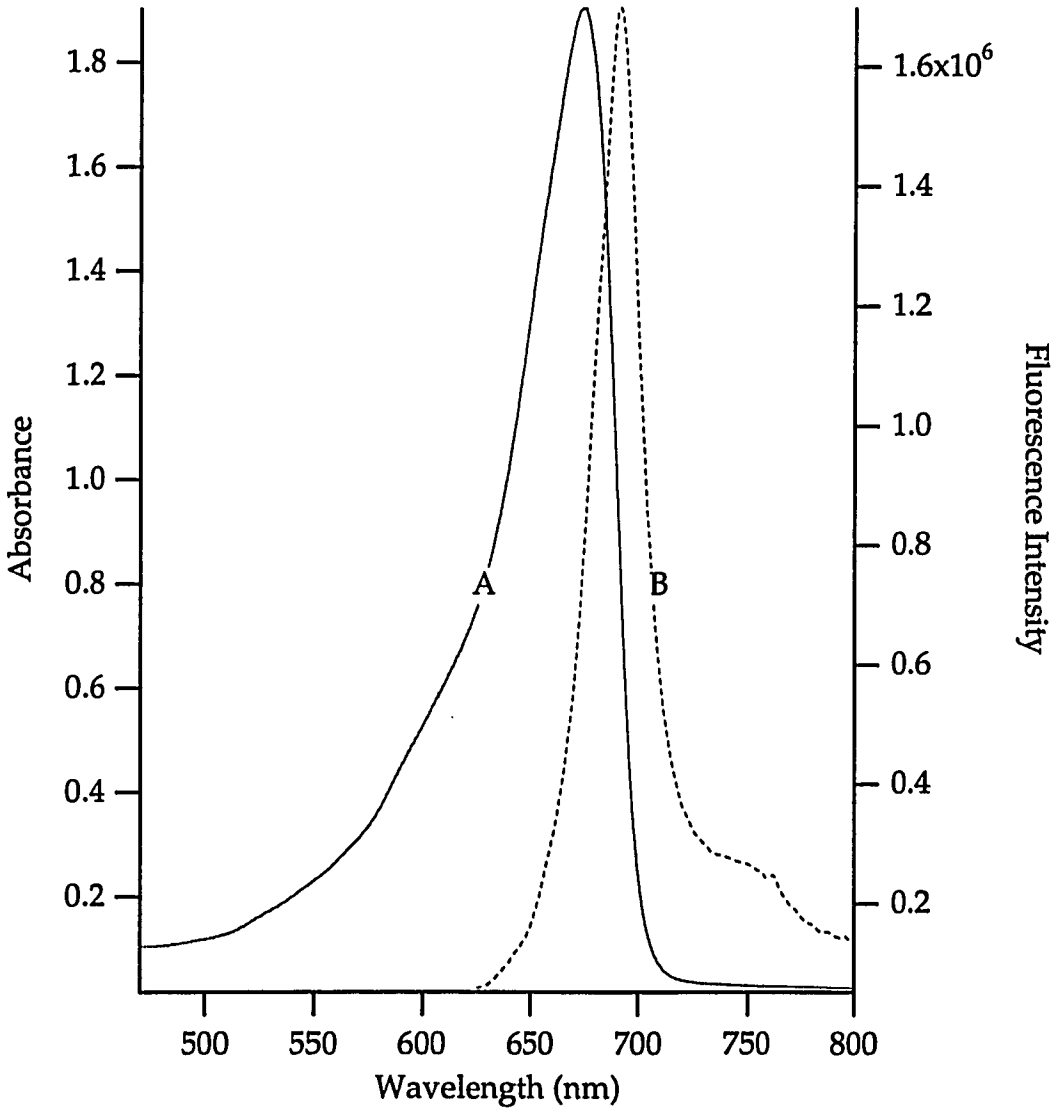

Figure 5.2. Absorption (A) and fluorescence (B) spectra of DBTC J-aggregate adsorbed on silica surface.

The shoulder at ca. 750 nm is again assigned to vibronic transitions of the J-aggregate. It remains unchanged whether the aggregate formed on the surface or in homogeneous solution.

5.3 Excited-State Dynamics of DBTC J-Aggregates

Fluorescence lifetime decays were obtained in order to get information about excited-state dynamics of DCTC J-aggregates. Fluorescence lifetime measurements of the J-aggregates have been carried out at room temperature using the Hamamatsu C4256 streak camera. The excitation source for the streak camera was a Coherent mode-locked Nd-YAG synchronously-pumped Kiton-Red dye laser, producing 5 ps pulses at 76 MHz. The system resolution was measured as 20 ps before experiments in single-shot mode. The excitation intensity at sample was 35 mW (0.43 nJ). The front-face excitation was used. The excitation wavelength was 635 nm. The spectral range of the system to monitor fluorescence was from 535 to 815 nm.

A) Fluorescence decay of the J-aggregate in homogeneous solution

Figure 5.3 shows the fluorescence decay of DBTC J-aggregate in homogeneous solution excited at 635 nm and monitored from 660 to 800

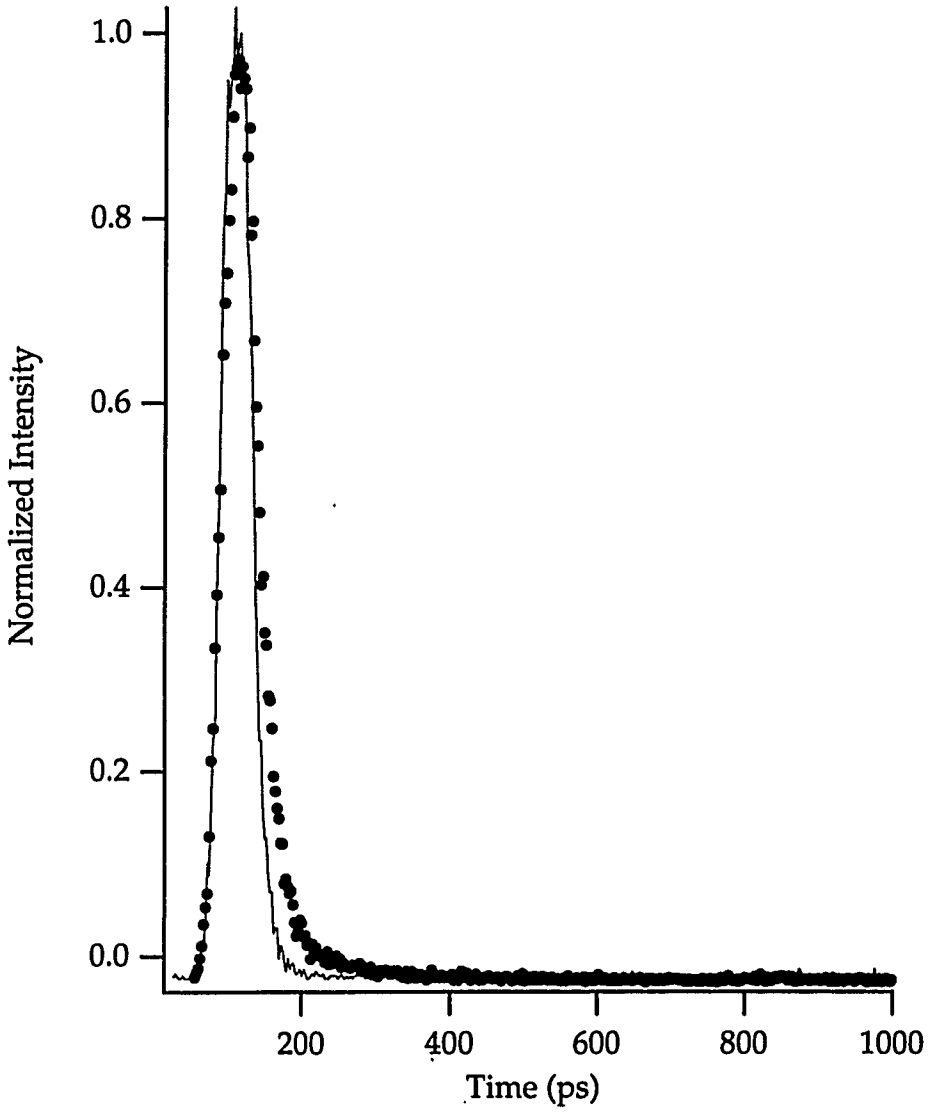

Figure 5.3. The fluorescence decay of DBTC J-aggregate formed in homogeneous solution

nm. The decays were analyzed by Hamamatsu U4290 fluorescence analysis software. The quality of fit is judged by the χ^2-test. The results are as follows: single exponential decays were recovered. The fluorescence lifetime of the J-aggregate, in the region from 670 to 725 which corresponds

to the band, is found to be 18.5 ± 0.2 ps with χ^2=1.5. It is the J-aggregate fluorescence decay time. The fluorescence decay was also measured in the region from 735 to 815 which corresponds to the shoulder. The fluorescence lifetime was found to be 12.4 ± 0.2 ps. This decay time is presumably shortened due to contribution of nonradiative relaxations due to existence of vibronic transitions or due to structurally different aggregate. The possibility of exciton annihilation, a bimolecular reaction, is eliminated because single-exponential decays are found.

The fluorescence lifetime of the J-aggregate in homogeneous solution is very short that indicates two possibilities: fast nonradiative relaxations or superradiance; i.e., enhanced radiative rate which scales linearly with the aggregate size. In order to determine effective mechanism for excited-state dynamics, one needs to calculate the radiative rate of the J-aggregate and that to compare to the monomer's radiative rate.

The monomer's radiative rate constant was determined to be 0.2 - 1.1 x 10^8 sec^{-1} in different solvents (16). Fluorescence quantum yield of the aggregate should be measured. However, it is rather difficult task because of resonance fluorescence which introduces reabsorption effects. To get around this problem one should use dilute solutions and front-face excitations, and corrections for equations. Another way to calculate radiative rate is to use the Strickler-Berg equation (17).

$$A_{u0\to l} = k_0 = \frac{1}{\tau_0} = \frac{8\pi.2303n^2}{c^2N} \frac{\int F(\bar{\nu})d\bar{\nu}}{\int \frac{F(\bar{\nu})d\bar{\nu}}{\bar{\nu}^3}} \int \varepsilon(\bar{\nu})d\bar{\nu} \qquad (5.1)$$

where $F(\nu)$ is fluorescence intensity, k_0 is the radiative rate constant, and τ_0 is the radiative lifetime, N is Avogadro's number, and $\varepsilon(\bar{\nu})$ is extinction coefficient. For resonance fluorescence transitions where the absorption and fluorescence occur at the same wavenumber $\bar{\nu}_{ul}$, equ. 5.1 simplifies to

$$\frac{1}{\tau_0} = 2.88x10^{-9}\bar{\nu}_{ul}^2 n^2 \int \varepsilon(\bar{\nu})d\bar{\nu} \ . \qquad (5.2)$$

The integral is over the electronic absorption spectrum, n is refraction index of solvent. The extinction coefficient was 2.5 x 10^5 $M^{-1}cm^{-1}$ which was measured. The radiative rate constant of DBTC J-aggregate is estimated to be 3 x 10^9 sec^{-1}. The ratio of the radiative rate constant of DBTC J-aggregate to the monomer's radiative rate is defined as "coherence size" that is found to be 30 - 150 which means 30 to 150 DBTC monomer units forms the aggregate. This implies enhanced fluorescence due to

aggregation and that superradiance is the mechanism of the excited-state dynamics of DBTC J-aggregates in solution.

However, it should be kept in mind, the the Strickler-Berg equation is an approximation to obtain radiative rate constant. Accurate results can be obtained by measuring the quantum yield of the aggregate. Additionally, exciton-phonon interactions should be studied. In our case, it is likely that exciton-phonon interaction may be estimated being weak because of the absence of the Stokes shift.

B) Fluorescence decay of the J-aggregate adsorbed on silica surface

Figure 5.4 shows the fluorescence decay of DBTC J-aggregate adsorbed on colloidal silica surface excited at 635 nm and monitored from 660 to 815 nm. The decay were analyzed by Hamamatsu U4290 fluorescence analysis software. The quality of fitness is judged by the χ^2-test. A single-exponential decay was recovered for the J-aggregate fluorescence from 658 to 690 nm; 35.4 ± 0.2 ps with χ^2=1.16. For the fluorescence from 691 to 715 nm, a double-exponential decay was obtained: 24.1 ± 0.1 ps with 88% of the decay, 134.4 ± 07 ps with 12% of the decay, χ^2=1.28. For the fluorescence from 730 to 800 nm, a single exponential with a decay time of 30.5 ± 0.3 ps was obtained with a χ^2=1.22.

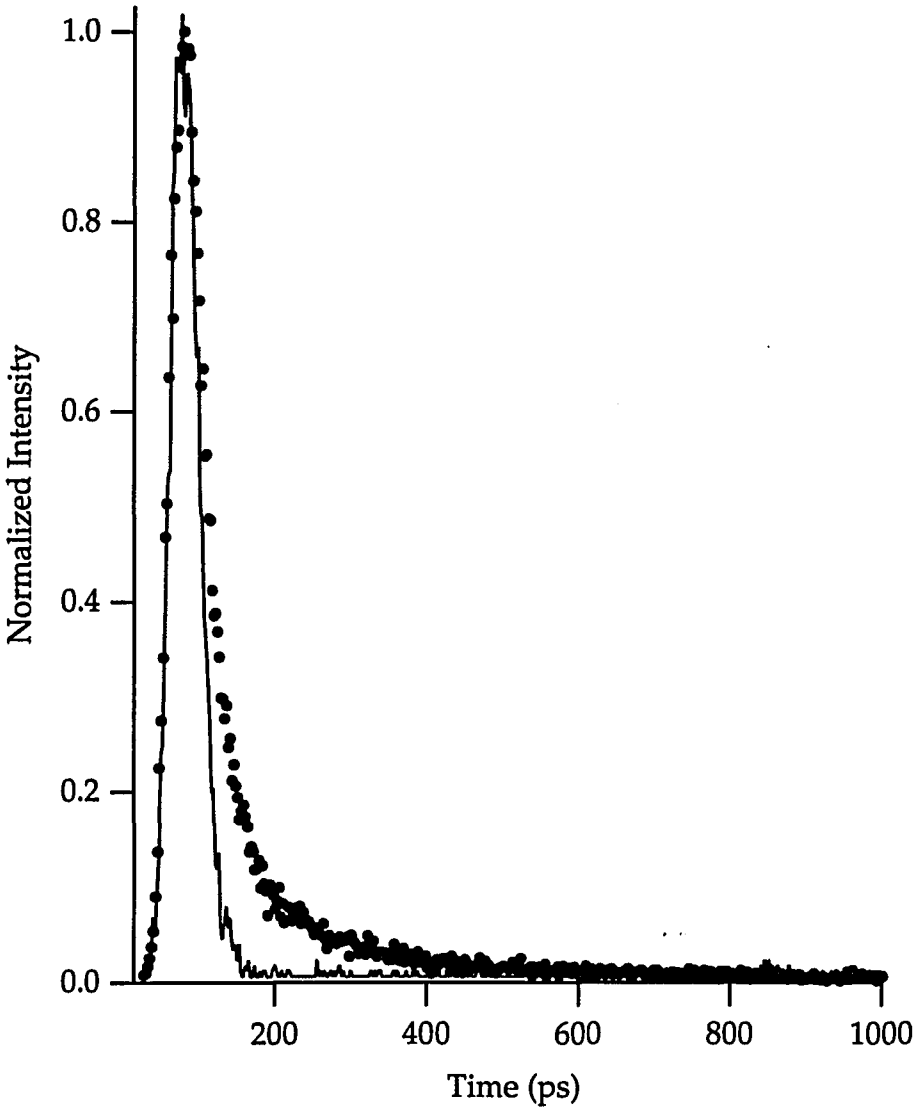

Figure 5.4. The fluorescence decay of DBTC J-aggregate adsorbed on silica surface

These measurements indicate that structurally different aggregates are formed on the silica surface. On the high-energy side of the J-aggregate fluorescence band, 658 to 690 nm, single lifetime was measured, indicating only one type aggregate is formed. On the other hand, on the low-energy

side of the J-aggregate fluorescence band, 691 to 715 nm, two substantially different decay times were measured, indicating two different aggregate structures. Their amplitudes should be related to their concentration in the excited-state. Therefore, the structure corresponding to the shorter decay seems more favorable than the longer one since the former's amplitude is bigger. In the lowest fluorescence wavelength range, 730 to 800 nm, one type of aggregate exists. I did not attemp to estimate the aggregate structure because more information is needed.

The discussion given for the J-aggregate in homogeneous solution is not valid for the J-aggregate adsorbed on the silica surface. The reasons come from the steady-state fluorescence spectrum: as was discussed the Stokes shift and broad bandwidth indicates nonradiative relaxations. Therefore fast nonradiative relaxations are responsible for the DBTC J-aggregate excited-state dynamics. The question arises about the mechanism that responsible for the fast nonradiative relaxations.

Potential mechanisms for the fast nonradiative relaxations are: interval conversion, triplet formation, dipole-dipole interaction, isomerization of monomers constituting J-aggregate, exciton trapping and dissociation.

Interval conversions may be induced by vibrations. The interval conversion rate constant is predicted for aggregates by Scharf and Dinur

(17). It is a function of aggregate size and in the strong coupling limit, decreases nonlinearly with size: the equation is

$$k_{IC}(J) = N^{-[(\Delta E/\hbar\omega)-1]} k_{IC}(M) \qquad (5.3)$$

where N is the aggregate size, $k_{IC}(J)$ is the aggregate interval conversion rate constant, $k_{IC}(M)$ is the monomer interval conversion rate constant, ΔE is the energy gap between S_1 and S_0, $\hbar\omega$ is vibration frequency of the accepting mode. $\Delta E = 14{,}000\ cm^{-1}$, $\hbar\omega = 1400\ cm^{-1}$ which is the strongest vibration frequency determined by Raman spectrum of the J-aggregate (18). $k_{IC}(M) = 0.05 - 2 \times 10^{10}\ sec^{-1}$ was determined in chapter 2 for for different solvents. For N=2, $k_{IC}(J) = 40$ to $1\ sec^{-1}$, for N=10, $k_{IC}(J) = 5$ to $200\ sec^{-1}$, therefore interval conversion can not explain the short lifetimes.

Triplet formation and exciton trap for the J-aggregate of the cyanines is, in general, considered to be negligible (11).

A dissociation mechanism is proposed for rhodamine B dimers in solution and dimers adsorbed on quartz (19, 20) to explain the short fluorescence lifetime of about 100 ps in both cases. But, dissociation is not observed for cyanine dimers and trimers (21). Pseudodissociation was proposed to explain very short fluorescence decay times of about 5 and 25 ps for J-aggregate of 5,5'-dichloro-3,3'-disulfopropyl-9-ethyl thiacarbocyanine adsorbed on AgBr and silica (11). The pseudodissociation was ascribed that it might be induced by unidirectional forces on the

surface. It could be operative for the DBTC J-aggregate adsorbed on silica surface.

Dipole-dipole interactions has been postulated to explain excited-state dynamics of dimers and trimers of 3,3'-diethylthiadicarbocyanine (21). It was proposed that the radiationless processes were induced by the very strong dipole-dipole interactions between the units of dimers and trimers. The rate of the nonradiative relaxations induced by dipole-dipole interactions is

$$k_{nr} \propto \frac{\mu^2}{\varepsilon_r R^3} F. \qquad (5.4)$$

where μ is the electronic transition dipole moment integral, R is the interunit distance between the two molecules in the dimer, ε_r is the dielectric constant of the medium and F is the Franck-Condon factor. Since the rate of the nonradiative relaxations contains the factor $1/R^3$, it is expected that the relaxation rate is quite sensitive to a change in R. It was shown that the Franck-Condon factor considerably decreases upon dimerization (17,21). The nonradiative rate constants of 3,3'-diethylthiadicarbocyanine dimer and trimer were calculated to be 4×10^{10} sec^{-1} and 2×10^{10} sec^{-1}, respectively, indicating weaker interaction in trimer. A weaker interaction could result from by a larger interunit distance in the trimer. Thus, it is reasonable that the interunit distance in the J-aggregate which is considered to be formed by large number of

repeating units that consists of up to four monomers could be larger than dimer and/or trimer. This consideration results in a lower nonradiative relaxation rate in J-aggregate. Dipole-dipole mechanism would be operative if its magnitude is about 10^{10} sec^{-1}.

Isomerization of the monomer could affect aggregate relaxation if the former mechanism rate is on similiar magnitude of the latter one. It is not reasonable to assume that when the aggregate band is excited energy finds its way into the isomerization coordinate of the monomer units and isomerization starts. Since the J-aggregate is excited at 635 nm which is lower than the monomer band located ca. at 600 nm, it is unlikely to induce monomer isomerization. Therefore, this mechanism is not operative in the J-aggregate oc DBTC.

As a result, dipole-dipole interactions and pseudodissociation of the J-aggregate is proposed as the operative excited-state relaxation mechanisms in the DBTC J-aggregate adsorbed on a silica surface.

REFERENCES

1. Hada, H.; Honda, C.; Tanemura, H. Photogr. Sci. Eng.1977, 21, 83.

2. Hada, H.; Honda, C. Photogr. Sci. Eng.1977, 21, 91.

3. Hada, H.; Honda, C. Photogr. Sci. Eng.1977, 21, 97.

4. Hada, H.; Honda, C. Photogr. Sci. Eng.1976, 20, 15.

5. Yonezawa, Y.; Mobius, D.; Kuhn, H. Ber. Bunsenges. Phys. Chem. 1986, 90, 1183.

6. Sato, T.; Yonezawa, Y.; Hada, H. J. Phys. Chem. 1989, 93, 14.

7. Yonezawa, Y.; Hayashi, T. J. Lumin. 1990, 47, 49.

8. Sato, T.; Yonezawa, Y.; Kurokawa, K.; Kurahashi, M.; Wada, Y.; Tanaka, T. Thin Solid Films 1992, 210/211, 172.

9. Sato, T.; Kurahashi, M; Yonezawa, Y. Langmuir, 1993, 9, 3395.

10. Takahashi, K.; Obi, K; Tanaka, I.; Tani, T. Chem. Phys. Lett. 1989, 154, 223.

11. Kemnitz, K.; Yoshihara, K.; Tani, T. J. Phys. Chem. 1990, 94, 3099.

12. Tani, T.; Suzumoto, T.; Kemnitz, K.; Yoshihara, K. J. Phys. Chem. 1992, 96, 2778.

13. Fidder, H.; Wiersma, D. A. J. Phys. Chem. 1993, 97, 11603.

14. Trosken, B.; Wiling, F.; Schwarzburg, K.; Ehert, A.; Spitler, M. J. Phys. Chem. 1995, 99, 5152.

15. Knox, R. S. Theory of Excitons; Solid State Physics Series, supplement no. 5, Academic Press, New York, 1963.

16. They were determined in chapter 2.

17. Scharf, B.; Dinur, U. Chem. Phys. Lett. 1984, 105, 78.

18. Raman spectrum of the J-aggregate of DBTC is obtained by Ozcelik, S. and Akins, D. L.; an unpublished study.

19. Smirl, A. L.; Clark, J. B.; Van Stryland, E. W.; Russel, B. R. J. J. Chem. Phys. 1982, 77, 631.

20. Kemnitz, K.; Tamai, N.; Yamazaki, I.; Nakashima, N.; Yoshihara, K. J. Phys. Chem. 1986, 90, 5094.

21. Sundstrom, V.; Gillbro, T. J. Chem. Phys. 1985, 83, 2733.

BIBLIOGRAPHY

The following references are used in this thesis.

Chapter 1

1. Jelley, E. Nature, 1936, 138, 1009.
2. Jelley, E. Nature, 1937, 139, 631.
3. Scheibe, G. Angew. Chem. 1936, 49, 563.
4. Scheibe, G. Angew. Chem. 1937, 50, 51.
5. Feher, G.; Okumura, M. Y. In "The Photosynthetic Bacteria"; Clayton, K.; Sistrom, W.F., Ed.; Plenum: New York, 1978.
6. Gilman, P. B. Photo. Sci. Eng. 1974, 18, 418.
7. Hanamura, E. Phys. Rev. B. 1988, 37, 1273.
8. Sasaki, F.; Kobayashi, S. Appl. Phys. Lett. 1993, 63, 2887.
9. Wang, Y. Chem. Phys. Lett. 1986, 126, 209.
10. Wang, Y. J. Opt. Soc. Am. B. 1991, 8, 981.
11. Kobayashi, S. Mol. Crys. Liq. Crys. 1992, 217, 77.
12. Fidder, H.; Knoster, J.; Wiersma, D. A. Chem. Phys. Lett. 1990, 171, 529.
13. Fidder, H.; Terpstra, J.; Wiersma, D. A. J. Chem. Phys. 1991, 94, 6895.
14. Grad, J.; Hernandez, G; Mukamel, S. Phys. Rev. A. 1988, 37, 3835.

15. Spano, F. C.; Mukamel, S. J. Chem. Phys. 1989, 91, 683.

16. Spano, F. C.; Kuklinski, J. R.; Mukamel, S. J. Chem. Phys. 1991, 94, 7534.

17. McRae, E.; Kasha, M. J. Chem. Phys. 1958, 28, 721.

18. Kasha, M. In Physical Processes in Radiation Biology. Academic Press, New York, 1964.

19. Kasha, M.; Rawls, H. R.; El_Bayoumi, M. A. Pure and Applied Chem., 1965, 11, 371.

20. Scheibe, G. In Optische Anregung Organischer Systeme. Ed. Foerst, W. Verlag Chemie, Weinheim, 1966.

21. Scheibe, G. Angew. Chem. 1939, 53, 631.

22. Dammeier, V. B.; Hoppe, W. Acta. Crystallogr. 1971, B27, 2364.

23. Czikklely, V.; Forsterling, H. D.; Kuhn, H. Chem. Phys. Lett. 1970, 6, 11.

24. Czikklely, V.; Forsterling, H. D.; Kuhn, H. Chem. Phys. Lett. 1970, 6, 207.

25. Stoeckli-Evans, H. Helv. Chim. Acta. 1974, 57, 1.

26. Duschl, C.; Frey, W.; Knoll, W. Thin Solid Films 1988, 160, 251.

27. Kuroda, S.; Ikegami, K.; Saito, K.; Saito, M; Sugi, M. J. Phys. Soc. Jpn. 1987, 56, 3319.

28. Mizrahi, V.; Stegeman, G. I.; Knoll, W. Phys. Rev. A 1989, 39, 3555.

29. Wolthaus, L.; Schaper, A.; Mobius, D. Chem. Phys. Lett. 1994, 225, 322.

30. Higgins, D. A.; Reid, P. J.; Barbara, P. F. J. Phys. Chem. 1996, 100, 1174.

31. Nolte, H. Chem. Phys. Lett. 1975, 31, 134.

32. Kirstein, S.; Mohwald, H. J. Chem. Phys. 1995, 103, 826.

33. Harrison, W. J., Mateer, D. L; Tiddy, G. J. T. J. Phys. Chem. 1996, 100, 2310.

34. Yu, Z. X.; Lu, P. Y.; Alfano, R. R. Chem. Phys. Lett. 1983, 79, 289.

35. Kopainsky, B.; Kaiser, W. Chem. Phys. Lett. 1982, 88, 357.

36. Rentsch, S. K.; Danielius, R. V.; Gadonas, R. A.; Piskarkas, A. Chem. Phys. Lett. 1981, 84, 446.

37. Brumbaugh, D. V.; Muenter, A. A.; Knox, W.; Mourau, G.; Wittmershaus, B.; J. Lumin. 1984, 31&32, 783.

38. Fink, F.; Klose, E.; Teuchner, K.; Dahne, S. Chem. Phys. Lett. 1977, 45, 548.

39. Sundström, V.; Gillbro, T.; Gadonas, R. A.; Piskarkas, A. J. Chem. Phys. 1988, 89, 2754.

40. De Boer, S.; Wiersma, D. A. Chem. Phys. 1989, 131, 135.

41. De Boer, S.; Wiersma, D. A. Chem. Phys. Lett. 1990, 165, 45.

42. De Boer, S.; Vink, K. J., Wiersma, D. A. Chem. Phys. Lett. 1987, 137, 99.

43. Muenter, A. A.; Brumbaugh, D. V.; Apolito, J.; Horn, L. A.; Spano, F. C.; Mukamel, S. J. Phys. Chem. 1992, 96, 2783.

44. Dorn, H-. P.; Muller, A. Appl. Phys. B. 1987, 43, 167.

45. Horng, M-L.; Quitevis, E. J. Phys. Chem. 1993, 97, 12408.

46. O'Brien, D. F. ; Kelly, T. M.; Costa, L. F. Photo. Sci. Eng. 1974, 18, 76.

47. Lindbrum, M; Glismann, A.; Moll, J.; Daehne, S. Chem. Phys. 1993, 178, 423.

48. Johnson, A. E.; Kumazaki, S.; Yoshihara, K. Chem. Phys. Lett. 1993, 211, 511.

49. Kamalov, V. F.; Struganova, I. A.; Tani, T., Y.; Yoshihara, K. Chem. Phys. Lett. 1994, 220, 257.

50. Kamalov, V. F.; Struganova, I. A.; Koyama, Y.; Yoshihara, K. Chem. Phys. Lett. 1994, 226, 132.

51. Gagel, R.; Gadonas, R.; Laubereau, A. Chem Phys. Lett. 1994, 217, 228.

52. Minoshima, K.; Taiji, M.; Misawa, K.; Kobayashi, T. Chem. Phys. Lett. 1994, 218, 67.

Chapter 2

1. Birks, J. B., In "Photophysics of Aromatic Molecules", Wiley-Interscience, New York, 1971.

2. Strickler, S. J.; Berg, R. B., J. Chem. Phys. 1962, 37, 814.

3. Akins, D. L. J. Phys. Chem. 1985, 98, 13476.

4. Dorn, H.-P.; Muller, A; Chem. Phys. Lett 1986, 130, 426.

5. Gray, W. E; Brewer, W.R; Bird, G. R. Photo. Sci. Eng. 1970, 14, 316.

6. Zuckerman, B. Photo. Sci. Eng. 1967, 11, 156.

7. Smith, D. L.; Luss, H. R. Acta Crystallogr., Sec. B 1972, 28, 2793.

8. Lakowicz, J. R. In "Principles of Fluorescence Spectroscopy". Plenum Press: New York, 1983.

9. Schäfer, F.P. In "Dye Lasers." 3rd Edition Springer-Verlag: Heidelberg, 1990.

10. Buettner, A. V. J. Chem. Phys. 1967, 46, 1398.

11. O'Brien, D. F. ; Kelly, T. M.; Costa, L. F. Photo. Sci. Eng. 1974, 18, 76.

12. Tredwell, C. J.; Keary, C. M. Chem. Phys. 1979, 46, 307.

13. Velsko, S. P.; Fleming, G. R. Chem. Phys. 1982, 65, 59.

14. Murphy, S.; Sauerwein, B.; Drickamer, H. G.; Schuster, G. B. J. Phys. Chem. 1994, 98, 13476.

15. Krieg, M.; Redmond, R. W. Photochem. Photobiol. 1993, 57, 472.

16. Kuzmin, V.A; Darmanyan, A. P. Chem Phys. Lett., 1978, 47, 123.

17. Krieg, M.; Bilitz, J. M., Srichai, M. B.; Redmond, R. W. Biochim. Biophys. Acta. 1994, 1199, 149.

18. West, W.; Pearce, S.; Grum, F. J. Phys.Chem. 1967, 71, 1316.

19. Chibisov, A. K. J. Photochem. 1976/77, 6, 199.

20. Siebrand, W; Williams, D. F. J. Chem. Phys. 1968, 49, 1860.

Chapter 3

1. Feher, G.; Okumura, M. Y. In "The Photosynthetic Bacteria"; Clayton, K.; Sistrom, W.F., Ed.; Plenum: New York, 1978.

2. Gilman, P. B. Photo. Sci. Eng. 1974, 18, 418.

3. Borsenberger, P. M.; Chowdry, A.; Hoesterey, D. C.; W. Mey J. Appl. Phys. 1978, 44, 5555.

4. Hanamura, E. Phys. Rev. B. 1988, 37, 1273.

5. Sasaki, F.; Kobayashi, S. Appl. Phys. Lett. 1993, 63, 2887.

6. Wang, Y. Chem. Phys. Lett. 1986, 126, 209.

7. Wang, Y. J. Opt. Soc. Am. B. 1991, 8, 981.

8. Kobayashi, S. Mol. Crys. Liq. Crys. 1992, 217, 77.

9. Jelley, E. Nature, 1936, 138, 1009.

10. Scheibe, G. Angew. Chem. 1936, 49, 563.

11. Fidder, H.; Knoster, J.; Wiersma, D. A. Chem. Phys. Lett. 1990, 171, 529.

12. Fidder, H.; Terpstra, J.; Wiersma, D. A. J. Chem. Phys. 1991, 94, 6895.

13. Muenter, A. A.; Brumbaugh, D. V.; Apolito, J.; Horn, L. A.; Spano, F. C.; Mukamel, S. J. Phys. Chem. 1992, 96, 2783.

14. Grad, J.; Hernandez, G; Mukamel, S. Phys. Rev. A. 1988, 37, 3835.

15. Spano, F. C.; Mukamel, S. J. Chem. Phys. 1989, 91, 683.

16. Spano, F. C.; Kuklinski, J. R.; Mukamel, S. J. Chem. Phys. 1991, 94, 7534.

17. Akins, D. L. J. Phys. Chem. 1986, 90, 1530.

18. Akins, D. L.; Lombardi, J. R. Chem. Phys. Lett. 1987, 136, 495.

19. Akins, D. L.; Akpabli, C. K.; Li, X. J. Phys. Chem. 1989, 93, 1977.

20. Akins, D. L.; Macklin, J. W. J. Phys. Chem. 1989, 93, 5999.

21. Akins, D. L.; Macklin, J. W.; Parker, L. A.; Zhu, H. -R. Chem. Phys. Lett. 1990, 169, 564.

22. Akins, D. L.; Macklin, J. W.; Zhu, H. -R. J. Phys. Chem. 1991, 95, 793.

23. Akins, D. L.; Zhu, H. -R. Langmuir 1992, 8, 546.

24. Akins, D. L.; Zhuang, Y. H.; Zhu, H. -R.; Liu, J. Q. J. Phys. Chem. 1994, 98, 1068.

25. Sato, T.; Yonezewa, Y., Hada, H. J. Phys. Chem. 1989, 93, 14.

26. Akins, D. L., Ozcelik, S.; Liu, J. Q. Pittsburgh Conference, 1994, Abstract # 936.

27. Ozcelik, S.; Akins, D. L. "Photophysics of Cyanine Dyes: I. Steady-State Spectroscopy and Fluorescence Lifetime of Monomeric Benzimidazolocarbocyanine," submitted to J. Phys. Chem., 1995.

28. West, W.; Pearch, S. J. Phys. Chem. 1965, 69, 1894.

29. O'Brien, D. F.; Kelly, T. M.; Costa, L. F. Photo. Sci. Eng. 1974, 18, 76.

30. Knudtson, J. T.; Eyring, E. M. J. Phys. Chem. 1974, 78, 2355.

31. Tredwell, C. J.; Keary, C. M. Chem. Phys. 1979, 43, 307.

32. Sundström, V.; Gillbro, T. J. Chem. Phys. 1985, 83, 2733.

33. Murphy, S.; Sauerwein, B.; Drickamer, H. G.; Schuster, G. B. J. Phys. Chem. 1994, 98, 13476.

34. Aramendia, P. F.; Negri, R. M.; San Romàn, E. J. Phys. Chem. 1994, 98, 3165.

35. Awad, M. M.; McCarthy, P. K.; Blanchard, G. J. J. Phys. Chem. 1994, 98, 1454.

36. Åkesson, E.; Sundström, V.; Gillbro, T. Chem. Phys. 1986, 106, 269.

37. Measurement made at General Food of Fort Lee, NJ by Dr. Stephen Habif.

38. Schafer, F. P. In "Dye Lasers." Springer-Verlag: New York, 1989.

39. Knapp, E. W. Chem. Phys. 1984, 85, 73.

40. Misawa, K.; Ono, H.; Minoshima, K.; Kobayashi, T. J. Lumin. 1994, 60&61, 812.

41. De Boer, S.; Vink, K. J., Wiersma, D. A. Chem. Phys. Lett. 1987, 137, 99.

42. Dorn, H-. P.; Muller, A. Chem. Phys. Lett. 1986, 130, 426.

43. Brooker, L. G. S.; White, F. L.; Sprague, R. H.; Dent Jr., S. G.; Van Zandt, G. Chem Rev. 1947, 41, 325.

44. Schmechel, D. E. V.; Crothers, D. M. Biopolymers 1971, 10, 465.

45. Yu, Z. X.; Lu, P. Y.; Alfano, R. R. Chem. Phys. Lett. 1983, 79, 289.

46. Kopainsky, B.; Kaiser, W. Chem. Phys. Lett. 1982, 88, 357.

47. Rentsch, S. K.; Danielius, R. V.; Gadonas, R. A.; Piskarkas, A. Chem. Phys. Lett. 1981, 84, 446.

48. Brumbaugh, D. V.; Muenter, A. A.; Knox, W.; Mourau, G.; Wittmershaus, B.; J. Lumin. 1984, 31&32, 783.

49. Fink, F.; Klose, E.; Teuchner, K.; Dahne, S. Chem. Phys. Lett. 1977, 45, 548.

50. Sundström, V.; Gillbro, T.; Gadonas, R. A.; Piskarkas, A. J. Chem. Phys. 1988, 89, 2754.

51. De Boer, S.; Wiersma, D. A. Chem. Phys. 1989, 131, 135.

52. De Boer, S.; Wiersma, D. A. Chem. Phys. Lett. 1990, 165, 45.

53. Dorn, H-. P.; Muller, A. Appl. Phys. B. 1987, 43, 167.

54. Lakowicz, J. R. In "Principles of Fluorescence Spectroscopy." Plenum Press: New York, 1983.

55. Demas, J. N; Crosby, G. A. J. Phys. Chem. 1971, 75, 991.

56. Melhuish, W. H. J. Phys. Chem. 1961, 65, 229.

57. Birks, J. B.; In "Photophysics of Aromatic Molecules", p. 92, Wiley-Interscience, 1971.

58. Di Bartolo, B.; In "Energy Transfer Processes in Condensed Matter", NATO-ASI Series B: Physcis, Vol. 114, Plenum Press, 1983.

59. Agranovich, V. M.; Galanin, M. D. In "Electronic Excitation Energy Transfer in Condensed Matter." North-Holland Pub. Co., Amsterdam, 1982.

60. Mejean, M.; Forel, M.T. J.Raman Spect. 1977, 6, 117.

61. Pace, L. J.; Pace E. L. Spectrochim. Acta. 1980, 36A, 557.

Chapter 4

1. Zuckerman, B. Photo. Sci. Eng. 1967, 11, 156.

2. Gray, W. E; Brewer, W.R; Bird, G. R. Photo. Sci. Eng. 1970, 14, 316.

3. Hochstrasser, R. M.; Kasha, M Photochem. Photobiol. 1964, 3, 317.

4. Smith, D. L.; Luss, H. R. Acta Crystallogr., Sec. B 1972, 28, 2793.

5. Herz, A. H Photo. Sci. Eng. 1974, 18, 323.

6. O'Brien, D. F. Photo. Sci. Eng. 1973, 17, 226.

7. O'Brien, D. F. ; Kelly, T. M.; Costa, L. F. Photo. Sci. Eng. 1974, 18, 76.

8. Lindbrum, M; Glismann, A.; Moll, J.; Daehne, S. Chem. Phys. 1993, 178, 423.

9. Johnson, A. E.; Kumazaki, S.; Yoshihara, K. Chem. Phys. Lett. 1993, 211, 511.

10. Kamalov, V. F.; Struganova, I. A.; Tani, T., Y.; Yoshihara, K. Chem. Phys. Lett. 1994, 220, 257.

11. Kamalov, V. F.; Struganova, I. A.; Koyama, Y.; Yoshihara, K. Chem. Phys. Lett. 1994, 226, 132.

12. Nabetani, A.; Tomioka, A.; Tamaru, H.; Miyano, K J. Chem. Phys, 1995, 102, 5109.

13. Thomas, J. K. J. Phys. Chem., 1987, 91, 267.

14. Weitz, D. A; Garoff, S.; Gersten, J. I.; Nitzan, A. J. J. Chem. Phys. 1983, 78, 5324.

15. Fox, M. A. Acc. Chem. Res. 1983, 16, 314.

16. Laane, C.; Willner, I.; Calvin, M. Proc. Natl. Acad. Sci., 1981, 78, 5928.

17. Willner, I.; Laane, C.; Otvos, J. W.; Calvin, M. In Inorganic Reactions in Organized Media; Holt., S. L., Ed.; American Chemical Society, Washington, DC, 1982, ACS Semp. Series No. 177, pp 71-95.

18. Iler, R. K. The Chemistry of Silica, 2nd edition; Wiley: New York, 1979.

19. Herz, A. Adv. Colloid. Interfac. Sci., 1977, 8, 237.

20. Herz, A.; Danner, R. P., Janusonis, G. A. In Adsorption from Aqueous Solution; Gould, R. F.; Ed.; American Chemical Society, Washington, DC, 1968, ACS Semp. Series No. 79, pp 173-197.

21. Czikklely, V. Forsterling, H. D.; Kuhn, H. Chem Phys. Lett., 1970, 6, 207.

22. Quitevis, E. L.; Horng, M-L.; Chen, S-Y. J. Phys. Chem., 1988, 92, 256.

23. Philpott, M. R. J. Chem. Phys., 1975, 63, 485.

24. Kamat, P. V.; Ford, W. E. J.Phys. Chem. 1989, 93, 1405.

25. Smith, D. L. Photo. Sci. Eng. 1974, 18, 309.

26. Emerson, E. S; Conlin, M. A.; Rosenoff, A. E.; Norland, K. S.; Rodriguez, H.; Chin, D.; Bird, G. R. J.Phys. Chem. 1967, 71, 2396.

27. Norland, K. S; Ames, A. E Photo. Sci. Eng. 1970, 14, 295.

28. McRae, E.; Kasha, M. J. Chem. Phys. 1958, 28, 721.

29. Kasha, M. In Physical Processes in Radiation Biology. Academic Press, New York, 1964.

30. Sundstrom, V.; Gillbro, T.; Gadonas, R. A.; Piskarkas, A. J. Chem. Phys., 1988, 89, 2754.

31. Brumbaugh, D. V.; Muenter, A. A.; Knox, W.; Mourou, G; Wittmershaus, B. J. Lumin., 1984, 31 and 32, 783.

32. Reid, P.; Higgins D. A.; Barbara, P. J. Phys. Chem., 1996, 100, 3892.

33. Paillotion, G.; Swenberg, E.; Breton, J.; Geactinov, N. E. Biophys. J., 1979, 25, 513.

34. Pope, M. and Swenberg, E. In Electronic Processes in Organic Crytals. p158-161.

35. Dexheimer, S. L.; Vareka, W. A.; Mittleman, D., Zettl, A.; Shank, C. V. Chem. Phys. Lett., 1995, 235, 552.

36. Gulbinas, V.; Chachisvilis, M.; Persson, A.; Svanberg, S.; Sundstrom, V. J. Phys. Chem., 1994, 98, 8118.

37. Kopelman, R.; Parus, S.; Prasad, J. Phys. Rev. Lett., 1986, 56, 1742.

38. Klymko, P. W.; Kopelman, R. J. Phys. Chem. 1983, 87, 4565.

39. Kamalov, V; Yoshihara, K. Time-resolved vibrational spectroscopy VII, p 28, 1995.

40. De Boer, S.; Wiersma, D. A. Chem. Phys. 1987, 131, 135.

41. Muenter, A. A.; Brumbaugh, D. V.; Apolito, J.; Horn, L. A.; Spano, F. C.; Mukamel, S. J. Phys. Chem. 1992, 2783.

42. Spano, F. C. Chem. Phys. Lett., 1995, 234, 29.

43. Gagel, R.; Gadonas, R.; Laubereau, A. Chem Phys. Lett. 1994, 217, 228.

44. Fidder, H; Knoester, J.; Wiersma, D. A. J. Chem. Phys. 1993, 98, 6554.

45. Minoshima, K.; Taiji, M.; Misawa, K.; Kobayashi, T. Chem. Phys. Lett. 1994, 218, 67.

46. Durrant, J. D.; Knoester, J.; Wiersma, D. A. Chem. Phys. Lett. 1994, 222, 450.

Chapter 5

1. Hada, H.; Honda, C.; Tanemura, H. Photogr. Sci. Eng.1977, 21, 83.

2. Hada, H.; Honda, C. Photogr. Sci. Eng.1977, 21, 91.

3. Hada, H.; Honda, C. Photogr. Sci. Eng.1977, 21, 97.

4. Hada, H.; Honda, C. Photogr. Sci. Eng.1976, 20, 15.

5. Yonezawa, Y.; Mobius, D.; Kuhn, H. Ber. Bunsenges. Phys. Chem. 1986, 90, 1183.

6. Sato, T.; Yonezawa, Y.; Hada, H. J. Phys. Chem. 1989, 93, 14.

7. Yonezawa, Y.; Hayashi, T. J. Lumin. 1990, 47, 49.

8. Sato, T.; Yonezawa, Y.; Kurokawa, K.; Kurahashi, M.; Wada, Y.; Tanaka, T. Thin Solid Films 1992, 210/211, 172.

9. Sato, T.; Kurahashi, M; Yonezawa, Y. Langmuir, 1993, 9, 3395.

10. Takahashi, K.; Obi, K; Tanaka, I.; Tani, T. Chem. Phys. Lett. 1989, 154, 223.

11. Kemnitz, K.; Yoshihara, K.; Tani, T. J. Phys. Chem. 1990, 94, 3099.

12. Tani, T.; Suzumoto, T.; Kemnitz, K.; Yoshihara, K. J. Phys. Chem. 1992, 96, 2778.

13. Fidder, H.; Wiersma, D. A. J. Phys. Chem. 1993, 97, 11603.

14. Trosken, B.; Wiling, F.; Schwarzburg, K.; Ehert, A.; Spitler, M. J. Phys. Chem. 1995, 99, 5152.

15. Knox, R. S. Theory of Excitons; Solid State Physics Series, supplement no. 5, Academic Press, New York, 1963.

16. They were determined in chapter 2.

17. Scharf, B.; Dinur, U. Chem. Phys. Lett. 1984, 105, 78.

18. Raman spectrum of the J-aggregate of DBTC is obtained by Ozcelik, S. and Akins, D. L.; an unpublished study.

19. Smirl, A. L.; Clark, J. B.; Van Stryland, E. W.; Russel, B. R. J. J. Chem. Phys. 1982, 77, 631.

20. Kemnitz, K.; Tamai, N.; Yamazaki, I.; Nakashima, N.; Yoshihara, K. J. Phys. Chem. 1986, 90, 5094.

21. Sundstrom, V.; Gillbro, T. J. Chem. Phys. 1985, 83, 2733.